Investigations into Expression and Function of the Murine *Fam181* Gene Family

Inaugural-Dissertation
to obtain the academic degree
Doctor rerum naturalium (Dr. rer. nat.)

submitted to the Department of Biology, Chemistry and Pharmacy
of the Freie Universität Berlin

by

Matthias Marks

from Görlitz

December, 2014

The present work was carried out at the Max-Planck-Institute for Molecular Genetics, Department of Developmental Genetics, in Berlin, Germany, between October 2010 and December 2014, under the supervision of Prof. Dr. Bernhard G. Herrmann.

1st Reviewer:

Prof. Dr. Bernhard G. Herrmann

Max-Planck-Institute for Molecular Genetics

Ihnestraße 63-73

14195 Berlin

2nd Reviewer:

Prof. Dr. Stephan Sigrist

Freie Universität Berlin

Takustraße 6

14195 Berlin

Date of Defense: 04/20/2015

"*When the snows fall and the white winds blow, the lone wolf dies but the pack survives.*" (George R. R. Martin)

~ To my fiancé and our Bohne ~

Contents

Abbreviations

Amp	ampicillin
AVE	anterior visceral endoderm
BMP	Bone morphogenetic protein
BSA	bovine serum albumin
Ci	Curie
CNS	central nervous system
Da	Dalton (proteins molecular weight)
DMEM	Dulbecco's Modified Eagle's Medium
DMSO	dimethyl sulfoxide
dNTP	deoxynucleotide triphosphate
dCTP	Desoxycytidintriphosphat
Dox	doxycyline
DTT	dithiothreitol
E	embryonic day
E. coli	*Escherichia coli*
EDTA	ethylenediaminetetraacetic acid
e.g.	for example (exempli gratia)
ES cell	embryonic stem cell
EtOH	ethanol
FCS	fetal calf serum
Fgf	fibroblast growth factor
Fig.	figure
G418^r	G418-resistant
h	hour(s)
HEPES	4-(2-hydroxyethyl)-1-piperazineethanesulfonic acid
hp	hairpin
i.e.	in especially
J	joule
KAc	potassium acetate
LB	Luria broth

LIF	leukemia inhibitory factor
LPM	lateral plate mesoderm
MeOH	methanol
min	minute(s)
mRNA	messenger RNA
miRNA	microRNA
NCC	neural crest cell
NCSC	neural crest-derived stem cells
NECD	Notch extracellular domain
NICD	Notch intracellular domain
NPC	neural progenitor cell
pA/polyA	polyadenylation signal
PBS	phsophate-buffered saline
PFA	paraformaldehyde
PNS	peripheral nervous system
PSM	presomitic mesoderm
qPCR	real-time quantitative PCR
RA	retinoic acid
rpm	rounds per minute
RT-PCR	reverse transcriptase PCR
RT	room temperature
SDS	sodiumdodecylsulfate
sec	second(s)
shRNAmir	short hairpin RNA in a microRNA-context
Spec	spectinomycin
SSC	saline-sodiumcitrate buffer
TBS	Tris-buffered saline
Tgf	Transforming growth factor
Tris	Tris(hydroxymethyl)aminomethane
TS	Theiler stage
U	Unit (enzyme activity)
V	Volt
vol.	volume
w/o	without
WISH	whole mount *in situ* hybridization

1 Introduction

1.1 General embryonic development of the mouse

For the understanding of fundamental molecular and cellular processes during development, model organisms are of great value. They offer certain advantages like a short life cycle and an easy maintenance, with the possibility to obtain results transferable to human embryogenesis. The model organism of choice used in this thesis was the house mouse (*Mus musculus*). As a mammal it is closely related to humans, has a maturation cycle of about 9-10 weeks (Fig. 1A), and allows for the generation of precisely targeted genetic mutations.

Murine embryonic development can be subdivided into the pre- and postimplantation phases (see blue and orange arrows in Fig. 1A). During the preimplantation development, the fertilized oocyte (Fig. 1B) moves through the oviduct, where it undergoes cleavages and forms a compact sphere of up to 32 cells, called a morula. Then the blastocoel, a central cavity, forms within the embryo, thus giving rise to the so-called blastocyst. At this time, there are already two cell types distinguishable in the embryo, namely the trophoblast cells forming the surrounding trophectoderm, and the pluripotent inner cell mass (Fig. 1C). The latter will later give rise to the embryo proper and the primitive endoderm (Gilbert, 2014). On a molecular level, this first specification event depends on the expression of the *POU domain class5 transcription factor1* (*Pou5f1/Oct4*, red in Fig. 1C) restricted to the inner cell mass by *Caudal type homeobox 2* (*Cdx2*, blue in Fig. 1C) (Nichols *et al.*, 1998; Strumpf *et al.*, 2005). Upon arrival of the blastocyst to the uterus between embryonic day (E)3.5 and E4.5, the zona pellucida is enzymatically removed and the embryo implants into the uterine crypts. This marks the end of the preimplantation phase.

Over the following days, the ICM further differentiates into the epiblast and the primitive endoderm (hypoblast) which is separating the epiblast from the blastocoel. Both tissues elongate to form a cup-shaped structure, called the egg cylinder. The hypoblast cells also spread laterally and will line the entire blastocoelic cavity thus giving rise to the yolk sac. The portion of the hypoblast covering the surface of the epiblast is called visceral endoderm (VE). Between E5.5 and E6.5 the anterior-posterior axis
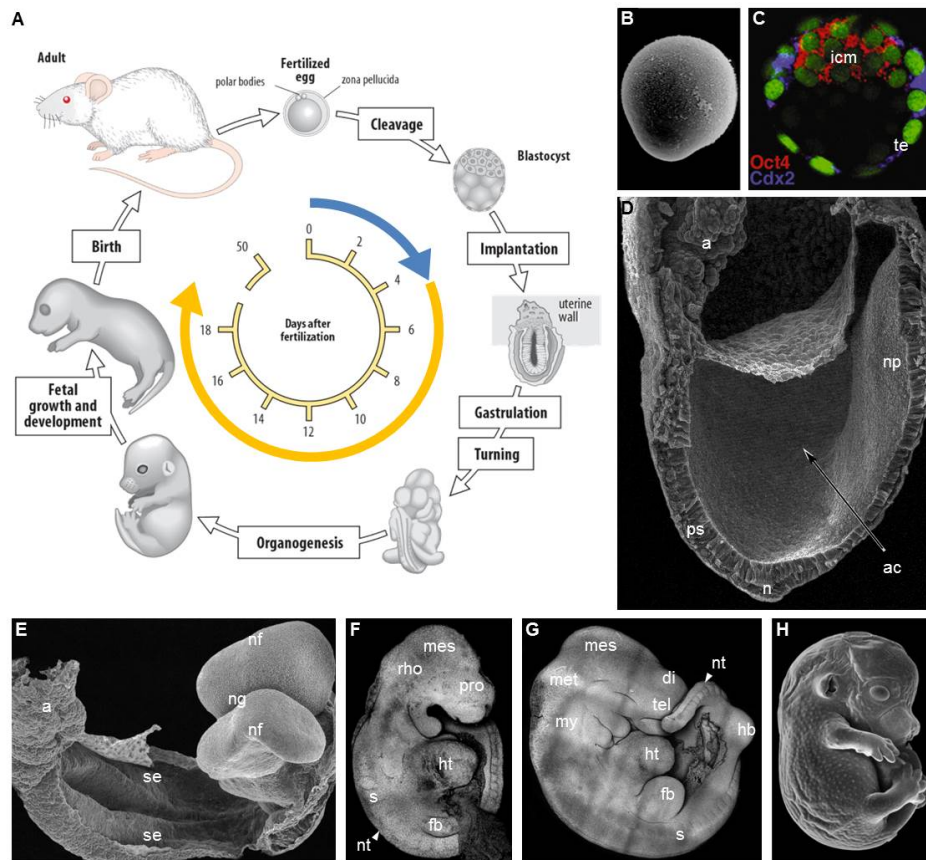
Figure 1. Life cycle and development of the mouse
A: Schematic representation of the mouse life cycle. The embryonic phase can be subdivided in pre- (blue arrow) and postimplantation (orange) development. Important events are mentioned. B: A fertilized oocyte before cleavage. C: Fluorescent *in situ* hybridization of for *Oct4* (red) and *Cdx2* (blue) on a mouse blastocyst. Nuclei were counterstained with YOYO1 (green). D: Scanning electron micrograph of a E7.0 gastrulating mouse embryo. E: Scanning electron micrograph of E8.0 mouse embryo. F-G: Laser scanning micrographs of carmine red stained E9.5 (F) and E10.5 (G) mouse embryos. H: E14.5 mouse embryos. a, allantois; ac, amniotic cavity; di, diencephalon; fb, forelimb bud; hb, hindlinb bud; ht, heart anlage; icm, inner cell mass; mes, mesencephalon, met, metencephalon; my, myelencephalon; n, node; nf, neural fold; ng neural groove; np, neural plate; nt, neural tube; ps, primtive streak; rho, rhombencephalons, somite; se, surface ectoderm; te, trophectoderm; tel, telencephalon A, B, and H modified after Wolpert *et al.* (2007), C modified after Oct4/Cdx2 Strumpf *et al.* (2005), D and E modiefed after Schoenwolf (2009)

becomes established by a subportion of the VE, the anterior visceral endoderm (AVE), whose cells migrate to the prospective anterior site of the embryo. They secrete several signalling inhibitors such as *Left right determination factor 1* (*Lefty1*), *Cerberus 1 homolog* (*Cerl1*), and *Dickkopf homolog 1* (*Dkk1*), thus inhibiting ectopic primitive streak formation in the underlying epiblast (Meno *et al.*, 1996; Perea-Gomez *et al.*, 2002; Kimura-Yoshida *et al.*, 2005). At about E6.5, the primitive streak forms at the prospective posterior end of the embryo, marking the onset of gastrulation, where mas-

sive amounts of cell migration and rearrangement lead to the formation of the three germ layers. The primitive streak expands towards the distal tip of the epiblast, where at about E7.0, at its anteriormost tip the node, the mammalian primary embryonic organizer, is formed (Fig. 1D). In concert with the AVE, the node will give rise to the head region of the embryo Knoetgen *et al.* (2000), while the trunk region is generated by the regressing primitive streak and the node (Wolpert *et al.*, 2007; Gilbert, 2014). Depending on the point of ingression between the node and the posterior end of the primitive streak, mesodermal cells will migrate to different positions within the embryo. The more posteriorly the cells ingress, the more laterally they will be positioned. This distribution gives rise to the different mesodermal lineages from the medialmost chordamesoderm, to the lateral plate mesoderm (LPM).

The cells not ingressing through the streak will become the ectoderm, giving rise to the surface ectoderm, the neural plate, and the neural crest (Gilbert, 2014). Around E7.5, primary neurulation starts in the anterior portion of the embryo. The contact region between the prospective surface ectoderm and the neural plate thickens to form the neural folds and the midline of the neural plate becomes anchored to the underlying notochord. This induces a size reduction in its neighbouring neural plate cells and leads to the formation of the neural groove. Between E7.75 and E8.0 the head process with the rapidly developing brain plate has emerged at the anterior end of the embryo and the neural folds move towards the embryonic midline (Fig. 1E; Gilbert, 2014). Posterior to the head region, metameric blocks of cells, the somites, form in an anterior-to-posterior sequence along both sides of the axis. Around the level of the 4th to 5th somite formed, the neural folds from both sides of the embryo come into contact with each other. This leads to the formation of the neural tube. This closure of the neural groove extends anteriorly and posteriorly in a zipper-like fashion. As the neural tube closes in the posterior direction, the neural crest forms between its dorsal site and the surface ectoderm. While the surface ectoderm expresses E-Cadherin, the neural plate instead produces N-Cadherin. That allows the release of the closed neural tube from the surface ectoderm (Detrick *et al.*, 1990). The neural crest cells express neither N- nor E-Cadherin, allowing them to migrate as single cells (Gilbert, 2014).

Between E8.5 and E9.0 the embryo goes through a process called turning, leading to the proper positioning of the three germ layers. By E9.0 the neural tube is closed anteriorly. Its head portion becomes temporally separated from the prospective spinal portion by a restriction of the lumen when closure occurs in this region. This allows for an increase of its lumen in the head, leading to the formation of the 3 primary brain vesicles: prosencephalon, mesencephalon, and rhombencephalon. Shortly before the closure of the neural tube, the cranial neural crest can be seen and the otic and optical

vesicals form. After the closure, the rhombencephalon subdivides into 7 discrete transient units, called rhombomeres (Gräper, 1913; Osumi-Yamashita *et al.*, 1996; reviewed in Jimenez-Guri and Pujades, 2011). On a molecular level they can be discriminated by the different subsets of genes they express and their neural crest cells will later give rise to different cranial nerves. At E9.5 the gut is closed and the neural tube remains open only at its posterior tip, the posterior neuropore. The forelimb bud emerges at the level of the 8th-12th somite (Fig. 1F). The primitive streak ceases and new cells for the three germ layers are now derived from the tail bud.

This also marks the start of secondary neurulation (Schoenwolf, 1984). Between E9.5 and E10.0, a round condensation of tail bud-derived cells, the medullary rosette, forms in the caudal end. Progressing anteriorly, a central cavity is generated and its lumen linked to the neural tube. Later, between E11.0 and E12.0, these cellular condensations are dorsoventrally flattened and called the medullary plate. The cavity also obtains a more slit-like form, but remains linked to the neural tube. At E10.0, the brain vesicles further subdivide. The prosencephalon forms the frontal telencephalon and the diencephalon, while the rhombencephalon divides into the anterior metencephalon and the caudal myelencephalon (Gilbert, 2014). The hindlimb bud emerges at the level of the 23rd-28th somite (see Fig. 1G for an E10.5 embryo). Also at this stage, organogenesis, the establishment of all major organ anlagen, starts. It will continue until about E14.5, when all major organs have developed (Fig. 1H). At about E11.5 the anterior limb bud has formed a distally rounded handplate, and at E12.0 the phalanges start to form. The hindlimb bud follows its anterior counterpart with an approximate 0.5 day delay. Finally, after about 18 to 21 days (depending on the strain), the pups are born, marking the end of embryonic development.

During the developmental processes described above, a complex multicellular organism arises from a single fertilised oocyte. In the embryo, cells are constantly being generated, and they require temporal and spatial instructions to ensure their correct positioning within the final body structure. As described for selected examples during the general murine embryonic development, the fundamental principle of these instructions is differential gene expression. The sum of these changes results in a temporally and spatially restricted gene activities and provides the instructions for further development and differentiation.

1.2 Signalling pathways as regulators of differential gene expression during development

One way to provide instructions for differential gene expression in the first place is through signalling pathways. Though the embryo becomes more and more complex with respect to the different tissues and cell types produced as development proceeds, the number of these intercellular communication systems is quite limited. Of major importance are signals of the Fibroblast growth factor (Fgf) family, the Hedgehog family, the Wnt family, the Transforming growth factor (Tgf)-β superfamily, as well as Notch and Retinoic acid (RA) signalling. The fundamental principle of all of these pathways is the same. A ligand binds to the extracellular portion of its receptor and thus activates an intracellular signalling cascade. The latter transduces the signal to the nucleus where it finally impacts on target gene expression. Depending on the distance with which these signals can be transmitted extracellularly, they can be discriminated between juxtacrine signalling pathways, limited to neighbouring cells, or paracrine signals. For the latter, the ligand is usually a secreted molecule. During development these signalling cascades do not act individually, but are instead interconnected. The spatial distribution of their activities as well as the temporal order with respect to each other, helps to increase the potential provided by these few pathways. For example, during patterning of the ectoderm, the spatiotemporal distribution of signalling activity from Wnt and Bone morphogenetic protein (BMP), which belongs to the Tgf-β superfamily, defines which regions of the embryo will give rise to surface ectoderm (epidermis), placodes, neural crest, or the central nervous system (Patthey *et al.*, 2008, see Fig. 2A)

Wnt ligands are small secreted proteins that can activate at least three signalling cascades intracellularly, namely the planar cell polarity (PCP) pathway, the Wnt/Ca^{2+} pathway, and the canonical Wnt pathway. The latter is involved in the regulation of a variety of developmental processes, cell proliferation, cell polarity, and cell fate determination (reviewed in Logan and Nusse, 2004; MacDonald *et al.*, 2009). It relies on β-Catenin (β-Cat) as terminal effector (Fig. 2B). There are two pools of β-Catenin within cells. One is bound to E-cadherins at the plasma membrane, where it exerts cytoskeletal functions, the other exists in the cytoplasm (reviewed in Valenta *et al.*, 2012). Without activation of Wnt sigalling by binding of the ligand to its receptors Frizzled (Frz) and Lipoprotein receptor-related protein 5 or 6 (LRP5/6), the cytoplasmic pool of β-Catenin is kept low by the work of the so-called destruction complex. This consists of the scaffolding proteins Adenomatous polyposis coli (APC) and Axin/Axin2 and the two kinases Casein kinase 1α (CK1α) and Glycogen synthase kinase 3 (GSK3).
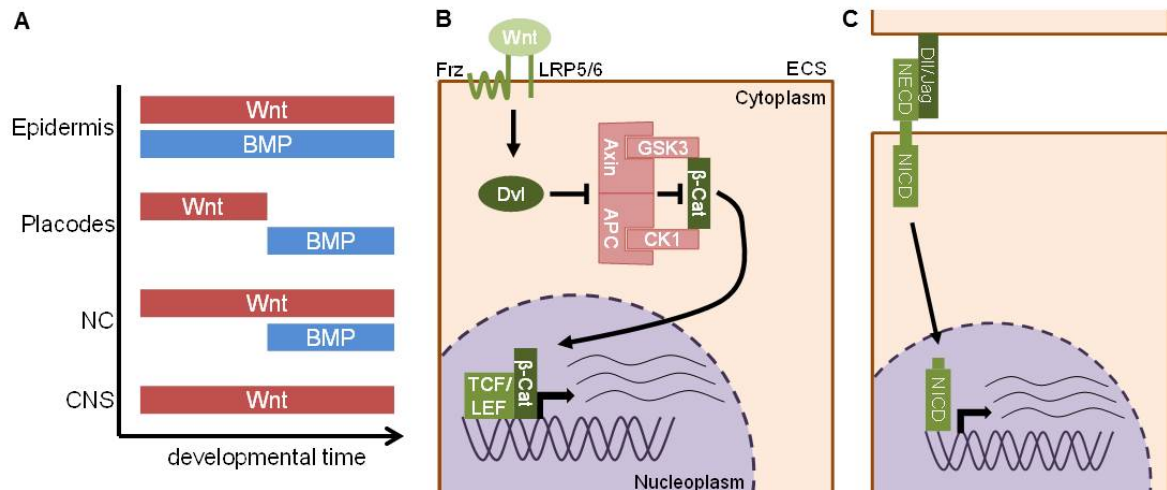
Figure 2. Signalling pathways in development
A: Schematic representation of the influence of the temporal order of BMP and Wnt signalling on ectoderm patterning. Depending which cells perceive the signals from both pathways, they differentiate into epidermal tissues, central nervous system (CNS), placodal, or neural crest (NC) cells. After (Patthey *et al.*, 2008; Gilbert, 2014). B: Schematic representation of the canonical Wnt pathway. Wnt-ligand binding to its receptors Frizzled (Frz) and LDL-receptor related protein (LRP) 5/6 activates Dishevelled (Dvl). This in turn inhibits the β-Catenin destruction complex, consisting of Adenomatous polyposis coli (APC), Axin/Axin2, Casein kinase 1α (CK1), and Glycogen synthase kinase 3 (GSK3). Thus β-Catenin is able to accumulate in the cytoplasm and shuttle into the nucleus, where it exerts its function in concert with T cell factor (TCF)/Lymphoid enhancer-binding factor (LEF) at response elements within the promoter to activate target genes. C: Schematic representation of the Notch signalling pathway. Binding of the Delta- and Serrate-like (called Jagged in mammals) ligands to the extracellular domain of the Notch receptor (NECD) induces an enzymatic cleavage, followed by the release of the Notch intracellular domain (NICD). The latter translocates to the nucleus and activates target gene transcription.

CK1α phosphorylates β-Catenin at serine residue 45 priming further phosphorylations by GSK3 at serine residues 33 and 37, and the threonine residue 41 thus activating ubiquitin-mediated destruction of β-Catenin (Liu *et al.*, 1999; Winston *et al.*, 1999; Wu and He, 2006). Upon ligand binding Dishevelled (Dvl) becomes activated and in turn inhibits the destruction complex. The exact mechanism of this remains a matter of discussion (Taelman *et al.*, 2010; Hernández *et al.*, 2012; Li *et al.*, 2012; Kim *et al.*, 2013). The accumulated β-Catenin is now able to shuttle to the nucleus, where it binds to the Lymphoid enhancer-binding factor (LEF) and T cell factor (TCF) DNA-binding proteins and activates target gene transcription.

The juxtacrine Notch signalling pathway is important for developmental processes such as lateral inhibition, boundary formation, and cell fate determination (reviewed in Fiúza and Arias, 2007). Both the Notch receptor and its ligands Delta (Dll) and Jagged (Jag) are single-pass transmembrane proteins. The intracellular domain of

Notch contains a transactivation domain, able to activate target gene expression in concert with its coactivators CBF1/*Drosophila* Su(H)/*C. elegans* LAG-1 (CSL) and Mastermind (Mam). The protein encoded by the mammalian *Notch* gene, is cleaved during its maturation (S1 cleavage) and both halves associate, forming the functional receptor dimer (reviewed in Fortini, 2009). Upon ligand binding, the extracellular domain (NECD) of the receptor is enzymatically removed (S2 cleavage), before two further cleavages (S3 and S4), mediated by the γ-Secretase complex, release the intracellular domain (NICD) from the plasma membrane (Fig. 2C). The NICD then shuttles to the nucleus and activates Notch target gene expression.

1.3 Methods for the investigation of differentially expressed genes

During embryonic development, differential gene expression provides the information that leads to commitment and differentiation of cells into various cell lineages and fates. Visualizing the spatial distribution of gene activity is an important step in identifying regulators of these developmental processes and can provide hints to the function of the expressed genes. The standard method to detect transcriptional activity in tissues is *in situ* hybridization (Wilkinson, 1998). Thereby, a labelled, complementary probe is hybridized to the RNA of interest directly within a specimen, which can be a piece of tissue, an entire embryo, or sections of them. The detection of the labelled probe allows for the visualization of the spatial distribution of the target RNA within the specimen (as for example shown for *Oct4* and *Cdx2* in Fig. 1C). Next to other methods, such as immunohistochemistry, *in situ* hybridization remains the gold standard for the investigation of differential gene expression and the identification of developmental regulators. The technical improvement of its protocols allowed for large-scale performance on mouse embryos (Shimizu *et al.*, 2009). This has led to the establishment of online-databases, such as MAMEP and others (Geffers *et al.*, 2012), to manage the high number of embryonic expression patterns.

Though the knowledge of the spatiotemporal distribution of a certain gene product can provide information about the developmental processes it is required for, other methods are needed to reveal its molecular function. In the mouse, such a functional analysis is usually done by gene targeting. This means the specific introduction of genetic modifications into a specific site of the genome (reviewed in Capecchi, 2005). Gene targeting is mediated by homologous recombination (Folger *et al.*, 1982) and can be done directly in mammalian cell lines (Thomas *et al.*, 1986; Thomas and Capecchi, 1987). That way it is possible to generate, for example, loss- and gain-of-function al-

leles. The impact of the introduced modification can further be restricted to certain tissues and developmental periods using recombinases and their specificity for certain recombination sites, or by using inducible systems (reviewed in van der Weyden *et al.*, 2011). The efficiency of the homologous recombination is very variable, mainly depending on the genomic locus supposed to be targeted. An alternative to bypass the targeting of lowly accessible loci is the recombinase-mediated cassette exchange (RMCE). This technique allows for the introduction of a transgene into the landing site provided by an already targeted locus. RCME can be used either to express genes, or to generate hypomorphic mutants via the RNA-interference machinery, as described in Vidigal *et al.* (2010).

Taken together, in the mouse there is a broad tool box to characterize and functionally analyse differentially expressed genes during embryonic development and later on.

1.4 Somitogenesis and the Segmentation clock

Depending on the tissue, the described changes in gene expression induced by the signalling pathways can occur in reiterating patterns at regular intervals. This is the case for somitogenesis. This process generates the metameric body pattern of vertebrates as is overt by examining the segmental arrangement of ribs, vertebrae, and spinal nerves.

Somitogenesis takes place in the paraxial mesoderm, which flanks the neural tube along the anteroposterior axis (Fig. 3A). In the head region, it forms together with the prechordal mesoderm the head mesenchyme, that will give rise to musculature and connective tissues of the head (Evans and Noden, 2006). In the trunk, the paraxial mesoderm is composed of an unsegmented portion called the presomitic mesoderm (PSM), and segmented epithelial block of cells called somites (Fig. 3B). The somites bud off pairwise from the anterior tip of the PSM with bilateral symmetry to the neural tube (Fig. 3C). The process proceeds in an anteroposterior fashion, whereby the most recently formed somite is always located directly anterior to the PSM. This offers a nomenclature system commonly used in the field of somitogenesis, in which the currently forming somite is labelled S0. The seperated somites anterior to it get positive numerals, starting with SI, and the predetermined somites posterior to it receive negative numerals (see yellow labels in Fig. 3C). From these cellular blocks develops the axial skeleton, the musculature of the trunk, and the dermis of the back (Christ and Ordahl, 1995). The differentiation of the somites into these tissues occurs in graded fashion, being more advanced the more anteriorly the somite is positioned.
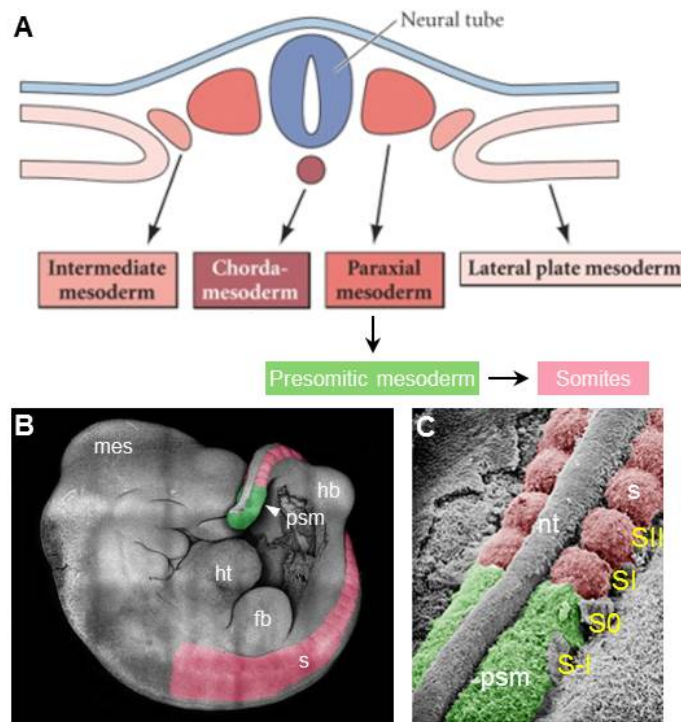
Figure 3. Mesoderm determination
A: Schematic representation of a transversal section of an amniote embryo, indicating the different mesodermal lineages. B: Laser scanning micrograph of a carmine red stained E10.5 mouse embryo. C: Scanning electron micrograph of the paraxial mesoderm and neural tube of a chicken embryo after removal of surface ectoderm. S-I - SII illustrates the nomenclature with respect to the currently forming somite S0. The presomitic mesoderm and the somites are highlighted in green and red respectively. fb, forelimb bud; hb, hindlimb bud; ht, heart; mes, mesencephalon; nt, neural tube; psm, presomitic mesoderm; s, somite. A and C modified after Gilbert (2014).

The intervals of somite formation and the number of pairs ultimately formed are specific for each species. In the mouse, a new pair forms about every 120 min between E7.75 and E12.25, leading finally to approximately 65 somite pairs (Tam, 1981). In chicken, somites form every 90 min, resulting in 50 pairs in total when somitogenesis has ceased (Palmeirim *et al.*, 1997). In the zebrafish, somites are formed even faster, with one pair every 30 min at 37°C, leading to a final count of 28-30 pairs (Holley *et al.*, 2000). In corn snakes a total of 315 somite pairs is formed, with one pair budding off from the PSM every 100 min, and the total number of generated somites can reach up to more than 500 pairs in several other snake species (Gomez *et al.*, 2008). To achieve such high numbers, two processes must be coordinated during somitogenesis. First, axial elongation must provide new cells derived from the primitive streak, and later the tail bud. Second, a subpopulation of these cells must become committed to the paraxial mesodermal lineage and added to the PSM posteriorly (reviewed in Dubrulle and Pourquié, 2004b). At its anterior end, the PSM is used up by the segmentation

process. The periodicity of this process is the key determinant of how many somite pairs can ultimately be generated from the PSM. The orchestration of these processes and an adoption of somitogenesis to individual body sizes requires complex molecular regulation. The PSM cells must be provided with spatial information about their current positioning within the anterior-posterior axis. Given that this axis elongates by adding new cells posteriorly, this alone is not sufficient for the periodic formation of regularly sized somites. The cell also require some kind of temporal information. A possible mechanism to achieve such a spatiotemporal control was already hypothesized by Cooke and Zeeman (1976), where a gradient or wavefront provides the spatial control, while a molecular oscillator provides the cells with the required temporal information.

1.4.1 Morphogen gradients provide the spatial information

Molecular analyses demonstrated the existence of posterior-to-anterior morphogen gradients of Fgf8 and Wnt3a, and an opposing gradient of RA (Dubrulle *et al.*, 2001; Aulehla *et al.*, 2003; del Corral *et al.*, 2003; Moreno and Kintner, 2004). The production of Fgf and Wnt is restricted to the primitive streak, and later the tail bud region (Aulehla and Herrmann, 2004; Dubrulle and Pourquié, 2004a). The enzymes for the synthesis of RA, namely Raldh2, are present in the somites and the anterior PSM (Swindell *et al.*, 1999). These gradients are thought to define a threshold level, the so-called determination front, above which the PSM cells are kept in an immature state, and when they fall below the threshold they are able to differentiate into somites (reviewed in Dequéant and Pourquié, 2008). Experimental manipulations of the PSM in chicken confirmed the existence of the determination front and showed that rostrally to it, the prospective somites already become predetermined in the anterior portion of the PSM (Dubrulle *et al.*, 2001).

1.4.2 The segmentation clock ensures temporal control

Evidence for the existence of the predicted molecular oscillator, the segmentation clock, was initially provided by Palmeirim *et al.* (1997). They identified *Hairy and enhancer of split 1* (*Hes1*) to be cyclically expressed in the PSM, thereby oscillating in-phase with morphological somite formation. Since then, a number of additional "cycling genes" have been discovered in various species, including the mouse. These exclusively belong to either the Notch-Dll (Palmeirim *et al.*, 1997), the FGF-MAPK (Dequéant *et al.*, 2006) or the canonical Wnt signalling pathways (Aulehla *et al.*, 2003). In principal, these oscillations are thought to be based on negative feedback loops within the signalling cascades (Palmeirim *et al.*, 1997). Activation of Notch signalling,

for example, leads to transcription of *Lunatic frindge* (*Lfng*, Forsberg *et al.*, 1998; McGrew *et al.*, 1998; Aulehla and Johnson, 1999; Morales *et al.*, 2002), an inhibitor of the Notch receptor (Dale *et al.*, 2003, see Fig. 4A).

Upon production of the LFNG protein, the Notch signalling cascade becomes inactivated. This also abolishes further *Lfng* expression and, after degradation of its protein and mRNA, releases the block on the Notch signalling cascade. A prerequisite for negative feedback regulators to achieve oscillations during somitogenesis are relatively short half-lives of their mRNA and protein (Ay *et al.*, 2013). Target genes of Wnt pathway oscillate out-of-phase with Notch target genes (Aulehla *et al.*, 2003), while Notch and Fgf signalling are synchronized by the *Hairy and enhacer of split 7* (*Hes7*) gene (Niwa *et al.*, 2007, reviewed in (Harima and Kageyama, 2013)). Notch signalling has another important function during somitogenesis, namely the synchronization of the segmentation clock between neighbouring PSM cells (Soza-Ried *et al.*, 2014). The synchronized, oscillating signalling activities finally lead to the wave-like propagation of the expression of their target genes, as is exemplified for *Lfng* in Fig. 4B. Both Fgf and Wnt participate at the level of the gradients, providing the spatial information, and the segmentation clock, thereby linking the processes under their control (Aulehla and Herrmann, 2004). This linkage is used as a basis for molecular models of somitogenesis as reviewed in Hubaud and Pourquié (2014).

1.5 *Fam181b* is a candidate gene identified from cycling screens

The study provided by Dequéant *et al.* (2006) was the first systematic approach to identify novel cyclic genes on a large scale. In this study, PSM samples were dissected and individually used for RNA extraction and expression profiling (Fig. 5A). The remaining portion of the embryo was subjected to whole-mount *in situ* hybridization for *Lfng*. This allowed a temporal alignment of the embryo samples to reconstitute one oscillation cycle of the gene using 17 time points. This alignment, in turn, allowed for the alignment of the corresponding expression profiles. Therein (Fig. 5B), and within a similar screen performed in our lab (Fig. 5C; P. Grote, L. Wittler, M. Werber, and B.G. Herrmann, unpublished data), the thus far uncharacterised gene *Fam181b* (synonym A830059I20Rik) was identified as an oscillating transcript with a possible function during segmentation. Both screens correctly displayed the expected anti-phase oscillations of Wnt and Notch/Fgf target genes. Interestingly, the cyclic expression of *Fam181b* was assigned to different phases, the Wnt phase in Dequéant *et al.* (2006) and the Notch/Fgf phase in our screen (compare *Fam181b* in respect to Notch/Fgf or
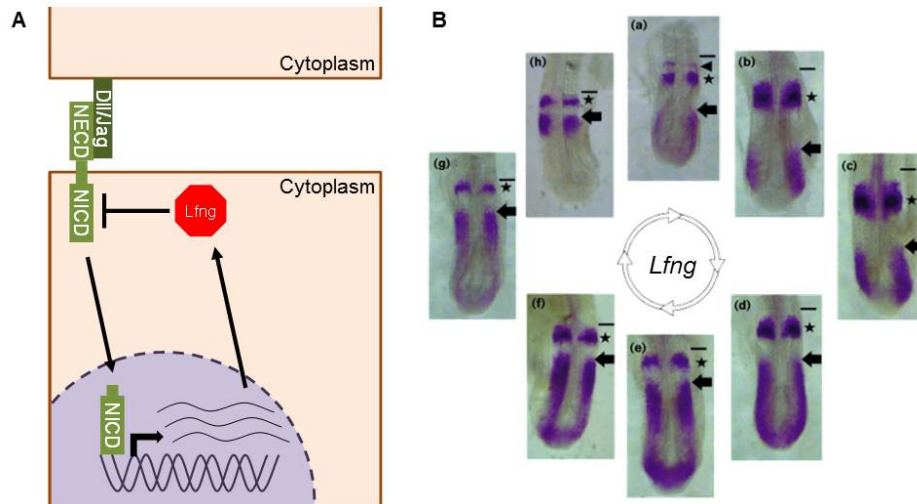
Figure 4. Oscillations of Notch signalling activity and its target gene _Lfng_
A: Schematic representation of the Notch signalling pathway. Upon activation of Notch signalling, the Notch intracellular domain (NICD) translocates to the nucleus and activates target gene transcription. Among these target genes are negative feedback regulators of the upstream signalling cascade, such as _Lfng_, enabling the regulation of the cyclic activity of the Notch pathway. B: WISH for _Lfng_ on mouse caudal ends (adopted from Forsberg _et al._ (1998)). Due to the established oscillations in Notch signalling activity and the synchronization of neighbouring PSM cells that it provides, its target genes display a reiterative wave-like propagation along the PSM.

Wnt targets between Fig. 5B and C).

1.6 The _Fam181_ gene family

Fam181b belongs to the _Fam181_ gene family, with its two family members, _Fam181a_ and _Fam181b_. _Fam181a_ (synonym EG544888) is located on mouse chromosome 12 and encodes a protein of 292 amino acid residues (~32kDa). Its paralogue, the intron-less _Fam181b_ gene is located on mouse chromosome 7 and is predicted to encode a protein with a length of 417 amino acids (~42kDa). Both genes are thus far uncharacterized, which formed the basis for the current work.

The work I describe in this thesis is aimed at characterizing _Fam181a_ and _Fam181b_. This comprises an initial expression analysis, followed by investigation into the function of the _Fam181_ gene family during murine development and in adult mice. _Fam181b_ was predicted to display cyclic expression in the PSM and was thus the main focus of my thesis.
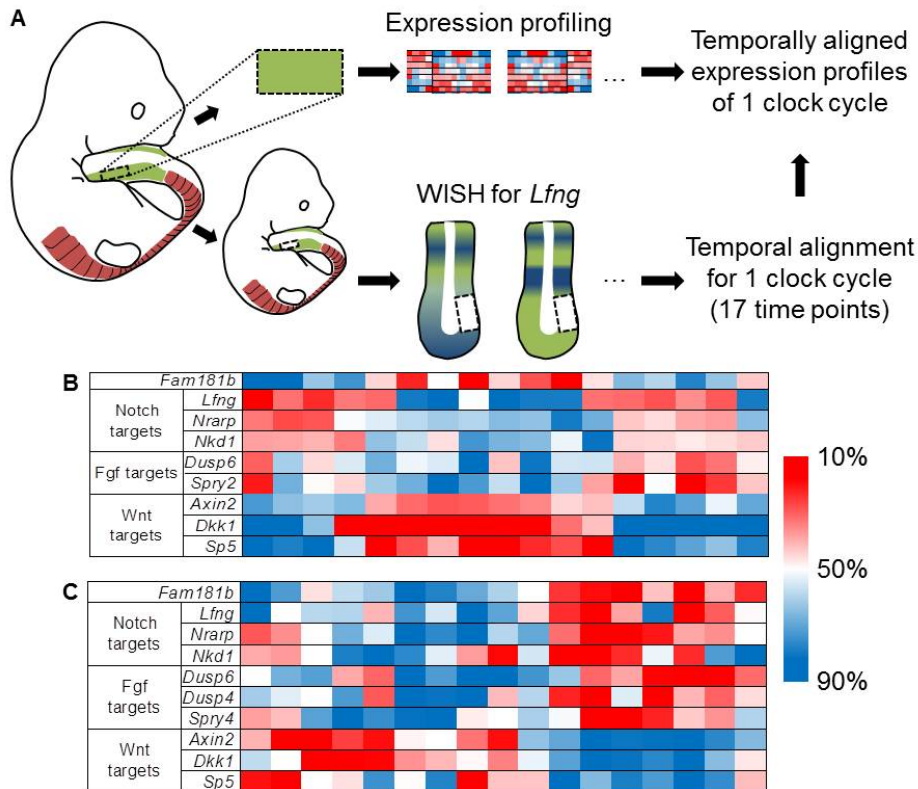
Figure 5. A screen for genes with cyclic PSM expression identifies *Fam181b*
A: Schematic representation of the workflow for the screen for oscillating PSM expression performed by Dequéant *et al.* (2006). A sample of the PSM is isolated and used for microarray-based expression profiling. The remaining embryo is subjected to whole-mount *in situ* hybridization (WISH) for the known cycling gene *Lfng*. This allows the temporal alignment of the embryo samples and their corresponding PSM expression profiles to reconstitute one cycle of the segmentation clock. The *Lfng* cycle was subdivided into 17 time points. B: 3-Colour-based quantile scaling of data selected from Dequéant *et al.* (2006). Next to *Fam181b*, known cycling target genes for Notch, Fgf and Wnt signalling were selected. All values are presented with respect to the arithmetic mean (set to 50%) of the corresponding gene. C: 3-Colour-based quantile scaling of data from a comparable screen performed in our lab (P. Grote, L. Wittler, M. Werber, and B.G. Herrmann, unpublished data).

2 Results

2.1 Analysis of *Fam181b*

In order to investigate *Fam181b* transcription in murine embryos, *in situ* hybridizations using a Digoxigenin-labled antisense RNA-probe were performed. This probe covered nucleotides 882-1813 of the transcript (NCBI: NM_021427.2), containing parts of the open reading frame (ORF) and the 3' untranslated region (UTR). Whole-mount *in situ* hybridizations were used for embryos up to embryonic day (E) 12.5 and selected samples vibratome-sectioned for a more detailed analysis. For E14.5 specimens, the embryos were embedded in paraffin and sectioned, following which *in situ* hybridization was done directly on the slides. To analyse *Fam181b* transcription in adult mice, real-time quantitative PCR (qPCR) and semi-quantitative PCR (RT-PCR) were done on various selected organs. Lacking a specific antibody for FAM181B, tagged versions were used for analysis of the FAM181B protein.

2.1.1 Expression of murine *Fam181b* on the mRNA level

Characterization of *Fam181b* presomitic mesoderm oscillations

Fam181b transcription was predicted to oscillate during mouse somitogenesis by two independent screens (Dequéant *et al.*, 2006 and Wittler, L., Grote P., Werber, M., and Herrmann,B.G., unpublished data). In the first screen, Dequéant and colleagues used isolated presomitic mesoderm (PSM) tissue, thereby guaranteeing the tissue-specific expression of the investigated genes. The antisense RNA probe generated in this thesis allowed visual detection of *Fam181b* mRNA in the PSM of E9.5 mouse embryos (Fig. 6A-A"), confirming this specificity. The anteroposterior expansion of this PSM expression domain varied between different specimens (compare brackets between Fig. 6A, A',A") . Given that different embryos are not phase-matched with respect to their segmentation clock cycle, these observed variations could reflect a response of *Fam181b* to the clock.

Since the discovery of the first cyclic gene, a standard experiment of proof for a periodic PSM expression of a gene which oscillates in synchrony with morphological
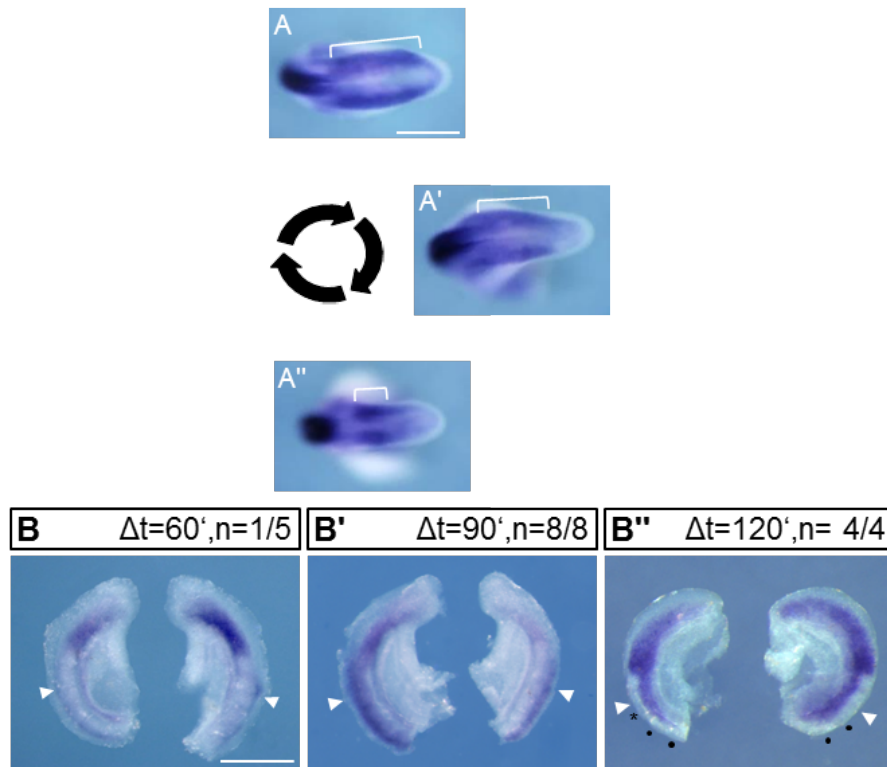
Figure 6. Oscillating *Fam181b* PSM expression
A-A": *Fam181b* expression in individual E9.5 mouse caudal ends. Brackets indicate differences
in the extension PSM expression domain. B-B": E9.5 caudal end half culture. The cultivated
half shows changes in *Fam181b* expression compared to fixed (t=0) half. Cultivation time
with respect to the fixed half (Δt) and number of samples with changes in expression (n)
are indicated. After 120 min of cultivation, a new somite has formed (asterisk in B"). White
arrowheads in B-B" mark anterior S0 somite boundary. Scale bar = 0.5mm.

somite formation and the segmentation clock is the caudal end half culture (Palmeirim
et al., 1997). Thereby, the caudal end is separated along the midline, thus producing
two halves phase-matched with respect to the segmentation clock.

Here, for this purpose, caudal ends of E9.5 mouse embryos were used. With one
half fixed and the other one incubated for a defined amount of time, the oscillatory
behaviour of a gene can be visualized by *in situ* hybridization. For *Fam181b* following
an incubation of 60 min, differences in the PSM expression of both halves were detected
in one out of five samples (Fig. 6B). After 90 min, the mRNA expression pattern
differed in all investigated sample pairs (Fig. 6B', n=8). In the mouse, somite formation
proceeds within a period of 120 min. An incubation for that amount of time resulted
in an additional somite in the cultured explant, while the PSM expression of *Fam181b*
was similar to those of their counterparts in all investigated samples (Fig. 6B", n=4).
This demonstrates that *Fam181b* expression in the PSM is indeed oscillating in-phase
with the segmentation clock.
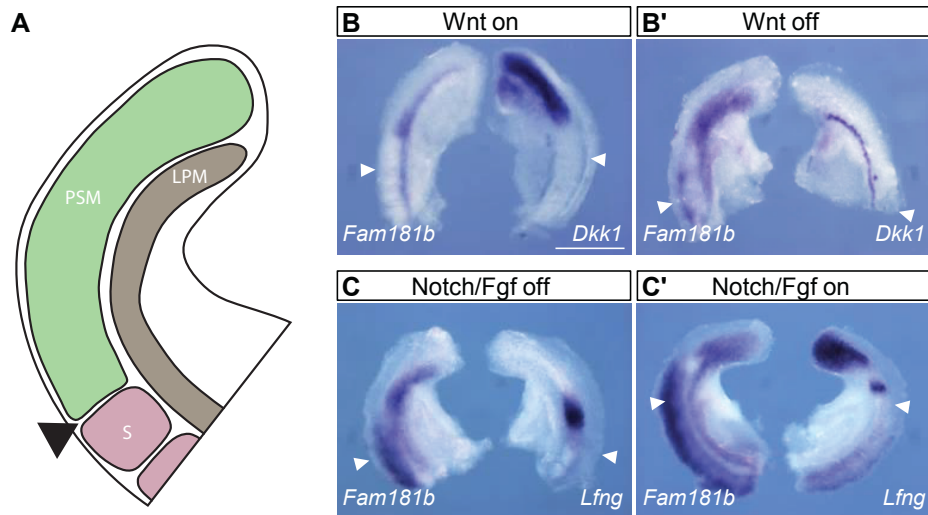
Figure 7. Corresponding signalling pathways for *Fam181b* oscillations
A: Schematic representation of a caudal end (lateral view). LPM, lateral plate mesoderm; PSM, PSM; S, somite. B/B': Comparison of *Fam181b* and *Dkk1* expression in individual E9.5 caudal end half pairs. C/C': Comparison of *Fam181b* and *Lfng* expression in individual E9.5 caudal end half pairs. (White arrowheads in A-B' mark anterior S0 somite boundary). Scale bar = 0.5mm.

While both screens predicted an oscillatory behaviour for *Fam181b* mRNA, their predictions regarding the corresponding signalling phase of the segmentation clock were contradictory. In the results of Dequéant *et al.* (2006), *Fam181b* oscillates in-phase with Wnt-targets and the cycling is in synchrony with Notch targets in the other screen (Wittler, L., Grote P., Werber, M., and Herrmann,B.G., unpublished data). To address which of these screens was correct in determining the phase for *Fam181b*, temporally identical caudal end halves were subjected to *in situ* hybridization with probes for *Fam181b* along with other characterized cyclically expressed genes. Probes for either the Wnt target gene *Dickkopf 1* (*Dkk1*; Niida *et al.*, 2004; Dequéant *et al.*, 2006), or the Notch target gene *Lunatic fringe* (*Lfng*; Forsberg *et al.*, 1998; McGrew *et al.*, 1998; Aulehla and Johnson, 1999; Morales *et al.*, 2002) (Fig. 7) were used. When Wnt signalling was activated as indicated by *Dkk1* expression in the entire posterior PSM, *Fam181b* mRNA was found to be restricted to a small stripe at the level of the prospective somite S-II, close to the determination front (Fig. 7A). During the phase of Wnt signalling inhibition, the *Fam181b* expression domain was largely extended in the PSM, while *Dkk1* transcripts were detectable in the intermediate mesoderm only (Fig. 7A'). When compared to the *Lfng* PSM expression, *Fam181b* mRNA showed a similar distribution intensity. Upon inactivation of Notch and FGF signalling in the posterior PSM, *Lfng* was expressed as a stripe at the level of the prospective somite S-I. In that phase, *Fam181b* transcription was detectable in the anterior PSM at the

S-II prospective somite level (Fig. 7B). During the contrary phase, *Lfng* was expressed in the caudal end including the posterior PSM (and additionally a narrow stripe in the anterior half of the S0 somite), the *Fam181b* transcriptional domain was also extended, ranging through the posterior 2/3 of the PSM (Fig. 7B'). Taken together, the observed oscillatory behaviour of *Fam181b* PSM expression demonstrates its oscillation in-phase with the Notch target *Lfng* and out-of-phase with the canonical Wnt target gene *Dkk1*. Note that Fam181b expression in the caudal end can also be detected in the lateral plate mesoderm (LPM) ventrally of the PSM (Fig. 7A).

Fam181b expression during murine embryonic development

During the analysis of *Fam181b* mRNA oscillations in E9.5 mouse embryos, further expression domains were detected besides the PSM. To investigate this in more detail, WISH was performed on wild-type embryos ranging from E6.5 to E12.5 to generate a temporal overview of *Fam181b* expression during midgestational development. For a better resolution of developmental time, E6.5 to E7.5 embryos were further staged according to Downs and Davies (1993), and E8.5 to E12.5 embryos in accordance with Theiler (1989).

In E6.5 mouse embryos, the earliest stage investigated, *Fam181b* transcripts were undetectable (data not shown). They became detectable at E7.5, in the anterior region of allantoic bud-stage embryos (Fig. 8A/A'). This region corresponds to the anterior neural plate. During morphological demarcation of the headfold, the transcriptional domain narrowed down and became restricted to the prospective midbrain region (Fig. 8B/B'). At Theiler stage (TS) 12, in addition to the midbrain expression (white dashed

---

Figure 8 *(facing page)*. **Fam181b expression from E7.5-E12.5**
A-B': Expression of *Fam181b* in E7.5 mouse embryos. Staging (indicated in the top right corner) according to Downs and Davies (1993). (A/B) lateral view, (A'/B') view of anterior end, brackets mark emerging expression in neural plate (A) or head fold (B). C-H''': Expression of *Fam181b* in E8.5-E12.5 mouse embryos. Staging according to Theiler (1989). White dashed line indicates midbrain expression domain; black dashed line marks PSM expression. C-D'': Red arrowheads highlight a rhombomeric expression domain anterior to the otic vesicle. D: At E9.5 expression arises in the intermediate mesoderm, (white solid line). E-F': Black arrow heads mark striped expression domains in early limb anlagen; black star in E highlights expression in 1st branchial arch, white stars in F mark expression in spinal nerve precursors. F-G'': From E10.5 on, multiple, distinct expression domains in more advanced forelimb (red arrows) and hindlimb anlagen (black arrows) can be distinguished. H-H''': At E12.5 expression domains in the developing phalanges (black bars) and the whisker pads (red arrow) become detectable. White stars in H' mark expression in spinal nerve precursors. LB, late allantoic bud stage; a, anterior; p, posterior; l, left; r, right; EHF, early head fold stage; TS, Theiler stage; ht, heart tube; nt, neural tube; ov, otic vesicle; fb, forelimb bud; hb, hindlimb bud.
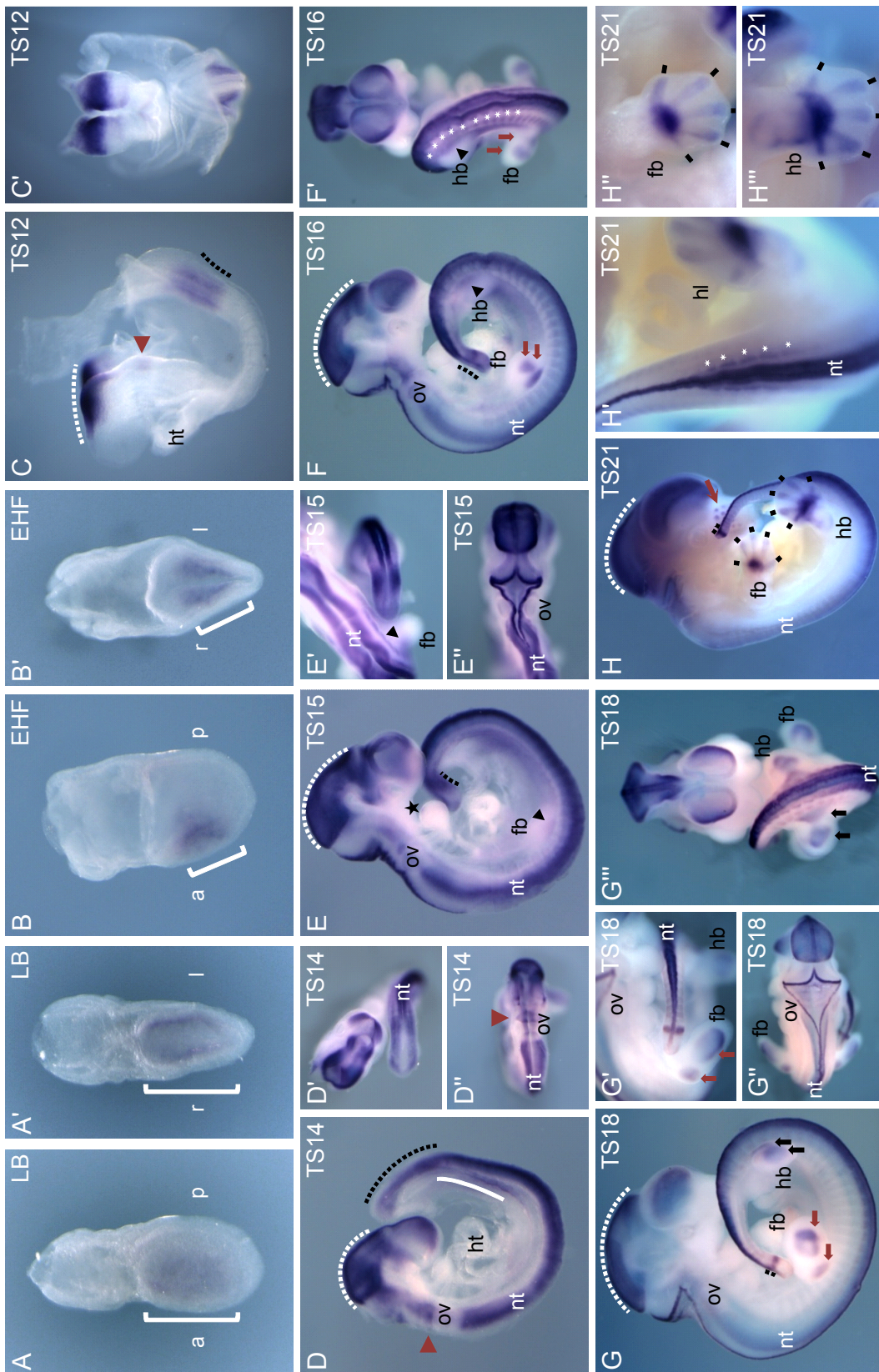
line), further *Fam181b* transcription domains arose, one in the PSM (black dashed line) and another in the rhombencephalon (red arrowhead) (Fig. 8C/C'). Both the PSM and the midbrain expression domain were detectable in all further stages investigated, while detection of the rhombencephalic signal was restricted between TS 12 to TS 14.

In embryos of TS14, additional signals for *Fam181b* mRNA were detected in the closed neural tube, the telencephalon and in the LPM (white solid line) (Fig. 8D-D"). The neural tube expression started posterior of the otic vesicle (ov) behind the rhomebencephalon and continued into the tail approximately at the level of the anterior-most PSM expression at the prospective somite S-II (Fig. 8D'/D"). The signal in the LPM was strongest around the level of the prospective forelimb bud (Fig. 8D). With the onset of morphological forelimb bud formation at TS15, this strong LPM expression emerged as a single domain in the medial portion of the bud (black arrowhead in Fig. 8E/E'), while at the level of the prospective hindlimb bud increased *Fam181b* mRNA levels were detected in the LPM (Fig. 8E). Neural tube staining for *Fam181b* in the roof plate was also observed, starting in the hindbrain and subsequently progressing posteriorly (Fig. 8E/E"-F). In contrast to the earlier appearing expression in the neural tube, which was absent from the rhombencephalic region around the otic vesicle, the roof plate expression was continuous throughout the entire hindbrain and continued without interruption into the trunk (compare Fig. 8D/E). A small domain of *Fam181b* transcriptional activity was also detectable in the anterior portion of the first branchial arch (black star in 8E) at this stage. At TS 16 the outgrowing forelimb bud showed a second, more distal *Fam181b* expression domain (Fig. 8F/F'). In parallel, with a single medial *Fam181b* mRNA signal, the emerging hindlimb bud began to recapitulate the expression pattern observed earlier within the forelimb bud (black arrowhead in Fig. 8F/F'). Along the dorsal side of the embryo, triangular-shaped protrusions from the roof plate expression domain (white stars in Fig. 8F') and a segmental expression in the dorsolateral portion of more advanced somites (Fig. 8F/F') were detected. The roof plate expression reached its maximum extension, ranging from the hindbrain towards the tip of the tail (Fig. 8F).

In TS 18 embryos, the distal expression domain in the forelimb bud was further extended. This was present as a distally positioned stripe and two weaker proximodistally expanded stripes (Fig. 8G/G'). The first seems to correspond to the position of wrist plate progenitors, while the latter likely corresponds to the progenitors of the ulna and radius. At this stage, the hindlimb bud also showed a second, more distal, and slightly proximodistally extended area of *Fam181b* transcription (Fig. 8G,G',G"'). The dorsolateral somitic expression and the *Fam181b* expressing domains emerging from the dorsal neural tube were still detectable along the posterior trunk at this stage

(Fig. 8G'''). Note that the signal detected in the roof plate was still clearly visible throughout the entire hindbrain and trunk into the tail (Fig. 8G-G"). After formation of hand and foot plate at TS 21, both forelimb and hindlimb anlagen exhibited signals in the forming digits (Fig. 8H,H",H"' black bars). While the staining in ulnar and radial regions of the forelimb were undetectable at this stage, the presumptive anlagen of tibia and fibula in the hindlimb showed expression (compare Fig. 8H" to H"'). Additional staining for *Fam181b* appeared in the whisker pads at this stage (red arrows in Fig. 8H). The detection of the roof plate expression became restricted to the posterior trunk region of the embryo (compare Fig. 8G-G" to Fig. 8H). A likely explanation for this observation is the progressive thickening of the epidermis at this stage, resulting in a more internalized positioning of the neural tube.
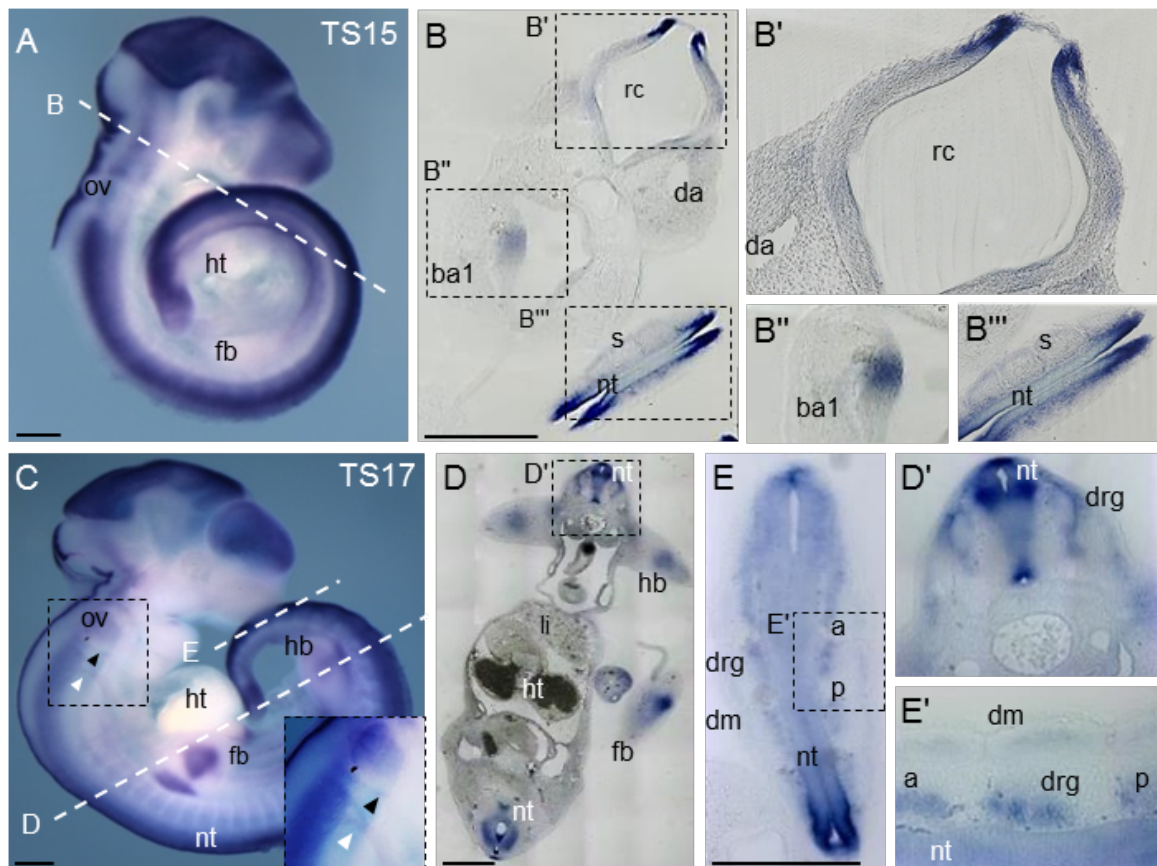
Figure 9. Detailed expression of *Fam181b*
A-E': Vibratome sections of TS15 (A-B"') and TS17 (C-E') mouse embryos. AC: Representative embryos are shown for each stage with indicated section planes (white dashed lines). Inset in C shows magnification of boxed region. Arrowheads in C highlight expression in glossopharyngeal (IX, black arrowhead) and vagus nerves (X, white arrowhead). B,D,E: Overview of sectioned region. B'-B"',D',E': Higher magnification of boxed regions in B,D,E. Scale bars = 0.5mm. a, anterior; ba1, 1st branchial arch; da, dorsal aorta; dm, dermomyotome; drg dorsal root ganglia; fb, forelimb bud; hb, hindlimb bud; ht, heart; li, liver anlagen; nt, neural tube; ov, otic vesicle; p, posterior; rc, rhombencephalon; s, somite; TS, Theiler stage.

To further examine the differential domains of *Fam181b* expression, selected WISH specimens were vibratome sectioned. This provided a better spatial mediolateral resolution of the more interior signals emerging along the trunk. At TS 15 a second neural tube expression domain emerged in the roof plate of the prospective hind brain region, while the earlier detectable neural tube signal was nearly undetectable in the rhombencephalic region (Fig. 9A-B"'). With its posterior progression, this roof plate staining became clearly demarcated from the earlier expression domain, which was restricted to the medial portion of the neural tube (Fig. 9D'). The vibratome sections also verified the small domain of *Fam181b* expression observed in the first branchial arch (Fig. 9B/B"). In sections of TS 17 embryos (Fig. 9C-E'), the expression domains protruding from the dorsal neural tube were identified as precursors of the peripheral nervous system, i.e. dorsal root ganglia and their projections (Fig. 9D'/E'). Besides the dorsal root ganglia expression of *Fam181b*, the TS17 specimen also showed signals in the cranial nerves, especially in glossopharyngeal (IX) and the vagus nerves (X)(Fig. 9C, black and white arrowheads respectively). The observed dorsolateral somitic signals corresponds to the dermomyotomal compartment of the differentiating somite (Fig. 9E/E').

Between E13.5 and E14.5 the mouse embryo develops its epidermis, which increases in thickness. This makes WISH analysis of the entire embryo difficult. Thus, to get more information about the *Fam181b* expression pattern at E14.5, fore- and hindlimbs were separated from the remaining embryo and used for WISH, followed by vibratome sectioning (Fig. 10A-F). This revealed that the expression detectable in the outgrowing digits of E12.5 limbs was now mainly localized to the cartilaginous regions between the phalanges, corresponding to the prospective joints (Fig. 10C-F). *Fam181b* expression in tibia and fibula, still present at TS21, was undetectable at this stage (compare Fig. 10E/F and 8H"'). To investigate domain of *Fam181b* transcriptional activity in internal structures of the E14.5 embryo, *in situ* hybridizations were performed on midsaggital

---

Figure 10 *(facing page)*. *Fam181b* expression at E14.5
A-F: Detailed expression of *Fam181b* in E14.5 limb anlagen. A-B: Representative E14.5 fore- (A) and hindlimbs (B) shown from dorsal and ventral sides. C-F: Longitudinal vibratome sections of fore- (C-D) and hindlimbs (E-F). G-G"": *In situ* hybridization for *Fam181b* on midsaggital paraffin sections of E14.5 wild-type embryos. G: Overview image. Black dashed line marks roof of neopallial cortex. Asterisks highlight cartilage primordia of turbinate bones. G'-G"": Higher magnification of boxed regions in G. Arrowheads in G"' mark follicle primordia of the vibrissa. Scale bars = 0.5mm. cp, choroid plexus; d, dorsal; drg dorsal root ganglia; fi, fibula; h, hyoid bone cartilage primordium; ht, heart; hu, humerus; igIX/sgIX, inferior/superior ganglion of glossopharyngeal nerve; lg, lung anlagen; li, liver anlagen; mb, lateral wall of midbrain; sm, submandibular gland; ti, tibia; tgV, trigeminal ganglion; ul, ulna; v, ventral; vcgVIII, vestibulocochlear ganglion.
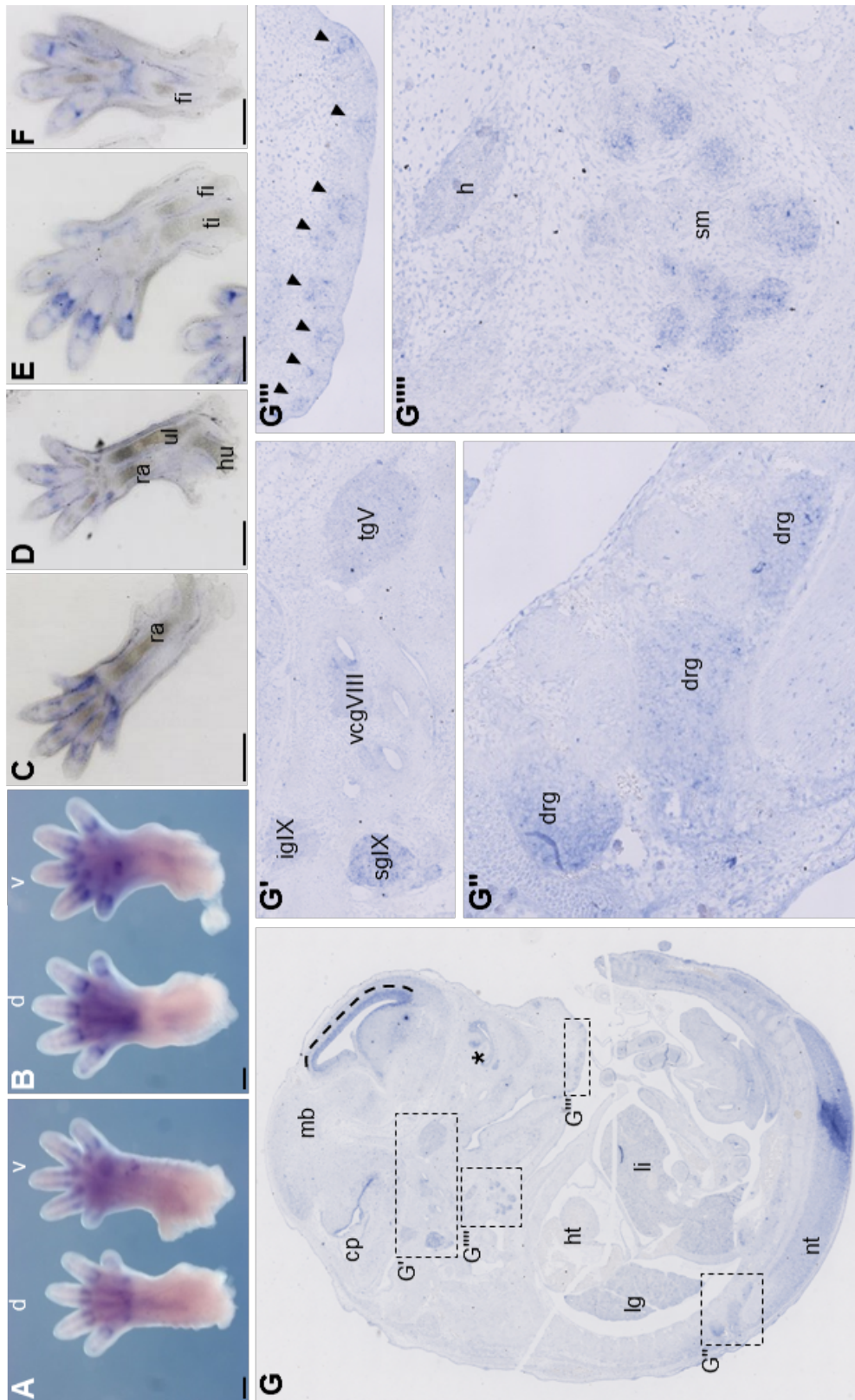
paraffin-sections (Fig. 10G-G""). These showed a strong signal within the inner surface of the forebrain, midbrain and the neural tube (Fig. 10G). They also confirmed expression in the dorsal root ganglia (Fig. 10G"), and revealed further expression in cranial nerves and associated ganglia, namely the trigeminal nerve (V) and the vestibulochochlear nerve (VIII), and confirmed the signal detected in glossopharyngeal nerve (IX)(Fig. 10G'). Other domains with *Fam181b* mRNA transcription were identified in the placodes of the vibrissal follicles (arrowheads in Fig. 10G"'), and the submandibular gland (Fig. 10G""), along with the cartilaginous primordia of the hyoid (Fig. 10G"") and the tubinate bones (asterisks in Fig. 10G).

Fam181b mRNA expression in mice with impaired Notch signalling

The analysis of cyclic *Fam181b* mRNA expression in the PSM revealed an oscillation in-phase with the Notch target gene *Lfng*. To investigate if Notch signalling activity has an impact on *Fam181b* transcription, WISHs were performed on loss-of-function mutants for the *Delta-like1* (*Dll1*) gene (*Dll1* $^{-/-}$) and their heterozygous and wild-type control littermates. Delta is a ligand for the Notch receptor, and *Dll1* one of its vertebrate homologues (Tax *et al.*, 1994; Bettenhausen and Gossler, 1995, reviewed in Nye and Kopan, 1995). In mice it is expressed in the paraxial mesoderm, especially in the PSM, and in the central nervous system, with a strong domain in the developing forebrain (Bettenhausen and Gossler, 1995; Bettenhausen *et al.*, 1995). The *Dll1* knock-out (KO) allele contains a β-galactosidase gene replacing the region coding for amino acids 2-116 of DLL1 (Hrabe de Angelis *et al.*, 1997). Homozygous mutants can be discriminated from their wild-type and heterozygous counterparts by defects in segmental patterning, which become overt from E8.5 onwards (Hrabe de Angelis *et al.*, 1997). In E9.5 and E10.5 wild-type and heterozygous control embryos, *Fam181b* expression was maintained as described above (compare Fig. 11A/C-C' to Fig. 8D-F'). In contrast, *Fam181b* transcripts were absent from the PSM and reduced in the forebrain of *Dll1* $^{-/-}$ embryos (Fig. 11B/D). While in the controls the mRNA signals from the ventrally protruding spinal nerves were regularly spaced along the trunk, in the homozygous mutants no discrete expression domains were detected (compare Fig. 11C' and D'). Instead *Fam181b* expression appeared as a uniform band ventrally expanding from the dorsal side of the neural tube. Taken together, this points to a regional dependency of *Fam181b* expression on Notch signalling, especially in the PSM and the telencephalon.
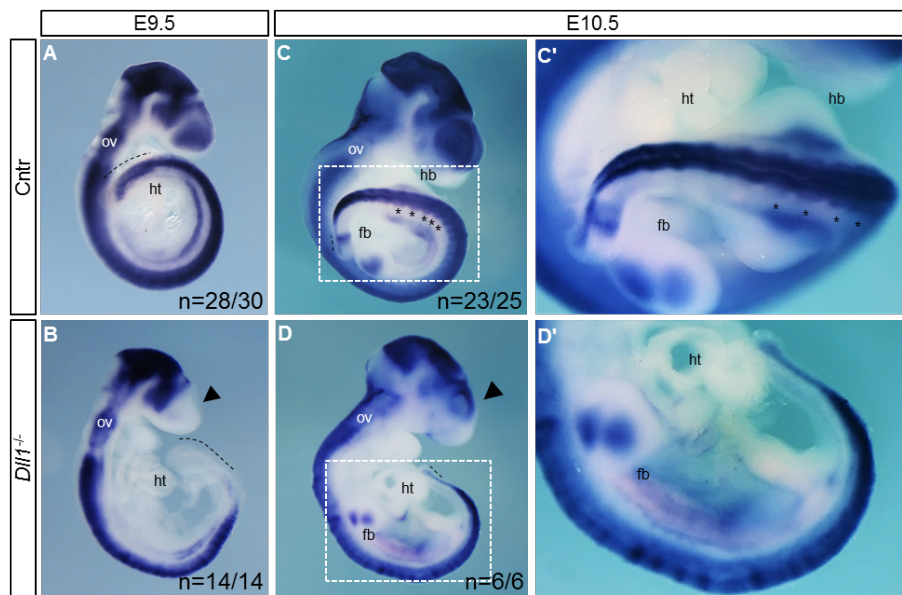
Figure 11. *Fam181b* expression in *Dll1* mutants
A-B: Representative E9.5 control (A; wt and het) and mutant (B) embryos. C-D: Representative E10.5 control (C) and mutant (D) embryos. C'-D': Magnification of boxed regions in C/D. Black arrowhead marks reduced telencephalic expression in *Dll1* $^{-/-}$; asterisks highlight the distinct expression domains in different spinal nerve precursors not distinguishable in the mutants, dashed black line in A-D marks PSM. Numbers of embryos with the observed expression out of the total number of analysed embryos are indicated in the bottom right corner. ht, heart; ov, otic vesicle; fb, forelimb bud.

Fam181b expression in various mouse strains

For investigation into the *Fam181b* expression pattern in Wnt pathway mutants, embryos mutant for *Dkk1* (Mukhopadhyay *et al.*, 2001) derived from *Dkk1*$^{+/-}$ intercrosses were genotyped and analysed by WISH for *Fam181b* expression. Most expression domains appeared unaltered between the littermates. Surprisingly, presomitic and lateral plate mesoderm expression of *Fam181b* was not detectable in any of the embryos investigated, irrespective of their genotype (Fig. 12A-A"). One major difference between the experiments described previously and the *Dkk1* mutant mouse line is their genetic background. For the description of the *Fam181b* expression pattern presented previously, only the CD1 and NMRI outbred strains were used, whereas the *Dkk1* embryos were the F1-offspring of 129s2 X C57BL/6J matings. Thus, to analyse if the genetic background used has an impact on embryonic *Fam181b* expression, wild-type embryos of the C57BL/6J and Sv129s2 inbred strains were dissected at E10.5/E11.0 and used for WISH analysis. As a control, CD1 embryos were used and all specimens were processed and stained in parallel, thus ruling out technical differences. Neither C57BL/6J (Fig. 12B-C') nor Sv129s2 embryos (Fig. 12D-E') showed *Fam181b* expression de-

tected in the PSM or the LPM. In the CD1 control embryos though, *Fam181b* mRNA was easily detected (see arrowhead and dashed line in Fig. 12F-F'). All other Fam181b expression domains identified and described above were maintained and no differences in the staining intensity was observed. This argues for a dependency of mesodermal *Fam181b* expression on the genetic background used.
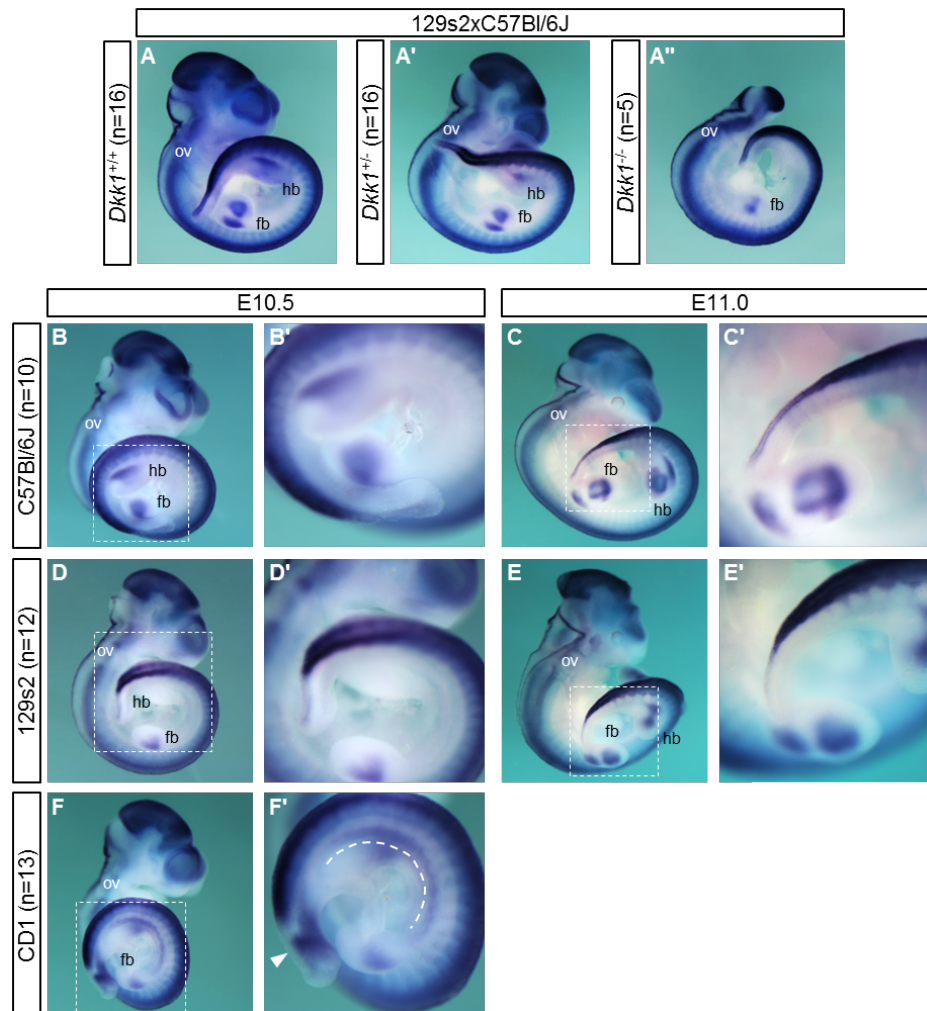
Figure 12. ***Fam181b*** **expression in** ***Dkk1*** **mutants and different mouse strains**
A-A"': Embryos derived from $Dkk1^{+/-}$ intercrosses were genotyped and analysed for *Fam181b* mRNA expression by WISH. B-F: C57BL/6J (B-C), 129s2 (D-E), and CD1 (F) wild-type embryos were analysed for the *Fam181b* expression pattern by WISH. B'-F': Magnification of boxed regions in B-F.White arrowhead in F' marks PSM expression, dashed line LPM expression. The number of embryos analysed are indicated. hb, hindlimb bud; ov, otic vesicle; fb, forelimb bud.

Fam181b expression in adult organs

To obtain information about *Fam181b* expression in adult mice, a 50 week-old female CD1 animal was sacrificed and tissue samples were taken from the lung, the heart, the

liver, the adrenals, the kidney, the spleen, the ovary, the cerebrum, and the cerebellum. These were then used for extraction of total RNA, followed by reverse-transcription into cDNA. The latter was used for quantitative real-time PCR (qPCR) (Fig. 13) and semi-quantitative RT-PCR (inset in Fig. 13). For qPCR, *Fam181b* levels were normalized to those of the *Phosphomannomutase2* (*Pmm2*) houskeeping gene, while for RT-PCR *Glyceraldehyde-3-phosphate dehydrogenase* (*Gapdh*) was used as a loading control.
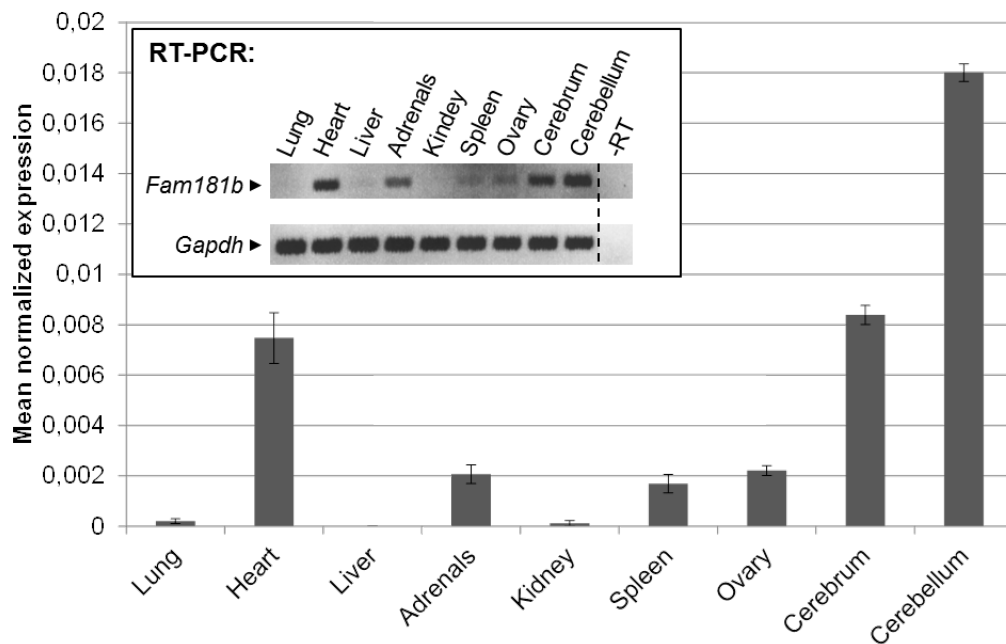
Figure 13. *Fam181b* expression in adults organs
Fam181b expression in organ samples of an adult female mouse (CD1). Total RNA was extracted from tissue samples of selected organs and reverse-transcribed into cDNA. A sample treated without reverse transcriptase was used as negative control. The cDNA was either used for RT-PCR (inset) with primers for *Gapdh* as loading control, or for quantitative real-time PCR (qPCR; graph), normalized to *Pmm2* and analysed by qGene. Dashed line in the inset indicates separation on the corresponding gel.

Both methods were congruent, and showed the presence of *Fam181b* transcripts in the brain, especially in the cerebellum, where the highest expression levels were measured with respect to all organs investigated. Strong *Fam181b* expression was also detected in the heart with transcript levels comparable to those of the cerebrum sample. In addition, *Fam181b* was present in the adrenals, the spleen, and the ovary. In these organs the transcript levels reached approximately 25% of heart and cerebrum expression, and about 12.5% of cerebellum expression, respectively. *Fam181b* transcription was nearly undetectable in the lung, the liver, and the kidney.

***Fam181b* expression during differentiation of ESCs into the neural lineage**

During embryonic development and in adults *Fam181b* transcripts were, to a large extent, associated with neural tissues. To test for a direct correlation between differentiation into neural lineages and induction of *Fam181b* expression, murine F1G4 ES cells (ESCs) were cultured according to the protocol established by Bibel *et al.* (2004). Using this cultivation procedure it is possible to differentiate the ES cells into a homogeneous population of neural progenitors, namely *paired box6* (*Pax6*)-expressing radial glial cells, which further develop into glutamatergic pyramidal neurons (Bibel *et al.*, 2004, 2007). During the time course, samples were taken and used for total RNA extraction. This was then used for cDNA synthesis, followed by qPCR to monitor changes in *Fam181b* and marker gene expression during the differentiation. *POU domain class5 transcription factor1* (*Pou5f1*/*Oct4*) was used as a stem cell pluripotency marker (Nichols *et al.*, 1998), and *Pax6* as a marker for the radial glia cells (Götz *et al.*, 1998; Heins *et al.*, 2002). To mark the terminally differentiated pyramidal neurons the *Neurotrophic tyrosine kinase receptor type2* (*Ntkr2*/*TrkB*) was used (Klein *et al.*, 1990; Bibel *et al.*, 2004).

The undifferentiated F1G4 ESCs served as reference sample and all other time points were set in relation to this sample. Between the ESCs and the neural progenitor cells (NP cells), samples were taken every 2 days (D2-D8) after formation of the cellular aggregates. According to the standard differentiation procedure, on D8, two hours after seeding the cells the NP cell sample was taken, and after 24h the Neuron sample was taken. During the differentiation, the stem cell marker *Oct4* steadily declined, while expression of *Pax6* reached its maximal levels between D6 and the NP cells, and rapidly dropped in terminal neurons. *TrkB* levels started to increase on D8 of differentiation and reached its maximum in the neuron sample. *Fam181b* expression was close to the detection limit of qPCR in ES cells, but continuously increased throughout the differentiation from D2 onwards. It reached its maximum in the NP cell sample, where an approximately 80-fold induction was seen relative to the ES cells. In the neuron sample *Fam181b* expression was slightly decreased. This demonstrates, that *Fam181b* expression is positively correlated with differentiation into the neural lineage of radial glia cells.

2.1.2 Expression of murine *Fam181b* on the protein level

Subcellular localization of FAM181B

For investigation into the subcellular localization of FAM181B, expression constructs for tagged versions of *Fam181b* were generated. Either the ORF or the entire transcript-
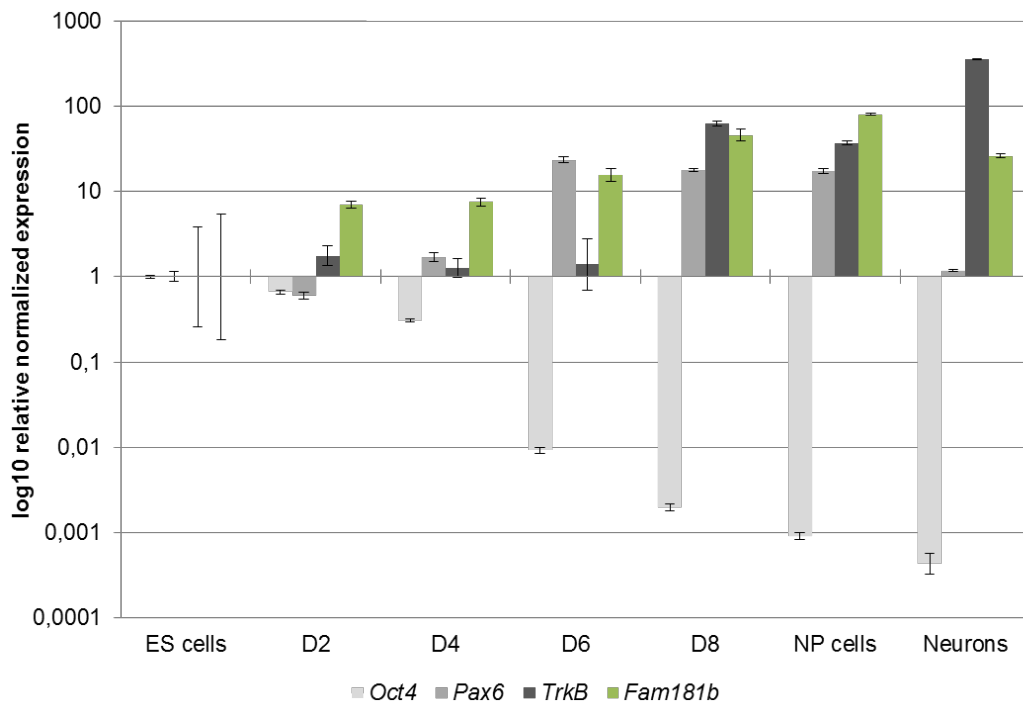
Figure 14. *Fam181b* **expression during differentiation of ESCs into the neural lineage**
Differentiation of murine F1G4 ES-cells into neural cells according to Bibel *et al.* (2007). During the differentiation procedure samples were taken (x-axis) and used for total RNA extraction and cDNA synthesis. *Fam181b* expression levels were analysed by qPCR. *Oct4* was used as a stem cell marker, *Pax6* as a marker for neural progenitors and *TrkB* for terminal neurons. Expression was normalized to *Pmm2*. The undifferentiated ES cells served as reference samples. The expression of *Fam181b* is maximally 80-fold upregulated in neural progenitor cells (NP cells).

coding region were amplified from a *Fam181b*-containing bacterial artificial chromosome (BAC) (*Fam181b* BAC, see 6.2.1), adding the V5-tag sequence either N- or C-terminally in frame to the ORF by Fusion-PCR. The PCR products were then inserted into the pcDNA3 expression vector and verified by sequencing. The plasmid allowed for ubiquitous expression under control of a Cytomegalo virus (CMV) promoter (Fig. 15A-B). The expression constructs were then used for transient transfection of NIH3T3 mouse fibroblast cells. To verify that the gene product detected by the αV5-antibody indeed corresponded to the FAM181B protein, cells were contransfected with microRNA (miRNA) expression constructs, encoding either a control-miRNA targeting no mammalian mRNA (Life Technologies) or a *Fam181b*-targeting miRNA (see 2.1.3 for more details). In whole cell lysates of the samples transfected according to the table in Fig. 15C, the V5-tagged protein was detected by immunoblot and quantified. LaminB1 was used as a loading control and for normalization (Fig. 15D-E). When miR-NAs targeting the *Fam181b* mRNA were co-transfected with the V5-tagged expression
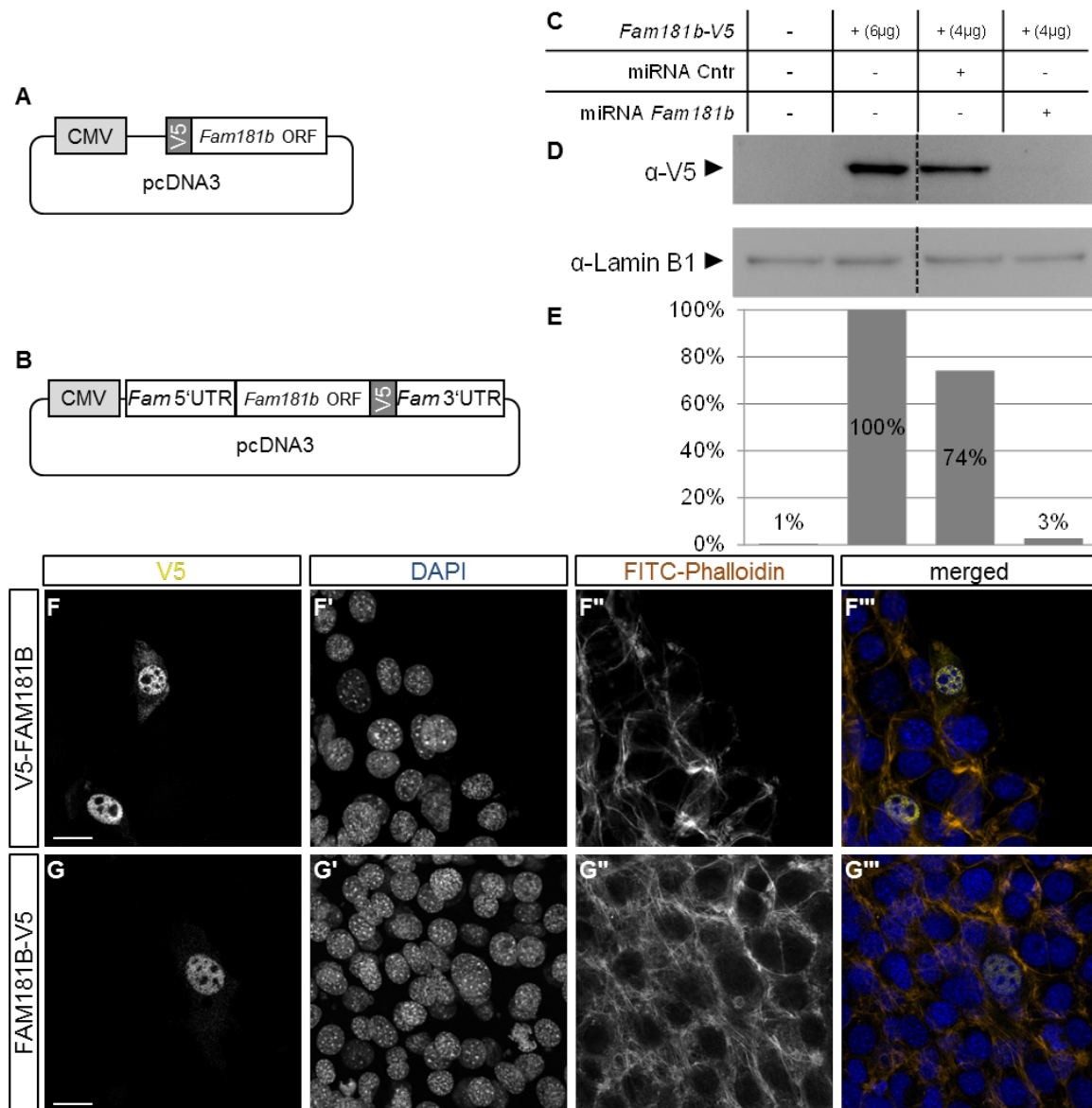
Figure 15. FAM181B subcellular localization
A-B: Schematic representation of either N-terminal (A) or C-terminal (B) V5-tagged *Fam181b* expression constructs. C: NIH3T3 cells were transiently-transfected with *Fam181b*-V5 (B), Contol-miRNA, or *Fam181* targeting-miRNA expression constructs as indicated. Total amount of transfected DNA was kept constant at 6µg. D: V5-immunoblot of whole cell lysate detected a protein of approximately 42kDa. Lamin B1 served as loading control. E: Densitometry of the V5-tagged protein detected in (B) normalized to Lamin B1. Co-transfection of a *Fam181b*-targeting miRNA expression construct reduced the amount of detectable V5-tagged protein. F-G"': NIH3T3 cells were transiently-transfected with the N-terminally (C-C"') or C-terminally (D-D"') V5-tagged *Fam181b* expression constructs. FAM181B was analysed by indirect immunofluorescence for V5. Counterstaining was performed with DAPI and FITC-Phalloidin, staining the nuclei and F-Actin respectively. Scale bar = 20µm.

construct (Fig. 15C-E, lane 4), the amount of protein detected by the αV5-antibody was decreased almost to the level of untreated cells (Fig. 15C-E, lane 1). In com-

parison, cells co-transfected with the control-miRNA allowed for detection of tagged protein in quantities correlating with the amount of *Fam181b* expression plasmid used for transfection (Fig. 15C-E, lane 3). This indicated, that the detected protein was indeed FAM181B. When the tagged FAM181B was analysed by indirect immunofluorescence, it was detectable in the nucleus of transfected cells, irrespective of whether it was tagged N- (Fig. 15F-F"') or C-termianlly (Fig. 15G-G"'). A similar localization was also observed when the murine myoblast C2C12 or the human HEK293 cell lines were used for transfection (data not shown). Also when a Green Fluorescent Protein (GFP)-tag was used instead of the V5-tag (either N- or C-terminally), localization in the nuclei of transfected cells was observed (Lars Wittler; unpublished data).

Knock-in of V5-tagged *Fam181b* into the endogenous *Fam181b* locus

The expression of the FAM181B protein under control of the CMV promoter and transiently-transfected into cell lines remains artificial. Thus, to be able to detect the endogenous protein without the laborious process of generating a specific antibody, a knock-in strategy was developed to introduce the V5-tag C-terminally to the ORF into the *Fam181b* gene. The transcript-encoding region and a 2.6kb 3' homology region were amplified from the *Fam181b* BAC and the V5 tag introduced by Fusion-PCR. Due to the construction design the 3' homology arm partially overlapped with the 3'UTR sequence, generating a 139bp repeat at its 5' end. Both DNA fragments were cloned into the PL451 vector (Liu *et al.*, 2003), the transcript-encoding region with the V5-tag sequence upstream, the 3' homology arm downstream of the neomycin selection cassette. The sequence for the region of interest was verified by sequencing and then linearised vector was used for targeting the *Fam181b* locus via homologous recombination in F1G4 ES cells (Thomas and Capecchi, 1987, see Fig. 16A). ES cell clones were selected with neomycin (G418) and correct integration in G418-resistant clones was verified by *Hind*III digest of genomic DNA (gDNA), followed by Southern blot analysis using a radioactively-labelled 5' external probe. The introduction of the additional sequence elements, mainly the FRT-flanked selection cassette, produced a restriction fragment length polymorphism resulting in a 10.6kb DNA-fragment in addition to the wild-type -allelic 8.5kb fragment (Fig. 16B, 5'probe). Out of 200 clones investigated, 1 ES cell clone showed the expected pattern.

It has been shown previously that the presence of a selection cassette can alter the expression of surrounding genes up to levels that can modify the phenotypic outcome of nearby targeted mutations (e.g. Takahashi *et al.*, 2007). To prevent such a disturbance for the V5 knock-in, the FRT-flanked nemoycin selection cassette was subsequently removed from the selected positive clone by transfecting a Flp-recombinase encoding
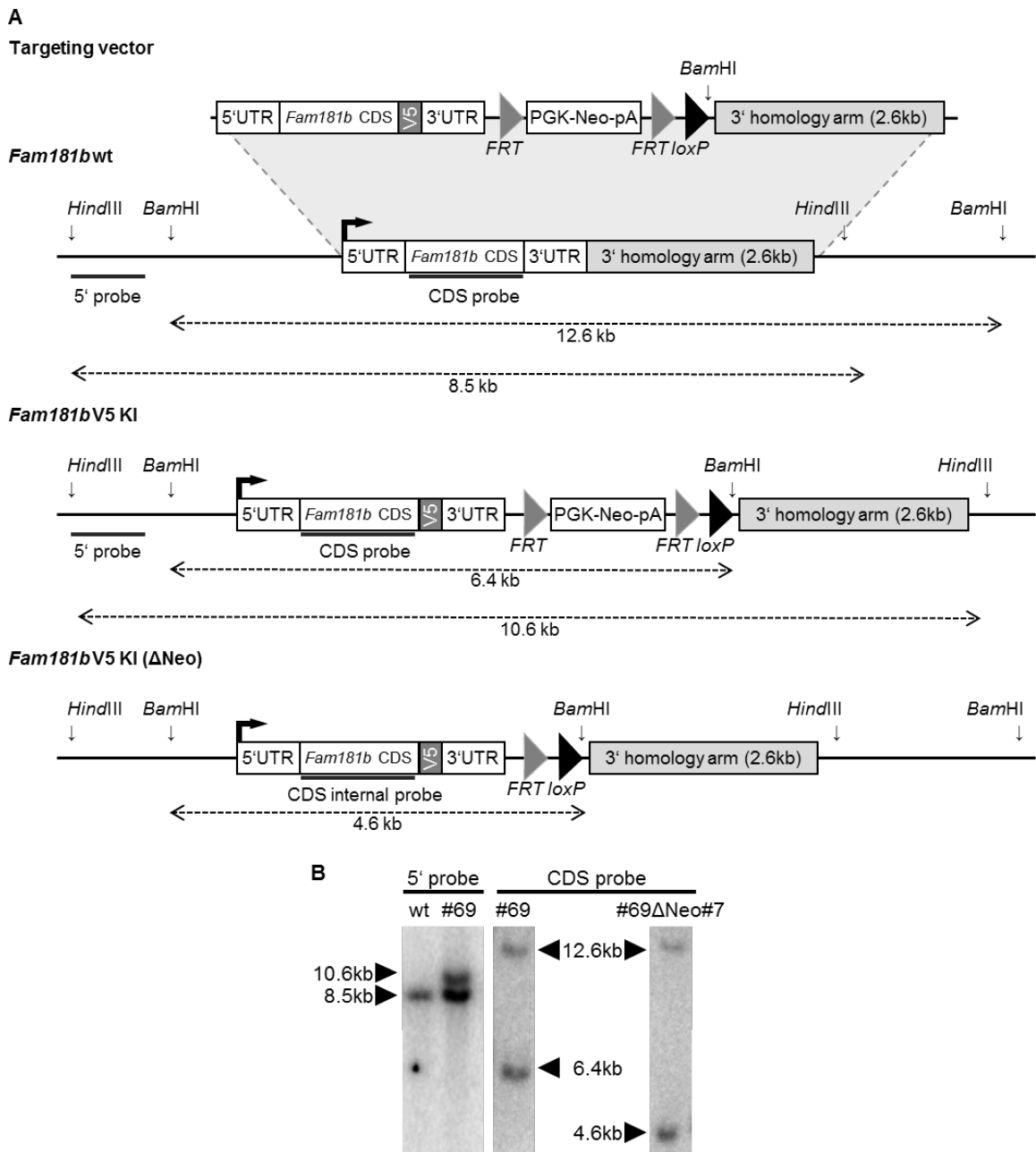
Figure 16. *Fam181b* V5 knock-in strategy
A: Schematic representation of the V5 knock-in into the *Fam181b* locus. F1G4 ES cells were targeted and selected for positive integration followed by removal of the neomycin selection cassette. B: Positive integration into F1G4 cells was verified by *Hind*III digest followed by Southern blot analysis using an external 5' probe (targeted band = 10.6kb). Subsequent removal of the selection cassette was checked by *Bam*HI digest and Southern blot analysis using an internal probe for the *Fam181b* coding sequence.

plasmid followed by negative selection (Fig. 16A). Genomic DNA of clones that lacked neomycin resistance was digested with *Bam*HI and analysed by Southern blot with a radioactively-labelled probe for the *Fam181b* coding sequence (Fig. 16B, CDS probe). The usage of this alternative probe and digest combination for the Southern blot was necessary because the targeted allele without the selection cassette yields a fragment of approximately the same size like the wild-type -allele when using *Hind*III digest and the 5' probe. In addition, the binding site for the 5' probe is located further upstream of the 5' *Bam*HI restriction site, preventing its usage with this digest.

The established ES cell line was then used to generate chimaeric embryos by diploid aggregation (Eakin and Hadjantonakis, 2006). Transgenic embryos together with wild-type embryos were dissected at E9.5, total protein extracted, and analysed by immunoblot (Fig. 17A). In the protein extract of transgenic, but not of wild-type embryos, a band of approximately 42 kDa was detected, corresponding to the calculated FAM181B-V5 protein size. This shows, that the predicted protein product encoded by the *Fam181b* gene is indeed expressed *in vivo*. In order to examine protein localization by immunofluorescence, the established V5 knock-in ES cells were differentiated *in vitro* into the neural lineage as described in 2.1.1. Again, besides *Fam181b* expression levels, *Oct4*, *Pax6*, and *TrkB* levels were assessed to verify that the differentiation procedure worked (Fig. 17B). Enrichment of *Fam181b* transcripts was observed in a comparable fashion to the experiments done on unmodified F1G4 ES cells (see 2.1.1). Highest expression levels were measured in the D8 and neuron samples. Due to limitations in the amount of cells, no NP cell sample was taken. The differentiated cells were subjected to indirect immunofluorescence with a αV5-antibody to detect FAM181B-V5 (Fig. 17D-D"'). In parallel, the differentiated unmodified F1G4 ES cells were used as negative control (Fig. 17C-C"'). The signals detected for the V5-tag were similar between the control and the *Fam181b-V5* expressing neurons, which most likely corresponds to background reactivity of the antibodies used (compare Fig. 17C and D). So although the FAM181B-V5 protein encoded by one of the two *Fam181b* alleles can be detected by immunoblot, it was not possible using immunofluorescence, as a result of the higher limit of detection for this type of analysis. In that respect, immunoblotting is the more sensitive method. This could point to either low quantities or a low stability of generated protein product, and would be in agreement with low amounts of *Fam181b* mRNA measured by qPCR.

2.1.3 Generation and analysis of *Fam181b* mutants

The expression pattern described in this thesis shows oscillation of *Fam181b* in-phase with the segmentation clock in the PSM and a strong association with developing
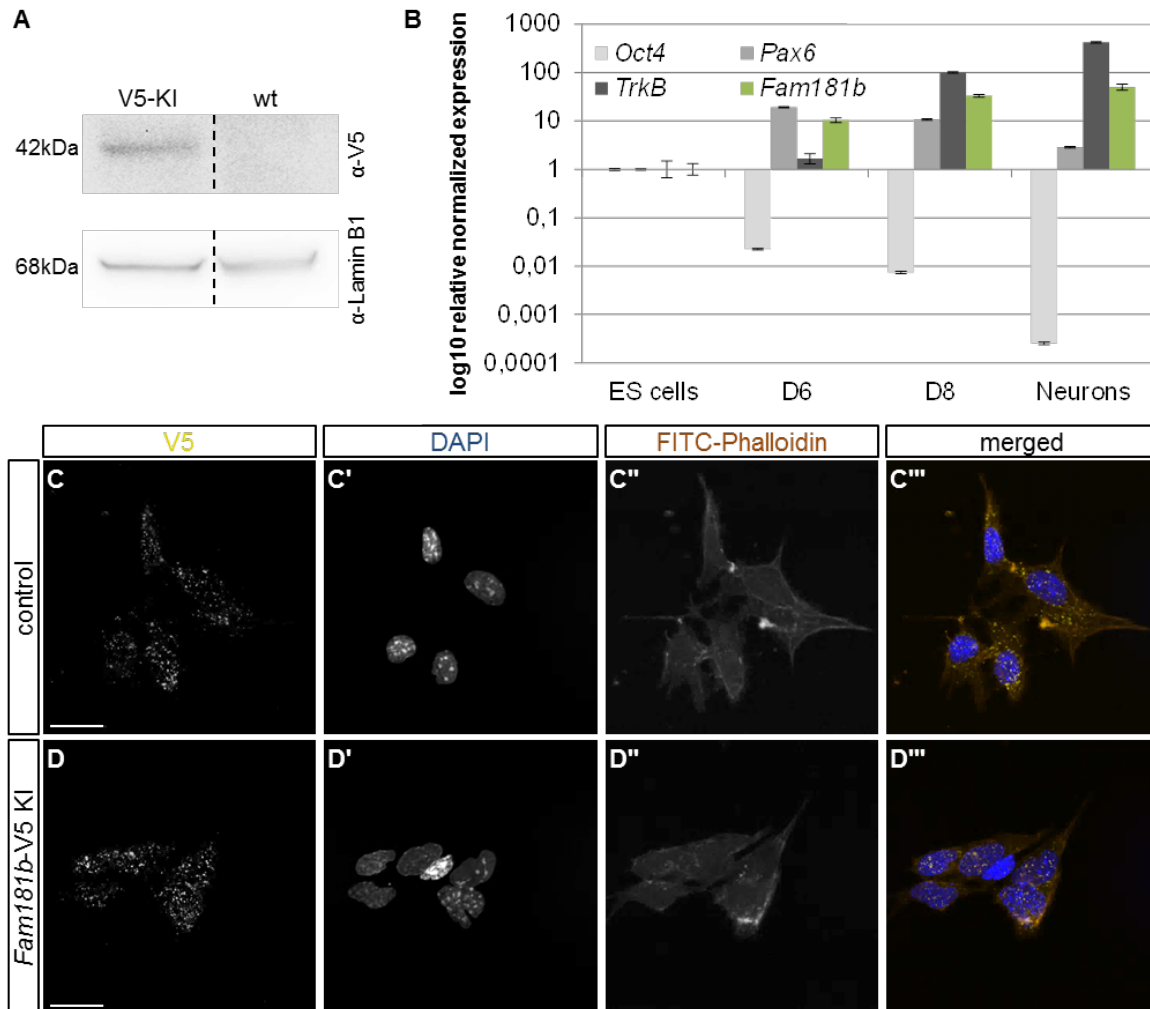
Figure 17. Analysis of V5-tagged endogenous FAM181B

A: Immunoblot from whole embryo lysate from *Fam181b*-V5 knock-in embryos generated by diploid aggregation (V5-KI) and wild-type embryos (wt) analysed for V5-tagged FAM181B expression. Laminin B1 served as loading control. B: *Fam181b*-V5 knock-in ES cells were differentiated into the neural lineage according to Bibel *et al.* (2007). On selected days, samples were taken and used for total RNA extraction and cDNA synthesis. *Fam181b* expression levels were analysed by quantitative real-time PCR. *Oct4* was used as a stem cell marker, *Pax6* as a marker for neural progenitors and *TrkB* for terminal neurons. C-D''': The terminally differentiated *Fam181b*-V5 knock-in cells (B) and F1G4 cells (differentiated in parallel as control) were analysed for FAM181B-V5 by indirect immunofluorescence for V5. Counterstaining was performed with DAPI and FITC-Phalloidin, staining the nuclei and F-Actin respectively. Scale bar = 20µm.

neural structures. This might point to an important function of *Fam181b* in these tissues. Thus, in order to functionally analyse its role during developmental processes in these tissues, gain- and loss-of-function mutants were generated and analysed for alterations in embryonic development and/or adulthood.

Fam181b gain-of-function mutants

To generate gain-of-function mutants for *Fam181b*, recombinase-mediated cassette exchange (RMCE) was used to integrate a transgene into a modified version of the *Gt(ROSA26)Sor* locus, which allowed for doxycycline (Dox)-inducible ubiquitous expression in embryos (Soriano, 1999; Vidigal *et al.*, 2010). For the generation the transgene, the *Fam181b* ORF was amplified by PCR and cloned into into a cassette exchange vector in-frame with an upstream tdTomato-T2A peptide coding sequence (Riemer *et al.*, 2014). After verification by sequencing, this plasmid was used for RMCE into ROSA26A F1G4 ES cells (Vidigal *et al.*, 2010, see Fig. 18A) thereby giving rise to the transgene *Tg(Fam OE)*. After neomycin selection, integration of the cassette in G418-resistant clones was verified by Southern blot analysis as described in Vidigal *et al.* (2010). The efficiency of the system was ≥85%, resulting in at least 7 positive clones out of 8 colonies picked. Correct clones were then tested *in vitro* by cultivation for 48h in either the absence or presence of doxycycline [2ng ml^{-1}]. Fluorescence of the tdTomato (Fig. 18B) and *Fam181b* transcript levels were assessed to verify functionality of the construct in the ES cells (Fig. 18C). The fluorescence signal was detectable in doxycycline-treated ES cells only. These cells showed a 50-fold increase in *Fam181b* expression as compared to control cells.

After confirming their functionality, the ES cells were used to generate embryos by diploid aggregation (Eakin and Hadjantonakis, 2006). These were dissected at E9.5 and checked for *Tg(Fam OE)* expression. The application of doxycycline to the drinking water of foster-mice from E2.5 onwards, resulted in tdTomato fluorescence in all embryos dissected from these mice (Fig. 19A'). Untreated control embryos remained non-fluorescent (Fig. 19A). While distribution of the tdTomato fluorescence marker appeared homogeneously at E9.5, differences in fluorescence intensity were visible in doxycycline-treated E10.5 embryos. The increase in *Fam181b* transcript levels (Fig. 19C, left bar) relative to untreated embryos and the ubiquitous distribution of *Fam181b* mRNA detected by WISH of doxycycline-treated embryos (compare Fig. 19D to D') further confirmed functionality of the *Fam181b* gain-of-function in the embryonic context. In addition, control embryos showed a similar *Fam181b* expression pattern as wild-type embryos of a comparable stage (compare Fig. 19D to Fig. 8D), which, in concert with the abscence of the tdTomato signal, confirmed the restriction of transgene
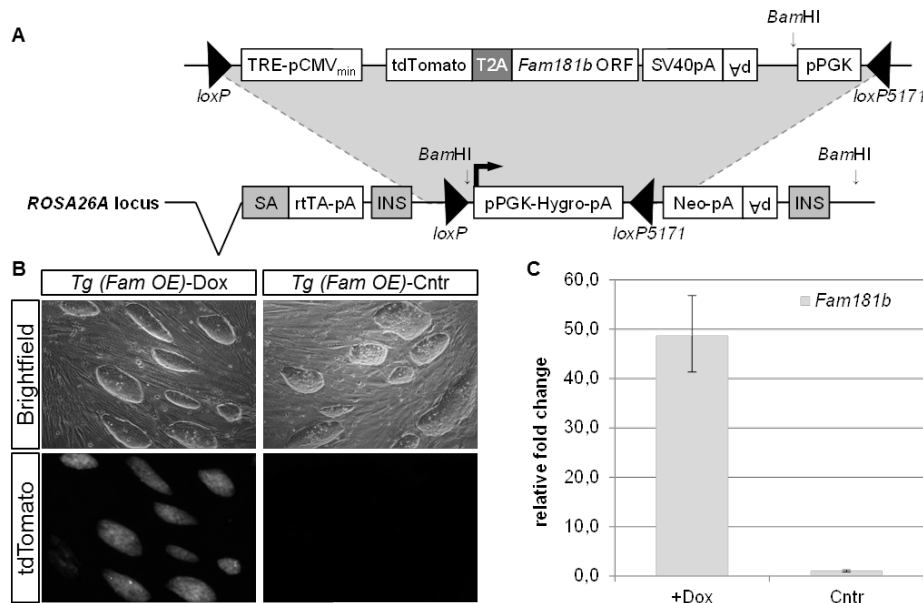
Figure 18. Generation of *Fam181b* gain-of-function ES cells
A: Schematic representation of the *Fam181b* gain-of-function construct. The cassette was integrated into ROSA26A (G4) ES cells and positive clones selected by Southern blot analysis as described in Vidigal *et al.* (2010). B-C: For testing of transgene activity, the generated ES cells were cultured either with or without doxycycline supplementation [2ng ml^{-1}] for 48h. Expression of the encoded tdTomato fluorescence marker was verified by live imaging (B). After imaging, total RNA was extracted from the cells, reverse-transcribed into cDNA, and was used for comparative quantification of *Fam181b* levels (C) normalized to *Pmm2*.

expression on induced embryos only.

For a phenotypic analysis of the *Fam181b* gain-of-function, embryos were generated by tetraploid aggregation (Eakin and Hadjantonakis, 2006). For activation of the transgene, foster mice were treated with doxycycline from E2.5 onwards. Embryos were dissected at E10.5, E12.5 and E17.5. In all stages investigated, *Tg(Fam OE)* expression was detectable in doxycycline-treated embryos only, as confirmed by tdTomato fluorescence (compare Fig. 19B and B' for E10.5, for other stages data not shown) and quantification of *Fam181* transcript levels (Fig. 19C right bars, for E17.5 data not assessed). An overall 8-fold increase of *Fam181b* expression was seen in induced embryos compared to controls. Independently of transgene induction, all stages analysed were properly developed and exhibited normal morphology (Fig. 20 A-B' for E10.5, C-C' for E17.5).

The *Fam181b* expression analysis revealed an association mainly with the developing neural system and cartilaginous precursors in the limb anlagen and craniofacial structures. To investigate if the gain-of-function resulted in alterations in nervous system development and patterning, *Sex determining region Y-box 2 (Sox2)* and *Sox10* were used as marker genes. *Sox2* is expressed in the epiblast, before its expression
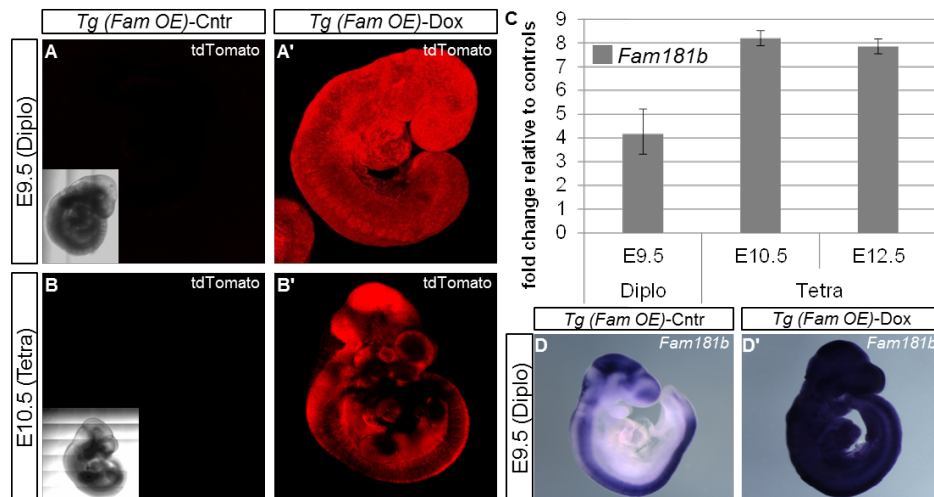
Figure 19. Transgene expression in *Fam181b* gain-of-function embryos.
A-D': Embryos were derived from the *Fam181b* gain-of-function ES cells by either diploid or tetraploid aggregation and dissected at E9.5 (diploid aggregation) or E10.5 and E12.5 (tetraploid aggregation). A-B': Embryos dissected from untreated (Cntr) or doxycycline-treated (+Dox) foster mice were analysed for tdTomato fluorescence. Fluorescence was observed in embryos from Dox-treated mice only, while it was absent from Cntr embryos. C: Quantification of the increase in *Fam181b* expression levels relative to control embroys was measured by qPCR. cDNA was generated from total RNA extracted from three pooled whole embryo lysates. Normalization was done to *Pmm2*. In all samples *Fam181b* expression was elevated compared to the corresponding control sample. D-D': Ubiquitous expression of *Fam181* from the *Gt(ROSA26)Sor* locus upon Dox-treatment was visualized by WISH. Untreated embryos showed a *Fam181b* expression pattern as described previously.

becomes restricted to the neuroectodermal lineage at E7.0-7.5 and later (Avilion *et al.*, 2003), whereas *Sox10* expression can first be detected in the forming neural crest and is maintained during further development of the peripheral nervous system (Kuhlbrodt *et al.*, 1998; Pusch *et al.*, 1998). The segmental arrangement of the outgrowing spinal nerves along the trunk depends on the anterior-posterior (A-P) polarity of the adjacent somites that is determined during somitogenesis (reviewed in Kuan *et al.*, 2004). The expression of both *Sox2* (Fig. 20 A-A') and *Sox10* (Fig. 20 B-B') was comparable between control and doxycycline-treated *Tg(Fam OE)* embryos at E10.5. The separation of the ventrally extending spinal nerve precursors was evenly spaced irrespective of the transgene activity, pointing to a correctly established A-P polarity in the embryos.

To investigate for alterations in chondrogenesis and skeletal development in the *Fam181b* gain-of-function embryos, skeletal preparations were performed at E17.5. The skeleton was stained with Alizarin Red for bone and Alcian Blue for cartilage. No differences were observed between the skeleton of control (Fig. 20D) and induced embryos (Fig. 20D'). Taken together, the *Fam181b* gain-of-function by ubiquitous inducible expression of an additional copy from the modified *Gt(ROSA26)Sor* locus resulted in

normally developed embryos up to E17.5, that were indistinguishable from controls.
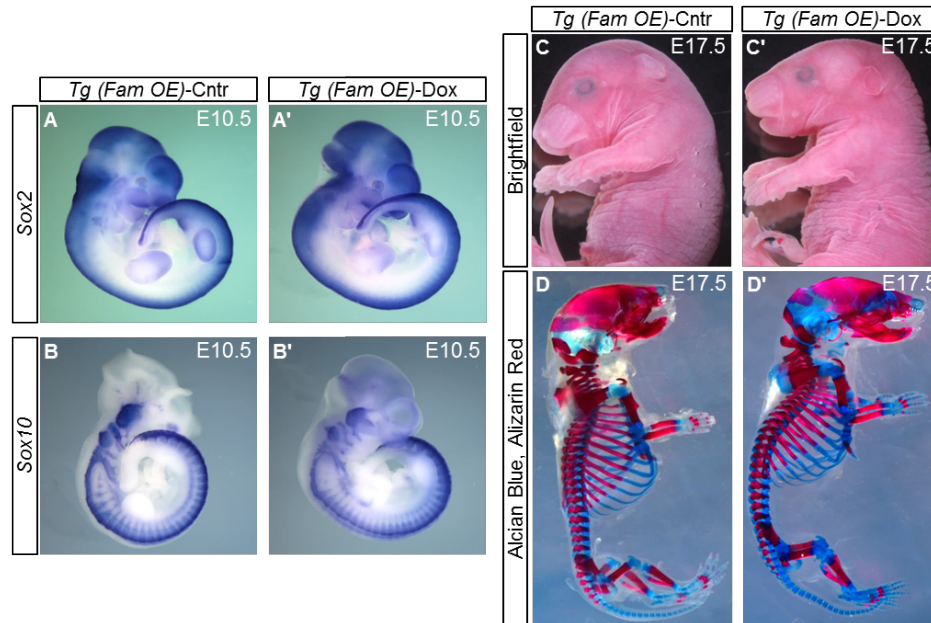
Figure 20. Phenotypic analysis of *Fam181b* gain-of-function embryos.
A-D': Control and Dox-treated *Fam181b* gain-of-function embryos generated by tetraploid aggregation were dissected at E10.5 (A-B') or E17.5 (C-D'). A-B': E10.5 embryos were subjected to WISH for either *Sox2* (A/A') or *Sox10* (B/B'). C-C': Bright-field images of E17.5 control (C) and Dox-treated embryos (C'). Treated and control embryos were indistinguishable by morphological criteria. D-D': Skeletal preparation with Alizarin Red/Alcian Blue at E17.5. No alteration between skeletons from control (D) or induced embryos (D') were detected.

Fam181b miRNA-mediated knock-down

To investigate if, contrary to the gain-of-function, a *Fam181b* knock-down results in altered embryonic development, a comparable approach, based on recombination-mediated cassette exchange (RMCE) and the modified *Gt(ROSA26)Sor* locus was used.

Instead of the *Fam181b* ORF, a short hairpin RNA in a microRNA context (shRNAmir)-expression cassette was integrated into the modified *Gt(ROSA26)Sor* locus of ROAS26A ES cells. As shown byVidigal *et al.* (2010), this allows for an RNA interference (RNAi)-mediated, doxycycline-inducible, ubiquitous knock-down of target genes in embryos generated from these cells. Three shRNAmirs were designed by applying the BLOCK-iT[TM] RNAi Designer tool (Life Technologies) to the *Fam181b* transcript (NCBI: NM_-021427.2), and then cloned into the pcDNA[TM] 6.2-GW/+EmGFP-miR plasmid (Life Technologies). This vector directly allowed for expression in eukaryotic cell lines. To verify that the shRNAmirs were indeed capable of targeting *Fam181b*, HEK293 cells were co-transfected with one of the generated hairpin (hp) expression constructs and a

pcDNA3-based *Fam181b* expression plasmid. To increase the putative knock-down potency, combinations of the shRNAmirs were generated and tested as well. A shRNAmir designed to target no known mammalian gene (Invitrogen) served as negative control. The EmGFP-fluorescence, encoded by the pcDNA$^{(TM)}$ 6.2-GW/+EmGFP-miR plasmids, was used to verify similar transfection efficiencies between the different samples (Fig. 21, lower panels). For each shRNAmir or combination of them, the test was done in biological triplicates. After 48h total RNA was extracted, transcribed into cDNA and used for qPCR (Fig. 21, graph, shRNAmir numbers indicated in the panels below). *Fam181* transcript levels were measured relative to the negative control. All *Fam181b* hp expression constructs tested, decreased the amount of *Fam181b* transcripts compared to the control shRNAmir. The maximum reduction for a single shRNAmir was observed for the *Fam181b* hp #2, reducing *Fam181b* levels down to 15%. The chaining of hp #2 with #1 (Fig. 21, *Fam181bS* hp #2+1) slightly increased the knock-down to 14% of the control levels.
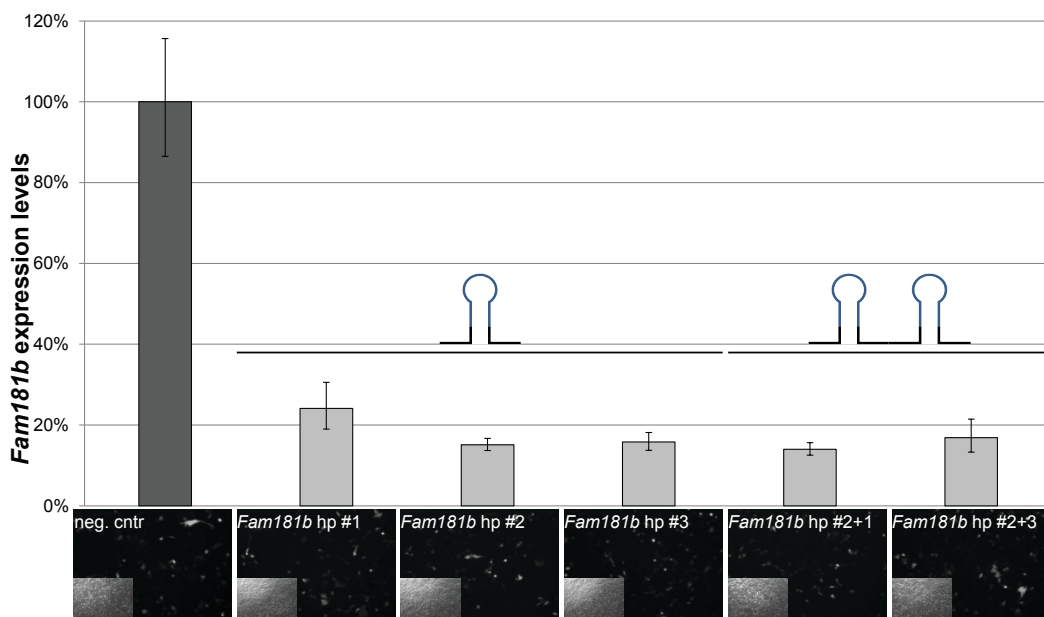
Figure 21. *Fam181b* hairpin test.
To compare the knock-down capacity of the different shRNAmirs, HEK293 cells were transiently co-transfected with expression plasmids for the murine *Fam181b* transcript and for the corresponding hairpin. Comparability of transfection efficiency was estimated by examining EmGFP fluorescence encoded by the shRNAmirs expression vector (lower panels, insets show brightfield images). To further increase knock-down efficiency, hairpins were chained and analysed similar to single hairpins. Transfections and real-time validation were each done in triplicate and human *Pmm2* was used as reference gene. To verify specificity, in the negative control sample a control hairpin provided by the manufacturer, targeting no known mammalian gene, was used.

After confirming functionality of the shRNAmirs, the two resulting in highest knock-down, *Fam181b* hp #2 and #2+1, were used for RMCE. Therefore, the EmGFP

upstream and the thymidin kinase polyA (TKpA)-signal downstream of the shRNAmir coding region of the pcDNA$^{(\text{TM})}$ 6.2-GW/+EmGFP-miR plasmids (Life Technologies) were all shuttled together into the cassette exchange vector (pDONR; Vidigal *et al.*, 2010). This was then used for cassette exchange into the modified *Gt(ROSA26)Sor* locus of ROAS26A ES cells (see Fig. 22A).Verification of correct cassette integration was done as described in Vidigal *et al.* (2010) with an efficiency comparable to the gain-of-function approach (see 2.1.3). The positive ES cell clones were then tested *in vitro* for their functionality. They were cultured for 72h either in the presence (+Dox) or absence (Cntr) of doxycycline. EmGFP was detected exclusively in doxycycline treated cells (Fig. 22B). After the cultivation, total RNA was extracted, cDNA synthesized from it and used for quantification of the *mir155* levels (Fig. 22C). The shRNAmirs used in this approach were all based on the murine *mir155* backbone (Life Technologies), therefore, levels of *mir155* could be used as a general quantitative marker for shRNAmir expression. Upon induction, the expression of mir155-based hairpins increased about 35x times in case of *Tg(Fam KD-#2)* and circa 20x times in case of *Tg(Fam KD-#2+1)*.

From the *Tg(Fam KD-#2+1)* ES cells, embryos were generated by tetraploid aggregation. Foster mice were either supplied with normal drinking water or drinking water supplemented with doxycycline from E2.5 onwards. Embryos were dissected at E9.5 and E12.5. The administration of doxycycline resulted in expression of the EmGFP in the entire embryo at both time points (Fig. 23A-A' and data not shown), as judged by fluorescence microscopy. Quantification of the *Fam181b* expression levels by qPCR showed a more than 80% reduction in doxycycline treated embryos at both, E9.5 and E12.5, as compared to their corresponding controls (Fig. 23B), demonstrating functionality of the transgene in embryos.

For further phenotypic analysis, more embryos were generated and half of the foster mice treated with doxycycline. To check for disorders of neural development, control and doxycycline-treated embryos were dissected at E9.5 and E11.5 (only Dox-treated), followed by WISH for *Sox2* and *Sox10* expression as described earlier (see 2.1.3). To identify alterations in skeleton development, skeletal preparations were done on embryos extracted at E17.5. At E9.5 control embryos were morphologically indistinguishable from doxycycline-treated embryos and no differences were observed for *Sox2* expression (Fig. 24A-A'). In doxycycline-treated E11.5 embryos, the *Sox10* mRNA pattern was comparable to those of *Fam181b* gain-of-function embryos, with evenly spaced spinal nerve precursors along the trunk (compare Fig. 24B to 20B-B'). At E17.5 all embryos treated with doxycycline had open eyelids (Fig. 24D-D'), and one showed further exencephaly (Fig. 24E). In comparison, control embryos developed normally (Fig. 24C-C'). Skeletons of the doxycycline-treated and control embryos were
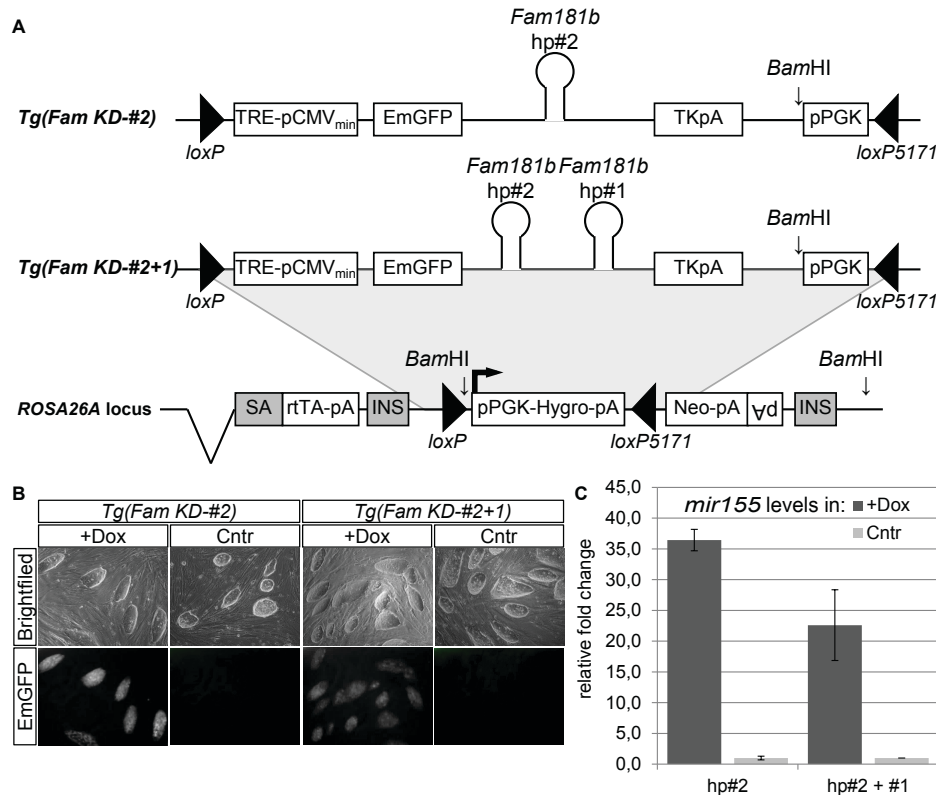
Figure 22. Generation of *Fam181b* knock-down ES cells.
A: Schematic representation of the generated *Fam181b* knock-down constructs. The cassette was integrated into ROSA26A (G4) ES cells and positive clones selected by Southern blot analysis as described in Vidigal et al.(2010). B-C: For testing of transgene activity, the generated ES cells were cultured either with (+Dox) or without (Cntr) doxycycline supplementation for 72h. B: Live imaging of the encoded EmGFP fluorescence marker, which became activated upon induction. C: After imaging, total RNA was extracted, reverse-transcribed into cDNA and used for quantification of *mir155* hairpin backbone levels normalized to *Pmm2*.

again indistinguishable from each other (Fig. 24F-F'). In summary, the generated knock-down transgene was functional in embryos. Upon application of doxycycline, *Fam181b* transcripts levels were measurably reduced and the induced embryos showed altered eyelid development at E17.5.

Fam181b loss-of-function by conventional knock-out

With the used knock-down approach, about 20% of *Fam181b* transcripts remained. This 20% could represent a sufficient amount of *Fam181b* activity to prevent other phenotypes. To address this point a conditional knock-out (cKO) allele was generated by targeting the endogenous *Fam181b* locus. This conditional allele was further used to establish the *Fam181b*-null allele using a general deleter line.

Therefore, the *Fam181b* transcript encoding sequence, together with a 2.9kb 5', and a 2.6kb 3'homology region were amplified from a *Fam181b*-containing BAC (*Fam181b*
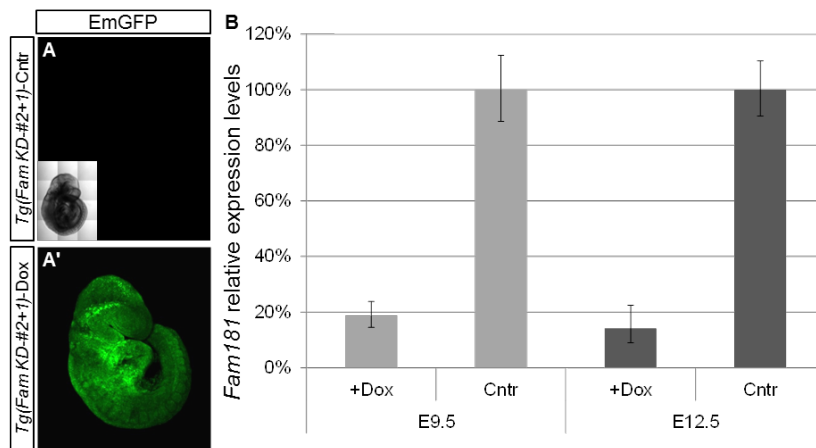
Figure 23. *Tg(Fam KD-#2+1)* expression in embryos.
A-A': E9.5 embryos generated from *Tg(Fam KD-#2+1)* ES cells by tetraploid aggregation (Eakin and Hadjantonakis, 2006) were checked for EmGFP expression. The application of Dox to the drinking water of foster mice from E2.5 onwards resulted in ubiquitous green fluorescence, while in control embryos no signal was detectable. B: Quantification of *Fam181b* expression levels at E9.5 and E12.5 in Dox-treated embryos relative to controls measured by qPCR. cDNA was generated from total RNA extracted from three pooled whole embryo lysates. Normalization was done to *Pmm2*.

BAC, see 6.2.1). A *loxP* recombination site was added upstream of the transcriptional start site. All sequence elements were then inserted into the PL451 vector (Liu *et al.*, 2003), the loxP-transcript coding region and the 5' arm upstream, the 3' arm downstream of the vectors neomycin selection cassette. As described for the V5 knock-in, the 3' homology sequence contained a 139bp repeat of the 3'UTR sequence at its 5' end due the construct design. The introduced sequence elements and the intervening selection cassette were verified by sequencing. The linearised vector was then used to target the endogenous *Fam181b* locus in F1G4 ES cells by homologous recombination (Thomas and Capecchi, 1987, see Fig. 25A). After neomycin selection, gDNA was extracted from the G418^r clones and used for Southern blot analysis. The inserted *Hind*III restriction site introduced between the loxP site and the transcript coding region allowed for discrimination of the targeted versus the wild-type allele. With a radioactively-labelled external 5' probe, the wild-type allele showed a DNA fragment of about 8.5kb, while upon correct targeting an additional fragment of 3.9kb was detectable (Fig. 25B). When this blot was further hybridized with an internal neomycin probe, a 6.8kb fragment, representing mainly the transcript coding region and the 3' homology arm, was observed (Fig. 25B). The combination of these two Southern probes thus verified the correct integration of the entire transgenic cassette into the *Fam181b* locus. Out of 500 ES cell clones analysed, 3 showed the expected pattern in the Southern analysis. Of these, the clones #81 and #221 were used for generation of
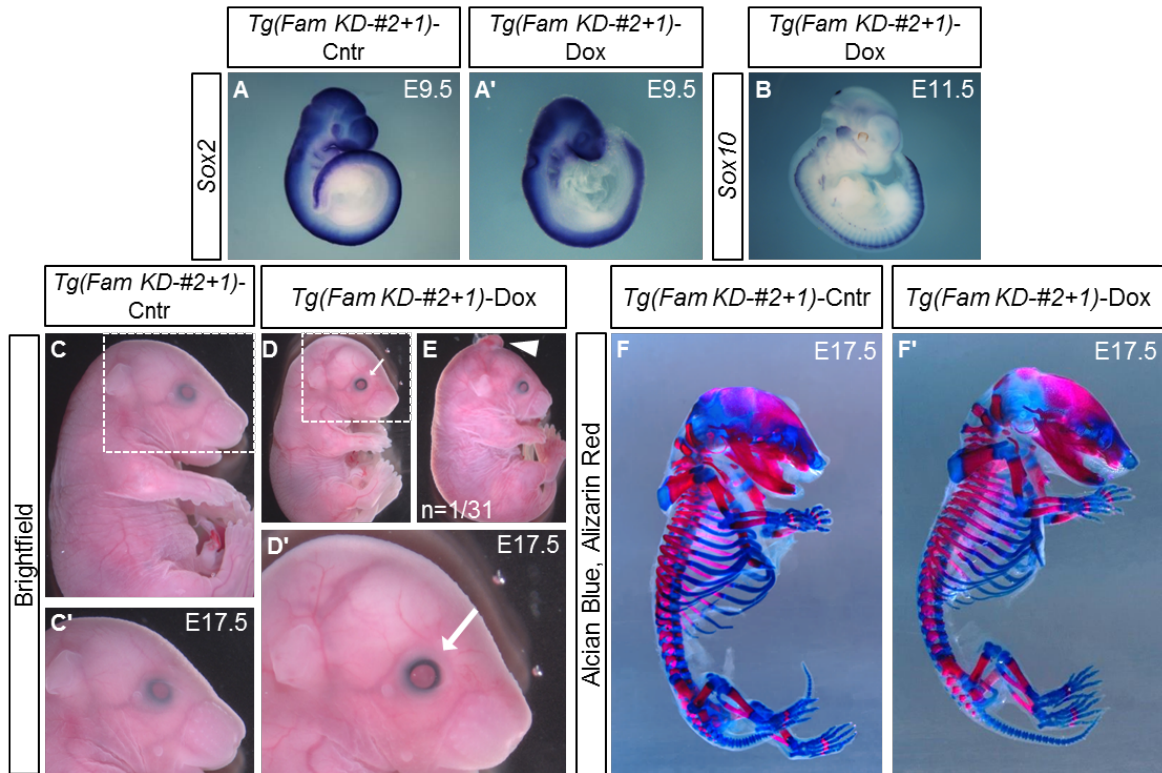
Figure 24. Analysis of *Tg(Fam KD-#2+1)* embryos
A-D': Control and Dox-treated Fam181b KD embryos generated by tetraploid aggregation (Eakin and Hadjantonakis, 2006) were dissected at E9.5 (A-A'), E11.5 (B) or E17.5 (C-F'). A-A': E9.5 embryos were subjected to WISH for *Sox2*. B: WISH for *Sox10* on E11.5 Dox-treated embryos. See Fig. 20B-B' for comparison. C-E: Brightfield images of E17.5 control (C-C') and Dox-treated embryos (D-E). C'/D': Magnification of boxed regions in C/D. If the phenotype was not representative for all specimens investigated, numbers are indicated in bottom left corner. Control embryos were normally developed, while all Dox-treated embryos had open eyelids (arrow in D,D'). One induced embryos showed exencephaly (E). F-F': Skeletal preparation with Alizarin Red/Alcian Blue staining of E17.5 embryos. No alteration between skeletons from control (F) or induced embryos (F') were detected.

chimeric F0 animals by diploid aggregation.

To obtain *Fam181b* loss-of-function animals, some of the F0 males were directly crossed to females of a general deleter line, expressing Cre-recombinase under control of the CMV promoter from a transgene located on the X-chromosome (Schwenk *et al.*, 1995). After germline transmission of the targeted allele, the ubiquitously provided Cre-activity resulted in excision of the entire *Fam181b* transcript coding region (Fig. 26A). Due to the accompanying deletion of the contained *Hind*III restriction site, the produced *Fam181b*-null allele was distinguishable from the wild-type allele by Southern blot with the 5' external probe. There it was detected as a 6.8 kb fragment next to the 8.5kb fragment of the wild-type allele (Fig. 26B). Heterozygous $Fam181b^{+/-}$ animals were crossed with each other to produce homozygous knock-out embryos. Females
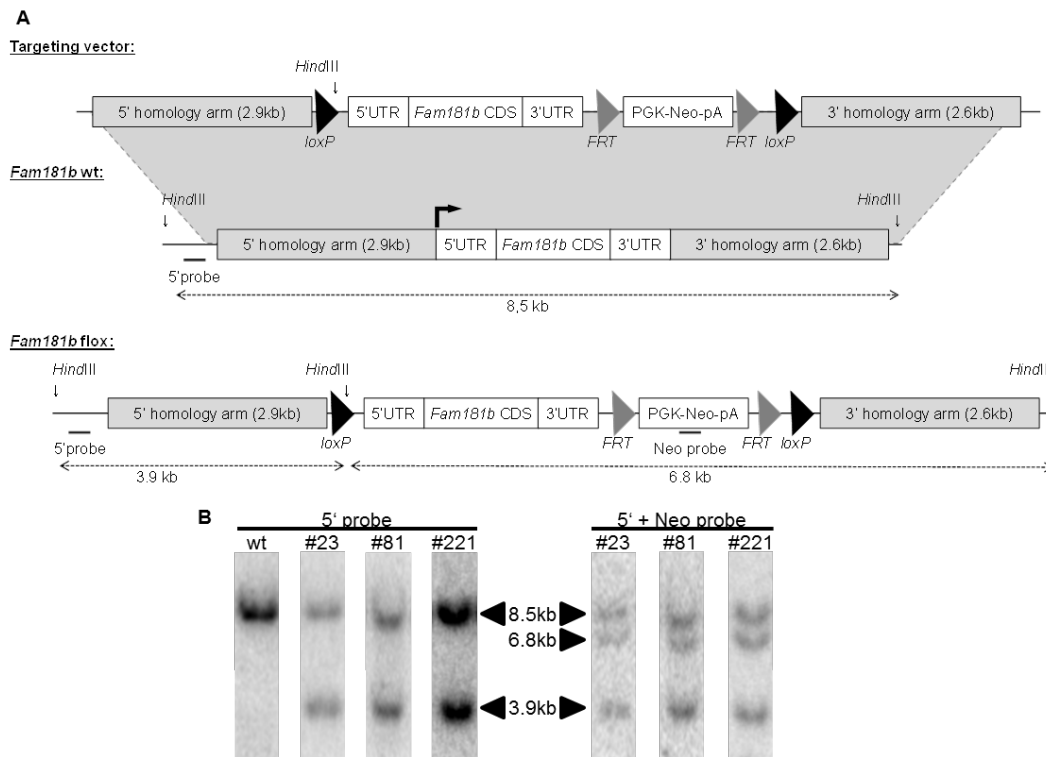
Figure 25. Strategy for generation of the *Fam181b* conditional knock-out
A: Schematic representation of the strategy for generation of the *Fam181b* conditional knock-out. The targeting vector was integrated into the *Fam181b* wild-type locus by homologous recombination. The additionally inserted *HindIII* restriction site allowed for discrimination between the wild-type and the floxed+neo allele. B: Southern blot analysis of ES cell clones. Due to the inserted *HindIII* site, an additional fragment of 3.9kb with the external 5' probe and a fragment of 6.8kb band using the internal Neo probe was detected in positive clones.

were then sacrificed to obtain embryos for analysis. The yolk sac and amnion were used for genotyping by Southern blot, where $Fam181b^{-/-}$ embryos now showed the 6.8 kb fragment of the null allele only (Fig. 26C). At E10.5, littermates could not be discriminated by morphology (data not shown). WISH for *Fam181b* revealed the absence of the transcript from $Fam181b^{-/-}$ embryos, demonstrating the loss-of-function (Fig. 26D).

To check for abnormalities in cranial nerve development, *Fam181b*-null embryos were subjected to αNeurofilament antibody staining (Fig. 27A). The observed nerve pattern was comparable to the expected wild-type pattern (compare to elsewhere, e.g. Cordes, 2001). Given that the knock-down resulted in a phenotype at E17.5, embryos of $Fam181b^{+/-}$ x $Fam181b^{+/-}$ matings were dissected at this stage. The amnion was used for genotyping by Southern blot as described previously. Morphologically, the littermates remained indistinguishable at E17.5, irrespective of their genotype (Fig. 27B-B'). Contrary to the doxycycline-treated knock-down embryos, neither defects in
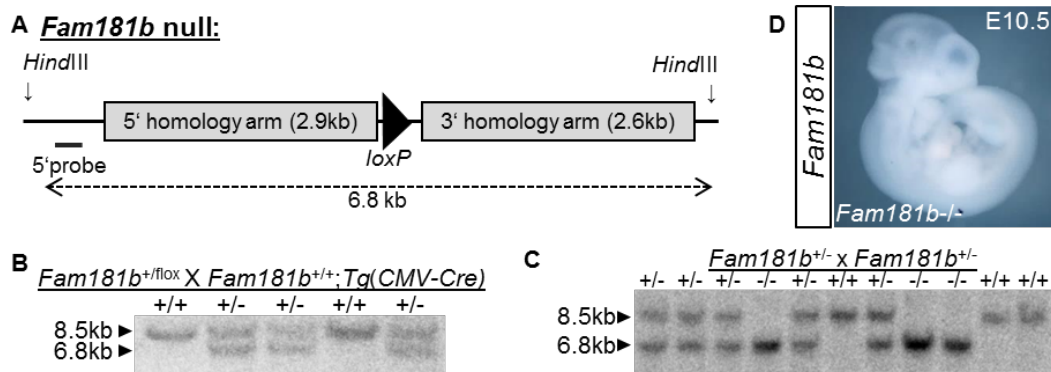
Figure 26. Generation of the *Fam181b*-null animals.
A: Schematic representation of the *Fam181b*-null allele. Deletion of the transcript coding region (and the selection cassette) from the targeted locus removed the internal *Hind*III site and produced a restriction fragment length polymorphism (RFLP). This allowed for discrimination between wild-type and null allele. B: Southern blot analyses of offspring from crossings of *Fam181b*$^{+/flox}$ animals with a CMV-Cre general deleter line. A 6.8kb fragment identified *Fam181b*$^{+/-}$ animals. C: *Fam181b*$^{+/-}$ animals were intercrossed to generate homozygous null animals, indicated by the absence of of the 8.5kb wild-type fragment by Southern blot analyses. D: Whole-mount *in situ* hybridization for *Fam181b* on E10.5 *Fam181b*$^{-/-}$ embryos revealed absence of a transcript.
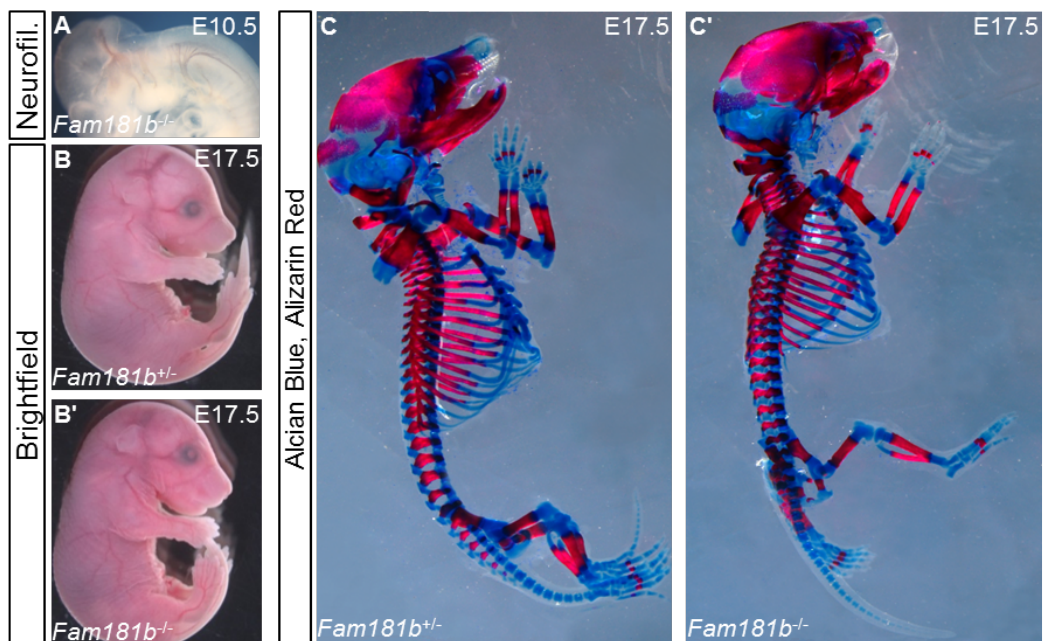
Figure 27. Analysis of *Fam181b*-null embryos
A: αNeurofilament antibody staining on E10.5 *Fam181b*$^{-/-}$ embryos. B-B': Brightfield images of E17.5 littermates heterozygous (B) or homozygous (B') for the *Fam181b* knock-out. C-C': Skeletal preparations of E17.5 littermates heterozygous (C) or homozygous (C') for the Fam181 knock-out. Alcian Blue and Alizarin Red staining was done to mark cartilage and bones respectively.

eyelid closure, nor the less frequent exencephaly were observed in the $Fam181b^{-/-}$ embryos. Skeletons of homozygous embryos were indistinguishable from those of their heterozygous and wild-type littermates (Fig. 27C-C').
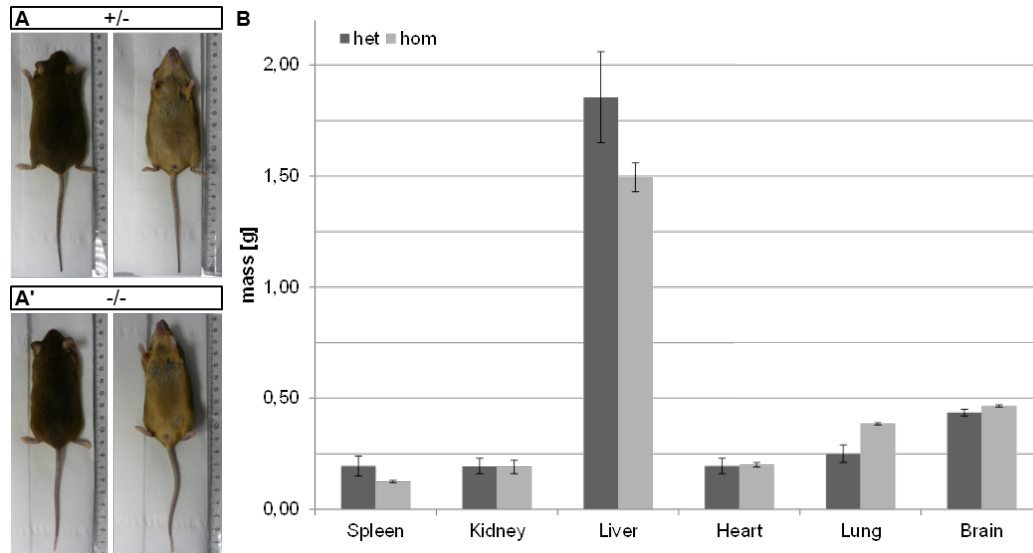
Figure 28. Postmortem examination of *Fam181b* KO animals
A-A': Dorsal (left) and ventral (right) view of 43 weeks old heterozygous (A, n=2) and homozygous (A', n=2) female *Fam181b* KO littermates were sacrificed for a postmortem examination. B: Comparison of organ mass between heterozygous (dark grey) and homozygous (light grey) littermates. No significant differences were measured.

Further, the $Fam181b^{+/-}$ intercrosses resulted in viable, fertile offspring of all genotypes. Distribution of the genotypes within the litters was in agreement with Mendelian ratios (data not shown). Judged by morphology, adult homozygous KO animals were indistinguishable from those heterozygous and wild-type for *Fam181b* (Fig. 28A-A'). To analyse if there were alterations in the internal morphology of $Fam181b^{-/-}$, postmortem examinations were done on 43 week-old female littermates either homozygous or heterozygous for the KO allele. After euthanising with CO_2, their abdomens were opened and the major organs weighed and checked for morphological abnormalities. All organs investigated were similar between $Fam181b^{-/-}$ and $Fam181b^{+/-}$ animals with respect to their morphology (data not shown) and mass (Fig. 28B).

While no morphological alterations were observed, alterations in the nervous system caused by the *Fam181b* loss-of-function could lead to neurological disorders. These might become overt through an abnormal behaviour. To assess such a putative behavioural phenotype, a test for activity upon stimulation (Fig. 29A-B) and a tail suspension test (Fig. 29C-D) were done and evaluated as described in Ordway *et al.* (1997). For both tests, all animals of one litter, including 2 heterozygotes and 5 homozygotes were used. Before the experiments they were kept individually in fresh cages
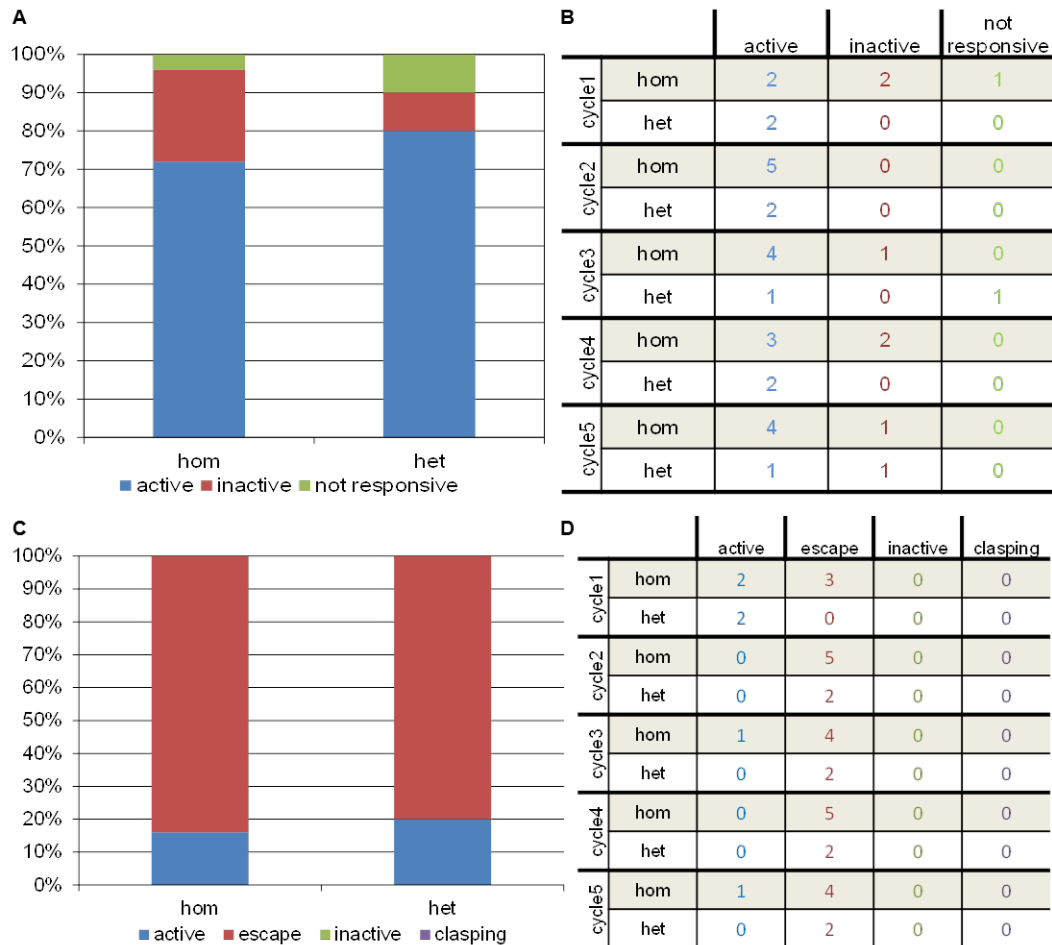
Figure 29. Behavioural tests of *Fam181b* KO animals
A-B: Activity upon stimulation. Heterozygous (n=2) and homozygous (n=5) littermates were placed separately under a fume hood, the cage lid removed, and their behaviour within the next 10 sec assessed. The test was repeated 5 times with 1h intervals. Active, mouse moves; inactive, does not move; not responsive, does not move when touched after 10 sec. C-D: Tail suspension test. Heterozygous and homozygous littermates (n as above) were lifted to about 35 cm, kept this way for 1 min and their behaviour assessed during that time. The test was repeated 5 times with 30 min intervals. Active, mouse spreads limbs away from its body; escape, reaches and climbs onto the holding hand; inactive, does not move; clasping, draws limbs towards its abdomen.

for two days. The experimental conditions during the monitoring were kept constant. Each experiment was done with 5 cycles within 1h intervals for the activity-test and 30 min intervals for the tails suspension test. The results for each cycle are listed in Fig. 29B and D, respectively. Between the two tests there was a break of 1 week during which the mice were maintained separately under equal conditions. The age of the mice at the time of the two tests was 13 and 14 weeks, respectively. The activity upon stimulation showed a greater number of inactive, and thus less active, homozygous animals compared to the heterozygous controls, although this result was not statistically

significant (Fig. 29A). No differences between homozygotes and heterozygotes were observed for the tail suspension test (Fig. 29C). To obtain a more reliable analysis, a greater number of animals and more age-matched litters have to be tested.

2.1.4 Phylogenetic analysis of the *Fam181* family

The *Fam181b* knock-out resulted in a normal phenotype, without any overt alterations of embryonic development. Furthermore, *Fam181b* knock-out animals proved to be viable and fertile. This raised the question, of whether the depletion of *Fam181b* function might be compensated for by the other *Fam181* gene family member, *Fam181a*.

Conservation of FAM181B and FAM181A in vertebrates

To obtain more information about the proteins encoded by the *Fam181* gene family, the predicted protein sequences of murine FAM181 proteins were compared with those of orthologues in other species. The mFAM181A and mFAM181B proteins themselves share 46% similarity on the amino acid level. A multiple sequence alignment with their human counterparts showed a similarity of about 77% for each of the proteins (Fig. 30A). Within this alignment, 4 conserved blocks were detected (Fig. 30A, red and green boxed regions). To further analyse this conservation, a protein-protein blast for non-redundant sequences was performed, using the mouse FAM181 protein sequences as input. This allowed for identification of putative orthologues by sequence similarity. The blast revealed that the FAM181 family is highly conserved among vertebrates. In most species two proteins were identified, one sharing higher similarity to mFAM181A and the other to mFAM181B. Several species, representing different taxa within the vertebrate phylum, were used as input for a multiple sequence alignment. This was further used to assemble a phylogenetic tree (Fig. 30B). For rooting of the tree, the starlet sea anemone *Nematostella vectensis* was used as an outgroup. The phylogram confirmed the conservation of the FAM181 proteins within vertebrates. A large portion of highly conserved amino acid residues were found in the N-terminal 3 conserved boxes (Fig. 30A, orange lettered residues). The fourth, most C-terminal box contained a proline-rich stretch (Fig. 30A, green region). Its proline-rich character was also conserved, though the exact position and total number of prolines varied between the species investigated. The two proteins identified in most species separated into two clusters, one for the FAM181A (Fig. 30B, blue) and another for the FAM181B proteins (Fig. 30B, green). In summary, this infers a conservation of FAM181 protein family in vertebrates with two paralogoues per species as the ancestral state.
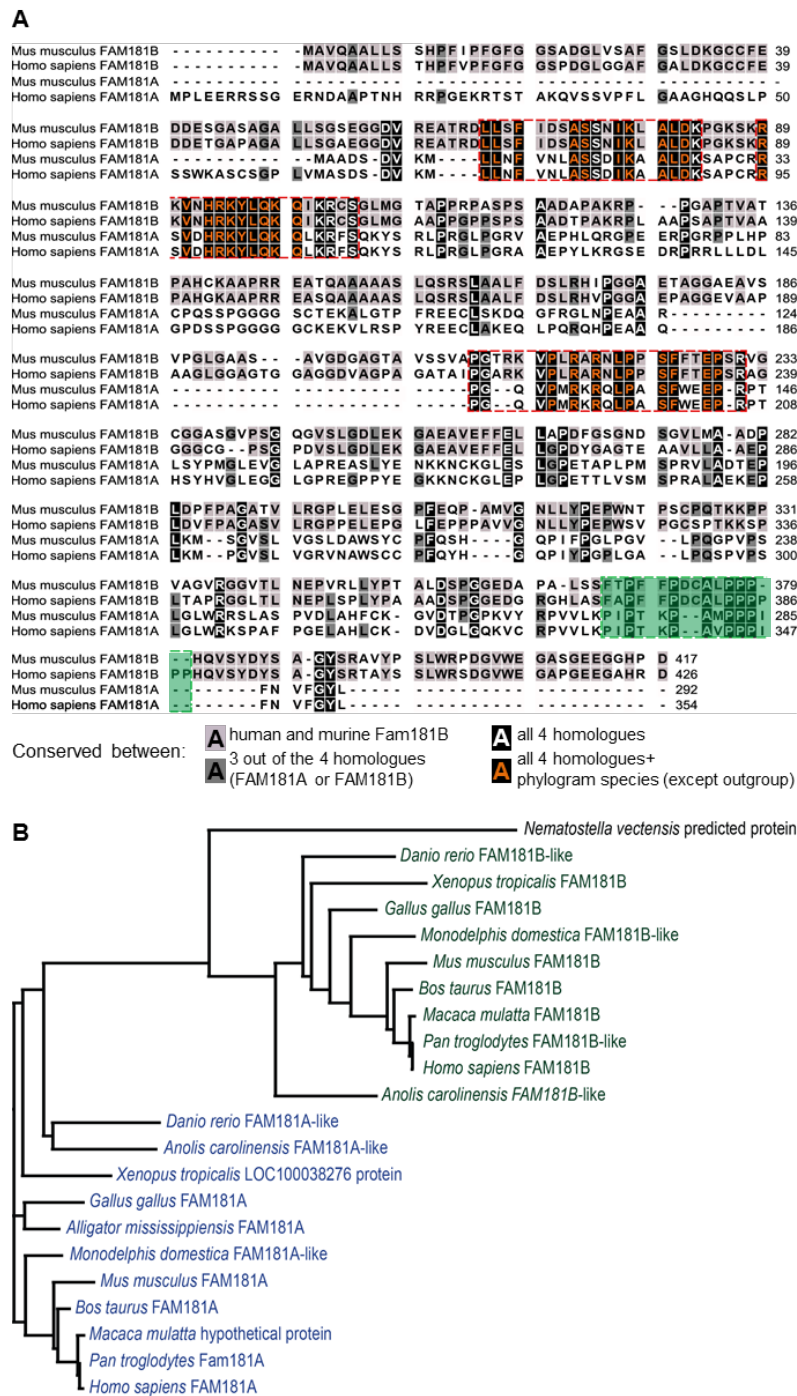
Figure 30. FAM181 family members in vertebrates

A: Multiple sequence alignment of mouse and human FAM181 protein homologues. Conserved residues between murine and human FAM181B are highlighted in light grey, residues conserved in 3 proteins by a dark grey background, and white lettered residues with a black background are those conserved in all 4 homologues. Red dashed and green boxes outline highly conserved motifs. Orange letters on a black background indicate residues conserved in all vertebrate species investigated in B. B: Phylogenetic tree of selected vertebrate species. The Cnidaria *Nematostella vectensis* was used as outgroup. FAM181B proteins are highlighted in green, FAM181A proteins in blue.

Deletion of the conserved box3 of FAM181B

Functionality is not necessarily linked to the primary sequence only, but can be transferred by structural domains. Phyre2 is an bioinformatic tool to predict a likely secondary structure and identify similarities to proteins of known structure (Kelley and Sternberg, 2009). A PSI-Blast is done on the input sequence and the identified sequences used to generate a Hidden Markov model. This is then scanned against the database of Hidden Markov models for known secondary structures. The primary sequence of the matching protein is then aligned against the amino acid sequence of the input protein to calculate the possible secondary structure. Using Phyre2 on mFAM181B, a model of the FAM181B protein was generated (Fig. 31A). Thereby, 16 residues (4%) of the protein were modelled with a confidence greater then 90% (highlighted in red in Fig. 31A). This stretch showed 59% similarity with a motif from the Hippo signalling effector Yes-associated protein 1 (YAP1, Fold libary IDs c3kysB and c3juaB). Based on these templates, 2 α-helices were predicted to be located upstream and within the conserved box 3 region. The model further calculated α-helices overlapping with the conserved boxes 1 and 2, though with lower confidence.

A protein-protein blast of the mFAM181B conserved box 3 amino acid sequence against all known, non-redundant mouse proteins confirmed the anticipated similarity with the mouse YAP1. In YAP1 the 2 helices-motif is required for the interaction with the DNA-binding protein TEAD4 and thus the nuclear localization of YAP (Chen *et al.* 2010; reviewed in Pan 2010). In FAM181A and B no known nuclear localisation signal was detected. An *in silico* search for such localization signals using NLStradamous (Nguyen Ba *et al.*, 2009) identified a possible motif in mFAM181B (amino acid residues 83-95: KPGKSKRKVNHRK), residing in between the conserved boxes 1 and 2, partially overlapping with them. A similar search for mFAM181A did not find any nuclear localization signal. Due to the conservation for both proteins it seems rather likely, that the observed nuclear localisation of mFAM181 proteins most likely depends on the similarity with the YAP-TEAD4 interaction domain. This might reflect a possible protein-protein-interaction enabled by the predicted 2 helices. To investigate this possibility, the conserved box 3 of mFAM181B was mutated. The entire region (amino acid residues 209-231) was deleted from a C-terminally V5-tagged expression construct by fusion PCR and the sequence-verified PCR product integrated into the pcDNA3 expression vector. The subcellular localization was analysed in transiently-transfected NIH3T3 cells by indirect immunofluorescence against the V5 tag. An unmodified FAM181B-V5 was used as control. FAM181B-V5 showed nuclear localisation, irrespective of the presence or abscence of box 3 (compare Fig. 31B-B" to C-C"). This infers that box three and its putative α-helix are dispensable for the subcellular localization
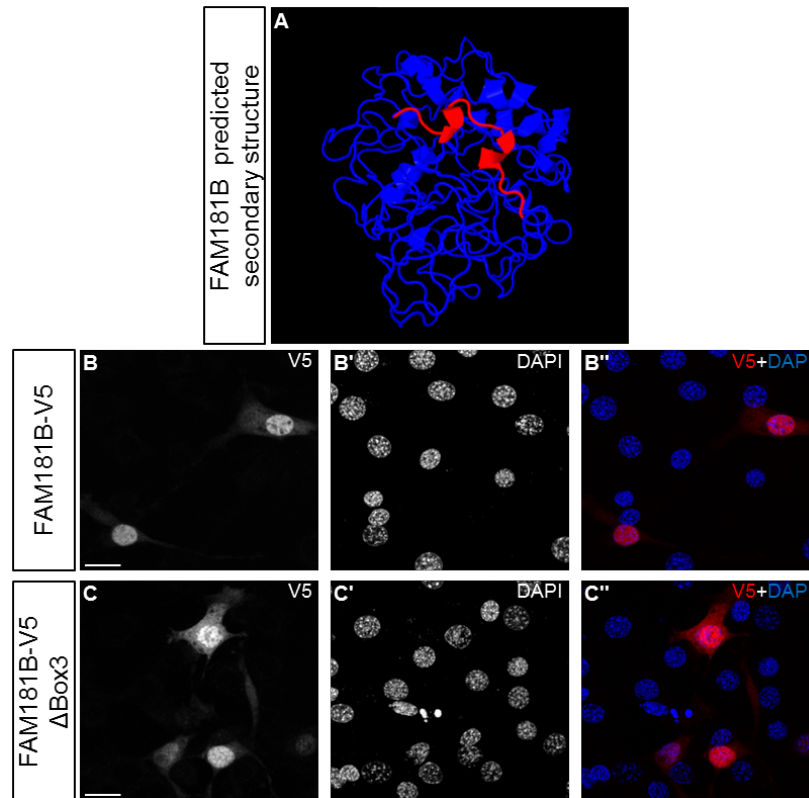
Figure 31. FAM181B structural analysis
A: The FAM181B protein secondary structure as calculated by Phyre2. Stretches highlighted in dark red showed ≥90% prediction confidence. B-C": C-terminally V5-tagged *Fam181b* expression constructs encoding either a wild-type (B-B") or box 3-depleted (ΔBox3; amino acid residues 209-231) (C-C") protein were transiently-transfected into NIH3T3 cells. FAM181B localisation was analysed by indirect immunofluorescence for V5. Counterstaining was performed with DAPI. Scale bar = 20μm.

of the FAM181 proteins.

2.2 Analysis of *Fam181a*

To analyse if *Fam181a* might be able to compensate for a *Fam181b* loss-of-function, its expression in mouse was analysed in more detail. Expression on the mRNA level was either investigated by WISH in embryos or by qPCR and RT-PCR in adults and cells. The probe used for the *in-situ* hybridisations corresponded to nucleotides 606-1343 of the transcript (NCBI: NM_001195726.1), covering parts of the ORF and the 3'UTR. Lacking specific antibodies, an initial protein analysis was done using tagged versions of FAM181A.

2.2.1 Expression of murine *Fam181a* on the mRNA level

Fam181a expression during murine embryonic development

WISHs were done on wild-type embryos between E7.5 and E12.5. Staging of E7.5 embryos was done according to Downs and Davies (1993), for older embryos in accordance with Theiler (1989). Earliest signs of *Fam181a* expression appeared at E7.5 in the prospective midbrain region of late headfold stage embryos (Fig. 32B-B'), while in younger embryos no signals were detected (Fig. 32A-A'). At TS12, *Fam181a* mRNA was further observed in the entire forming neural tube and with a distinct domain in the rhombencephalon anterior to the otic vesicle (Fig. 32C-C', arrowhead highlights rhombencephalic expression). At later stages, *Fam181a* transcriptional activity remained localised mainly to the neural tube and the developing brain, while the rhombencephalic signal became undetectable from TS14 onward. A new distinct domain of expression arose in the developing eye anlagen and remained visible until TS19 (Fig. 32D-H, red arrowhead). Only in embryos of TS14, the expression domains in the brain vesicles and in the neural tube were separated by a small gap at the level of the otic vesicle (Fig. 32D-D'), while such a separation was not present in older embryos (compare to Fig. 32E-J). Between TS16 and TS19, the midbrain *Fam181a* expression domain became clearly demarcated from the surrounding neural expression domains by an increased staining intensity (Fig. 32E-H", white dashed line). Overall, *Fam181a* expression was limited to neural tissues through all stages investigated. There it might compensate for the *Fam181b* loss-of-function. No signal for *Fam181a* mRNA was detected in the PSM or limb anlagen.

Figure 32 *(facing page).* **Fam181a expression from E7.5-E12.5**
A-B': Expression of *Fam181a* in E7.5 mouse embryos. Staging (indicated in the top right corner) according to Downs and Davies (1993). (A/B) lateral view, (A'/B') view of anterior end, bracket in B marks emerging expression in prospective midbrain region. C-I": Expression of *Fam181a* in E8.5-E12.5 mouse embryos. Staging according to Theiler (1989). C/C': Black arrowheads highlight a rhombomeric expression domain anterior to the otic vesicle. D-H": At E9.5 expression arises in the eye anlagen and remains detectable up to E11.5 (red arrowheads). F-J: Around E10.5 the midbrain expression domain becomes distinguished by an increased staining intensity (white dashed line). a, anterior; EHF, early head fold stage; fb, forelimb bud; hb, hindlimb bud; ht, heart tube; l, left; LHF, late head fold stage; nt, neural tube; ov, otic vesicle; p, posterior; r, right; TS, Theiler stage.
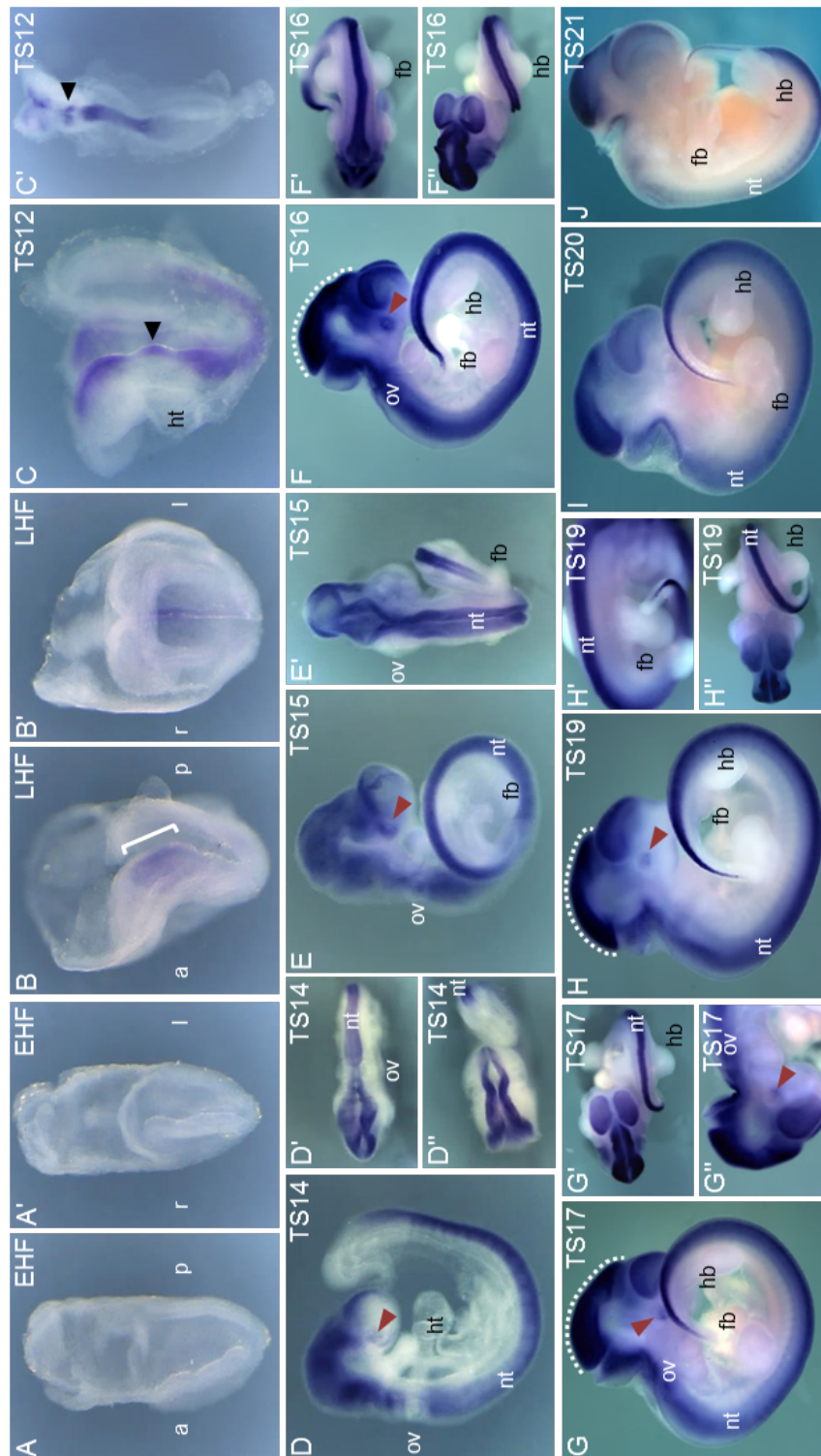
Fam181a expression in adult organs

To analyse *Fam181a* expression in adult mice, qPCR and RT-PCR were performed on the cDNA generated from the same tissues as for *Fam181b* (2.1.1). The qPCR was normalized to *Pmm2*, while for the RT-PCR *Gapdh* served as loading control.
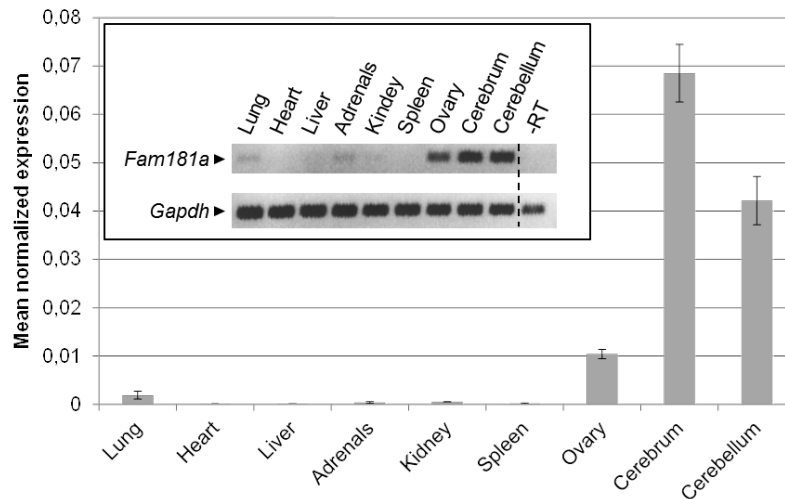
Figure 33. *Fam181a* expression in adult organs
Fam181a expression in organ samples of an adult female mouse (CD1). Total RNA was extracted from tissue samples of selected organs and reverse-transcribed into cDNA. A sample treated without reverse transcriptase was used as negative control. The cDNA was either used for RT-PCR (inset) with primers for *Gapdh* as loading control, or for quantitative real-time PCR (qPCR; qraph). qPCR was normalized to *Pmm2* and analysed by qGene. Dashed line in the inset indicates separation on the corresponding gel.

Using both methods, highest expression levels were measured in the brain samples, the cerebrum followed by the cerebellum (Fig. 33), overlapping with expression of its paralouge *Fam181b*. High *Fam181a* levels were further detected in the ovary, equalling about 24% of cerebellum and 15% of cerebrum expression. Low, barely detectable expression was measured in lung, adrenals and kidney. The lung expression measured about 4.5% of cerebellum and 2.8% of cerebrum levels. *Fam181a* transcripts were not detectable in heart, liver or spleen.

Fam181a expression during differentiation of ESCs into the neural lineage

Both the WISH analysis on embryos and the transcript quantification on adult organs showed *Fam181a* expression in the central nervous system (CNS) and their developmental precursor structures. To investigate if there is a direct correlation of *Fam181a* expression and differentiation into neural lineages, the samples of the *in vitro* differentiation generated earlier (see 2.1.1) were reused and *Fam181a* transcript levels quantified

by real-time qPCR. *Oct4*, *Pax6*, and *TrkB* levels are shown again to illustrate the different steps of differentiation during the protocol. *Fam181a* levels reached a plateau of maximum expression between day 8 (D8) and the neural progenitor sample (NP cells) (see Fig. 34). This reached about the 220x times of the ES cell values. This points to a positive correlation of *Fam181a* expression with differentiation into the radial glia lineage.
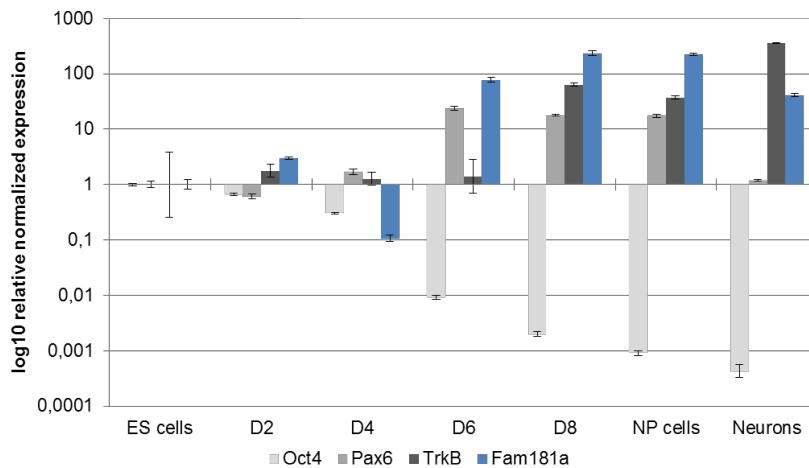
Figure 34. *Fam181a* expression during differentiation of ESCs into the neural lineage
Differentiation of murine F1G4 ES-cells into neural cells according to Bibel *et al.* (2007). During the differentiation procedure samples were taken (x-axis) and used for total RNA extraction and cDNA synthesis. *Fam181b* expression levels were analysed by qPCR. *Oct4* was used as a stem cell marker, *Pax6* as a marker for neural progenitors and *TrkB* for terminal neurons. Expression was normalized to *Pmm2*. The undifferentiated ES cells served as reference samples. The expression of *Fam181a* is maximally upregulated (230-fold) in the day 8 (D8) sample.

2.2.2 Expression of murine *Fam181a* on the protein level

To obtain more information about the FAM181A protein, the amino acid sequence was used as input into Phyre2. The predicted secondary structure showed similarities with that of FAM181B (Fig 35A). Forty-six residues (16%) of the protein were modelled with an accuracy greater than 90% (dark red in Fig 35A). This stretch shared about 45% identity with a motif of YAP1 (Fold libary IDs c3kysB and c3juaB) and predicted one α-helix in the conserved box 3 and another upstream of it. Further, two α-helices were predicted to be overlapping with the conserved boxes 1 and 2. With about 60% confidence another stretch, showing 71% identity to a knottin fold motif, C-terminal of box 3 was predicted by Phyre2 (light red in Fig 35A). Knottins are small cystein-rich proteins of various functions and are grouped together based on their knotted 3D structure (Gracy *et al.*, 2008). The murine FAM181A protein contains 7 cystein

residues (about 2.4% of the total protein) that might be sufficient for the 3 disulfide-bridges required for classification as a knottin. However, the Knoter1D algorithm (Gracy *et al.*, 2008) predicted it unlikely that mFAM181A belongs to the knottin protein class.
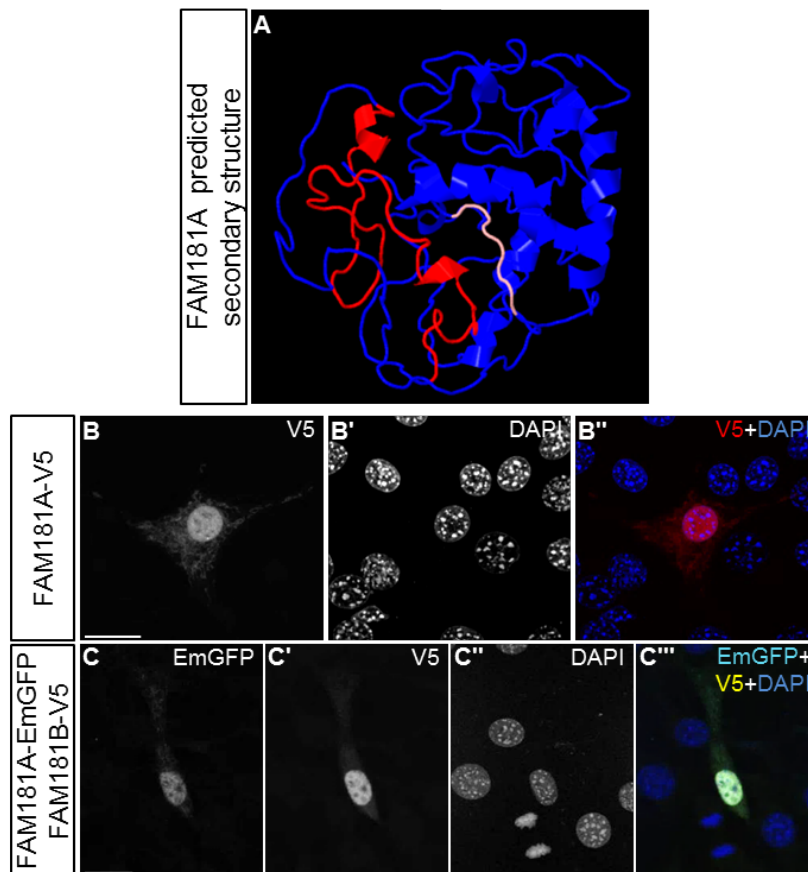
Figure 35. Analysis of FAM181A
A: The FAM181A protein secondary structure as calculated by Phyre2. Stretches highlighted in light red were predicted with a confidence of $\geq$60%, those highlighted in dark red $\geq$90%. B-B": A C-terminally V5-tagged *Fam181a* expression construct was transiently-transfected into NIH3T3 cells and FAM181A analysed by indirect immunofluorescence for V5. C-C"': A C-terminally EmGFP-tagged *Fam181a* and a C-terminally V5-tagged *Fam181b* expression construct were transiently co-transfected into NIH3T3 cells and both proteins analysed by indirect immunofluorescence for EmGFP and V5 respectively. Counterstaining was performed with DAPI. Scale bar = 20µm.

To investigate its subcellular localization, expression constructs encoding C-terminal tagged FAM181A proteins were generated and transiently-transfected into NIH3T3 cells. The distribution of the tagged protein within the cell was then analysed by indirect immunofluorescence. C-terminally V5-tagged FAM181A was detected in the nucleus (Fig 35B-B"). A combined transfection of a C-terminally EmGFP-tagged FAM181A and a V5-tagged FAM181B showed an overlapping localization in the nucleus (Fig 35B-

B").

2.2.3 Generation of mutants for analysis of *Fam181* gene family function in mice

To obtain functional data for *Fam181a* and the entire gene family, two transgenic ES cell lines were generated. One was a classical KO performed by homologous recombination into the endogenous locus in F1G4 ES cells, that will allow for single analysis of the *Fam181a* loss-of-function in embryos and adult mice. The generation of this mouse line and the further generation of *Fam181a/b* compound KO animals and embryos is a very time consuming approach and is, thus, still underway. A faster possibility to obtain information about the *Fam181* family loss-of-function was the generation of a doxycycline-inducible double knock-down of both genes in ES cells and embryos derived from them.

Generation of a *Fam181a* knock-out

To generate a classical KO of *Fam181a*, a 2.7kb 5' and a 2.8kb 3' homology arm were amplified from the a *Fam181a*-containing BAC (*Fam181a* BAC, see 6.2.1) and integrated upstream and downstream of the neomycin selection cassette of the PL451 (Liu *et al.*, 2003) vector respectively.

After sequence verification, the linearised vector was used for targeting of the endogenous *Fam181a* locus in murine F1G4 ES cells. Given that the homology arms directly flanked the *Fam181a* protein coding sequence, homologous recombination resulted in replacement of the ORF by the *FRT* recombination site-flanked selection cassette (Fig. 36A). After the neomycin selection, the *Bam*HI restriction site present in the transgene allowed for identification of clones with correct integration by Southern blot analysis (Fig. 36B). Besides the 15.9kb wild-type fragment, an additional 6.6kb fragment should be detectable in positive clones using an external 5' probe. This smaller fragment was detected solely with a internal probe for neomycin, again confirming correct integration into the *Fam181a* locus and ruling out additional integrations somewhere else in the genome. One ES cell line was established (#95) out of 200 clones analysed. These ES cells are currently being used to generate F0 animals for establishing the *Fam181a* KO mouse line.
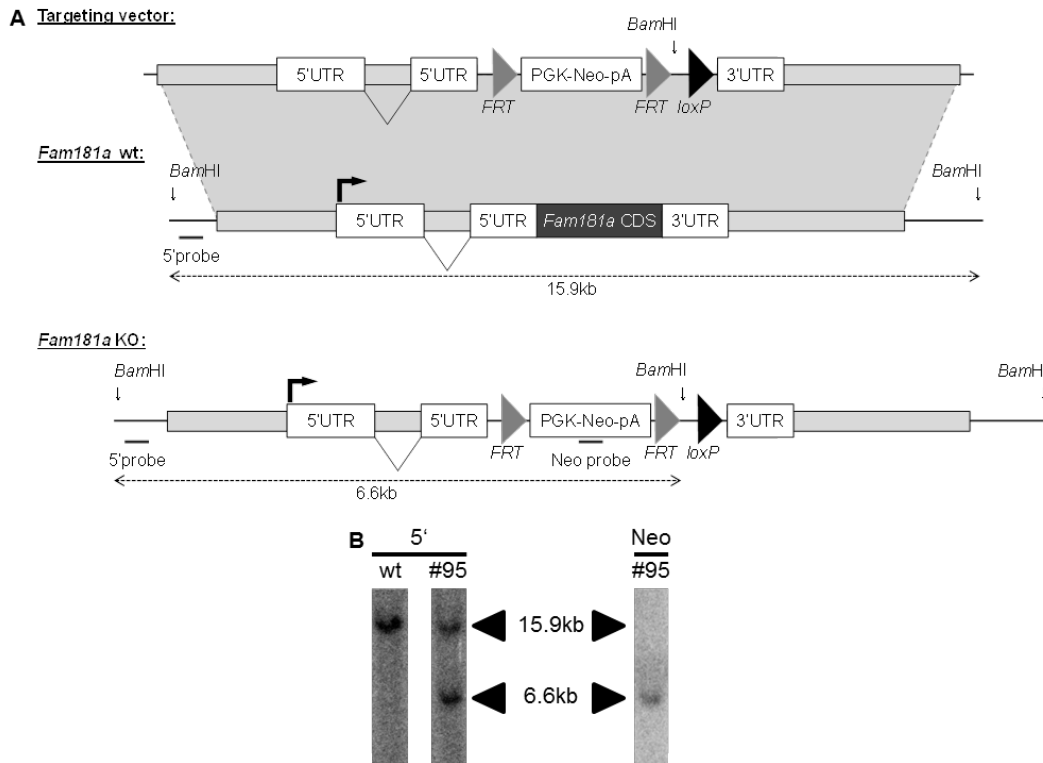
Figure 36. Generation of *Fam181a* knock-out ES cells
A: Schematic representation of the strategy to generate a *Fam181a* knock-out. The targeting vector was integrated into the *Fam181a* wild-type locus by homologous recombination in F1G4 ES cells. The additionally inserted *Bam*HI restrictions site allowed discrimination between the wild-type and the knock-out allele. B: Southern blot analysis of ES cell clones. Due to the inserted *Bam*HI site, an additional fragment of 6.6kb was detected in positive clones using an external 5' probe . The same fragment was detected with an internal Neo probe.

Fam181a/b double knock-down

The *Fam181b* KO showed a wild-type phenotype in embryos. This might be due to compensation of *Fam181b* function by *Fam181a*. To investigate this possibility, three shRNAmirs were designed by applying the BLOCK-iT$^{(TM)}$ RNAi Designer tool (Life Technologies) to the *Fam181a* transcript (NCBI: NM_001195726.1). These were cloned into the pcDNA$^{(TM)}$ 6.2-GW/+EmGFP-miR plasmid (Life Technologies) and tested by co-transfection with a *Fam181a* expression plasmid into HEK293 cells. The control shRNAmir targeting no known mammalian gene (Invitrogen) was used as reference control to calculate knock-down efficiencies. EmGFP fluorescence, encoded by the pcDNA$^{(TM)}$ 6.2-GW/+EmGFP-miR plasmid, was used to verify comparable transfection efficiencies between the different samples (Fig. 37, lower panels). Forty-eight hours after transfection, total RNA was extracted from the cells and reverse-transcribed into cDNA. This was used for real-time qPCR to quantify the *Fam181a* transcript levels relative to the negative control. With a knock-down of greater than 80% *Fam181a*

hp#3 was the most potent shRNAmir tested (Fig. 37, graph). This was followed by *Fam181a* hp#1 and *Fam181a* hp#2 with a reduction of transcript levels down to 40% and 60%, respectively.
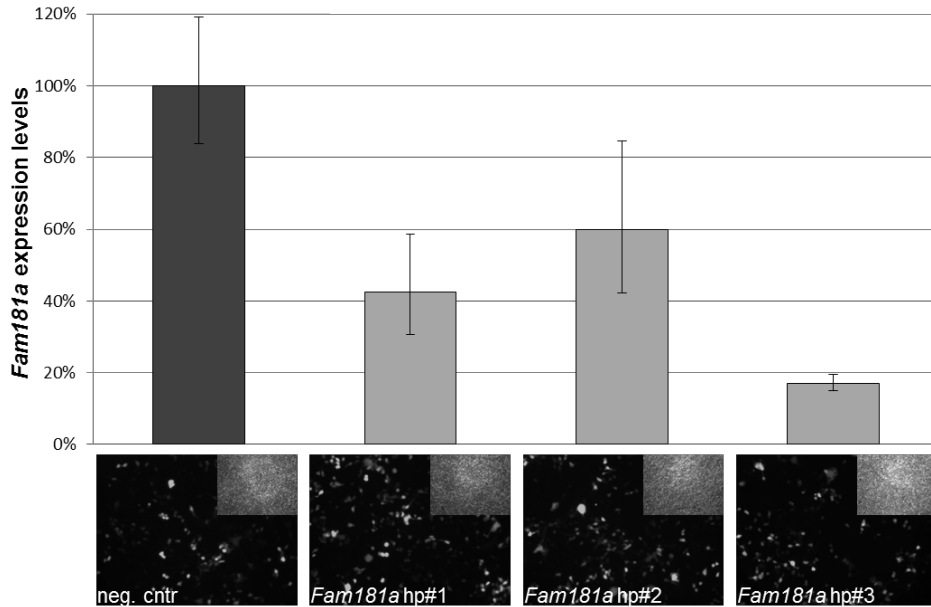
Figure 37. *Fam181a* hairpin test
Knock-down capacity of the *Fam181a* targeting shRNAmirs was analysed by co-transfection of HEK293 cells with expression plasmids for the murine *Fam181a* transcript and for the corresponding shRNAmirs indicated in the panels below. Comparability of transfection was verified by EmGFP fluorescence (lower panels, insets show brightfield images). Transfections and qPCR measurements were each done in triplicates. Human *Pmm2* was used for normalization. A control shRNAmir targeting no mammalian gene (Life Technologies) was used as reference sample (dark grey).

While the chaining of shRNAmirs for the same target is purported to increase knock-down efficiency, the chaining of shRNAmirs targeting different genes decreases knock-down efficiency for the single genes. To obtain the maximal potent combination of shRNAmirs for the double knock-down, the three hairpins for of *Fam181a* and the three for *Fam181bb* were chained. Together with the upstream encoded EmGFP marker and the downstream polyA signal of pcDNA$^{(TM)}$ 6.2-GW/+EmGFP-miR, this chain of 6 shRNAmirs was cloned into the pDONR vector. This allowed for integration into the modified *Gt(ROSA26)Sor* locus of ES cells (Fig. 38A). ES cell clones with correct integration were identified as described in Vidigal *et al.* (2010). From these *Tg(FamA+B KD)* ES cells, embryos were generated by tetraploid complementation. A subgroup of the foster mice was treated with doxycycline from E2.5 onwards and embryos were dissected at E10.5 and E17.5.

The functionality of the transgene was examined by analysing the EmGFP expression from the cassette and quantification of the knock-down of *Fam181a* and *Fam181b*
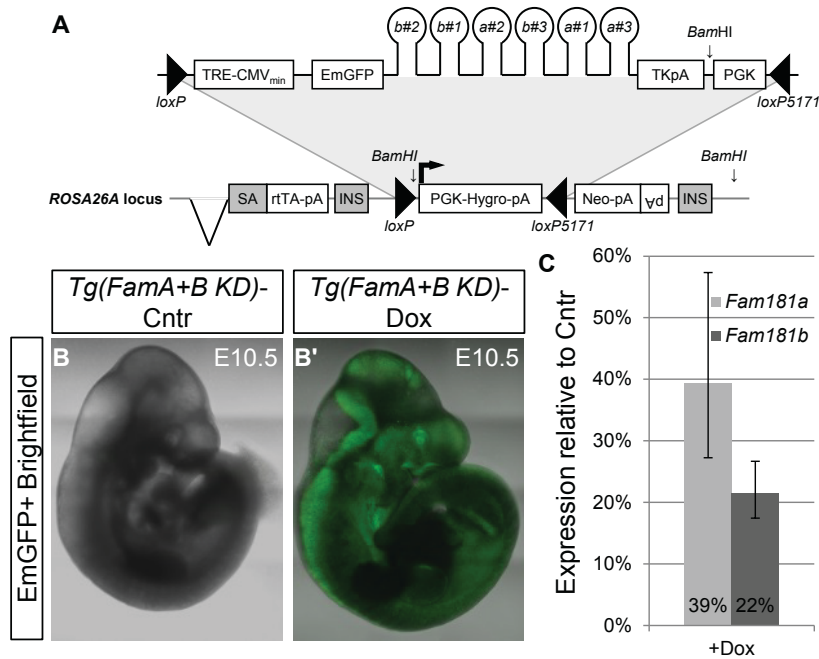
Figure 38. Generation of a *Fam181a/b* double knock-down
A: Schematic representation of the double knock-down construct integrated into the modified
Gt(ROSA26Sor) locus of ROSA26A ES cells. B-B': E10.5 Embryos derived by tetraploid
aggregation show EmGFP expression , upon treatment of foster mice with Dox from E2.5
onwards (B'). Embryos from untreated mice (B) did not show fluorescence. C: Real-time
quantification of *Fam181a* and *Fam181b* from E10.5 whole embryo lysates relative to control
embryos (n=2 for each). Normalization was done to *Pmm2*.

in induced embryos. The administration of doxycycline to the foster mice resulted
in an ubiquitous green fluorescence in E10.5 embryos, which was absent from control
embryos (compare Fig. 38B to B'). The quantification of transcript levels on cDNA
derived from total RNA of whole embryo lysates (n=2 for each) showed a decrease for
both *Fam181a* and *Fam181b* down to 39% and 22% respectively, compared to control
embryos (Fig. 38C). This shows functionality of the transgene, though a portion of
Fam181 gene products remained after induction. The induced transgenic embryos were
indistinguishable from the controls. Further analysis by WISH for *Sox2* and *Sox10*,
showed a similar expression of those marker genes in control (Cntr) and doxycycline-
treated embryos (Dox; see Fig. 39A-B'). The neurofilament antibody staining to high-
light the cranial nerves showed the normal, expected patterning (Fig. 39C; compare to
compare to elsewhere, e.g. Cordes, 2001). At E17.5 only one induced embryo and no
control embryos were retrieved (foster mice n=1 each). The single doxycyline-treated
embryos showed only partially closed eyelids (Fig. 39D-D'), while its skeleton appeared
normally developed (Fig. 39E, compare to 20D or 24F).

In summary, the double knock-down of *Fam181a* and *Fam181b* did not appear
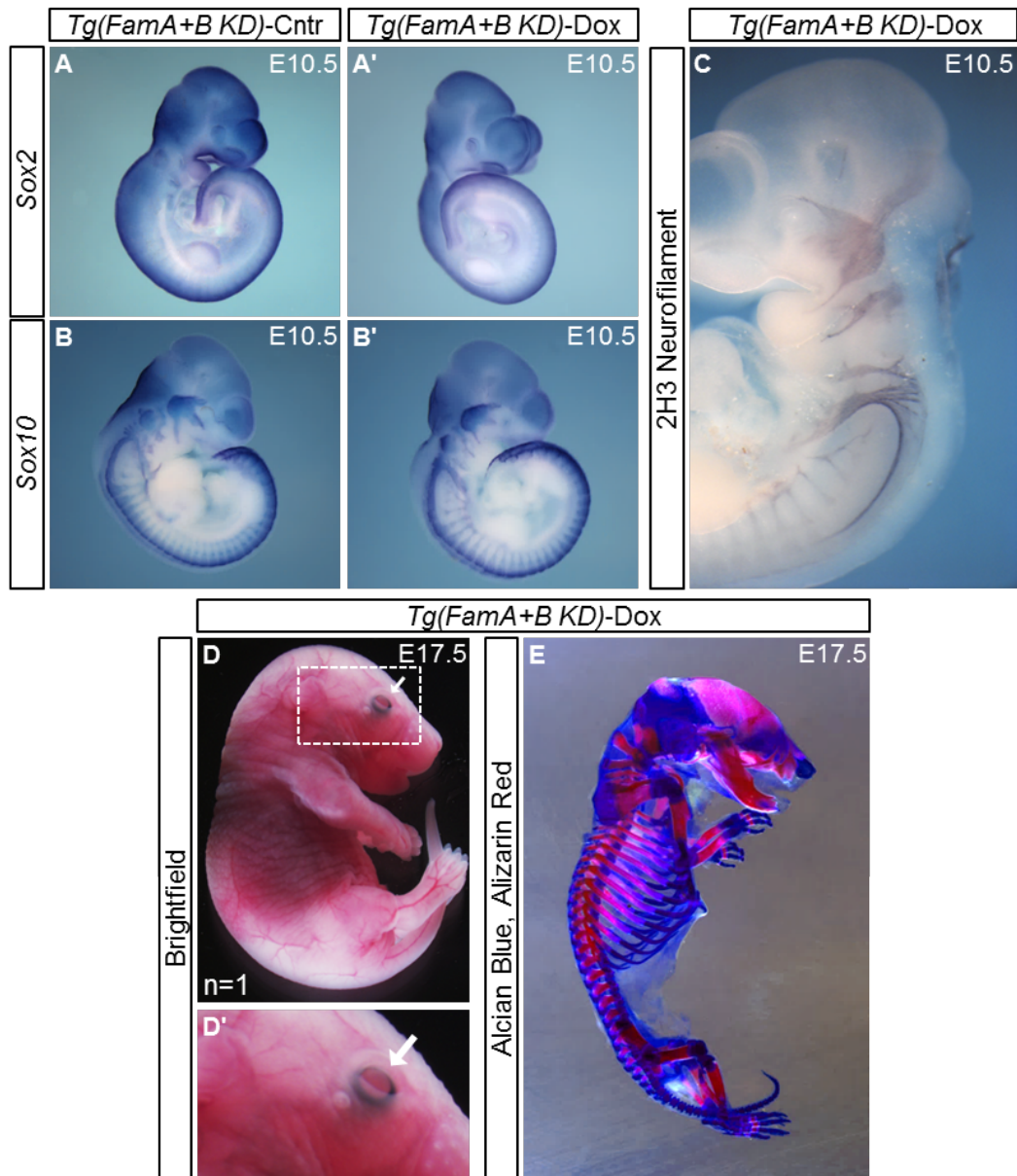
Figure 39. Analysis of Tg(*FamA+B KD*) embryos

A-B': WISH on E10.5 Tg(*FamA+B KD*) embryos generated by tetraploid aggregation hybridized with a probe for either *Sox2* (A-A') or *Sox10* (B-B'). For transgene induction, Dox was applied to foster mice from E2.5 onwards. C: αNeurofilament immunostaining on E10.5 embryos Dox-treated since E2.5. D-E: At E17.5, the single Dox-treated embryo retrieved from the foster mouse showed partially open eyelids (D-D'). D': Magnification of boxed region in D. E: Skeletal preparation of E17.5 embryo stained with Alcian Blue and Alizarin Red to highlight the cartilage and bones, respectively.

to alter embryonic development up to E17.5. Using the described combination of 6 shRNAmirs, about 60% of total *Fam181* activity remained after transgene induction from E2.5 onwards. In E17.5 embryos a eyelid closure defect was observed, though this observation was limited to one embryo. Further experiments are required to investigate

the phenotypic outcome of the *Fam181a/b* loss-of-function.

2.3 Experimental contributions

Lars Wittler, Phillip Grote, and Bernhard G. Herrmann conceived and supervised the project. Lars Wittler and Phillip Grote identified *Fam181b* as candidate gene from the cycling screen performed in our department and began the initial analysis. Sandra Währisch generated the ROSA26A recipient cell line. Vibratome sections and *in situ* hybridization on paraffin sectioned were done in collaboration with Tracie Pennimpede. Immunoblot analysis were done in collaboration with Lisette Lange. Karol Macura, Judith Fiedler, and Lars Wittler performed the diploid and tetraploid complementation assays. Behavioural tests were designed by me and executed by Dijana Wrembel. Mouse caretaking was done by Christin Franke and Dijana Wrembel. All other experiments were planed and executed by me, including tests, cloning of exchange vectors and targeting constructs, generation and verification of transgenic ES cell lines, *in situ* hybridisation experiments, and embryo analysis.

3 Discussion

The aim of this study was to characterize and analyse the murine *Fam181* gene family during development. This family contains two, so far uncharacterized genes, namely *Fam181a* and *Fam181b*. The latter is a candidate which was previously identified in a screen for cyclic genes within the presomitic mesoderm (PSM) and thus served as the main focus for the current work.

The phylogenetic analysis described here revealed the *Fam181* family as conserved within the vertebrate phylum, with both paralogues being present in almost all species investigated. Thus, it is likely that the presence of both *Fam181a* and *Fam181b* reflects the ancestral state in vertebrates. Further, this study provides the first comprehensive analysis of their expression patterns during development, as well as their presence in several adult organs. The expression was found to be mainly associated with structures of the nervous system, an observation confirmed by *in vitro* differentiation experiments. Both proteins share several highly homologous regions, and were found to localize to the nucleus. Given that the mutation of *Fam181b* alone did not disturb normal embryonic development, both genes are likely able to compensate for one another in their, yet to be identified, function.

3.1 *Fam181b* oscillates in-phase with Notch target genes in the mouse segmentation clock

Fam181b was already predicted to exhibit oscillatory gene expression by a screen for cyclic for cyclic expression within the PSM (Dequéant *et al.*, 2006) as well as through a similar screen independently performed in our department (Wittler, L., Grote P., Werber, M., and Herrmann,B.G., unpublished data) (see Fig. 5B-C). With the *in situ* probe generated in this thesis it was possible to visualize, and thus verify, the expression in the PSM. The observed pattern of *Fam181b* mRNA expression in the PSM varied between embryos with respect to its antero-posterior expansion. By using tail half cultures it was possible to prove that these changes indeed reflected an oscillatory PSM expression. In mouse, the segmentation clock and its target genes show oscillations about every 120 min (Tam, 1981). Using different temporal delays between the two

tail halves cultured *in vitro*, it was possible to show that the changes observed for the *Fam181b* pattern reflected an oscillation in-phase with the segmentation clock. When the delay was smaller than 120 min, differences between both halves were observed (see Fig. 6B-B'), while a delay of 120min resulted in a similar pattern in both halves (see Fig. 6B").

The mouse segmentation clock consists of alternating phases of Wnt- and Notch-/Fgf-signalling activity (Aulehla *et al.*, 2003; Dequéant *et al.*, 2006). While both screens predicted cyclic PSM expression of *Fam181b*, their positioning with respect to the Notch and Wnt phase of the clock were contradictory. In the screen by Dequéant *et al.* (2006), *Fam181b* oscillated in-phase with typical Wnt-target genes such as *Axin2* (Aulehla *et al.*, 2003), *Dkk1* (Niida *et al.*, 2004; Dequéant *et al.*, 2006), and *Trans-acting transcription factor 5* (*Sp5*; Harrison *et al.*, 2000; Weidinger *et al.*, 2005; Dequéant *et al.*, 2006). The screen performed in our department, on the other hand, suggested a position in-phase with known targets of Notch- and Fgf-signalling, like *Lfng* (Forsberg *et al.*, 1998; McGrew *et al.*, 1998; Aulehla and Johnson, 1999; Morales *et al.*, 2002) or *Dual specificity phosphatase 4* (*Dusp4*; Dequéant *et al.*, 2006; Niwa *et al.*, 2007). By comparison of the *Fam181b* expression pattern with either that of *Lfng* or *Dkk1* in-phase-matching caudal end halves, it was possible to show that *Fam181b* cycles in synchrony with Notch-target genes (Fig. 7). This confirmed the prediction of the screen performed in our department. Both screens accurately verified the expected antiphase oscillations of known Wnt- and Notch-/Fgf-target genes, thus demonstrating their general functionality. One major difference between the two screens was the mouse strain used: CD1 in the screen by Dequéant *et al.* (2006) and NMRI in our screen. The tail half cultures shown in this thesis are based on CD1 embryos, though similar results were obtained for NMRI (Marks, 2010). There are several more biological, technical, and bioinformatic differences between the two cycling screens, such as the portion of the caudal end tissue used, and the microarray used. It is likely that the sum of these differences, together with the relatively low expression levels of *Fam181b* noted in this thesis, are able to account for the identified discrepancies. On the tissue level, *Fam181b* transcriptional oscillations are clearly in-phase with Notch-target genes. The analysis of *Dll1* null mutants further showed a dependency of *Fam181b* PSM expression on Notch signalling activity. In these mutants, PSM is still formed but its segmentation is heavily impaired (Hrabe de Angelis *et al.*, 1997). *Fam181b* PSM expression was absent from the null mutants (see Fig. 11B,D-D'). The improper segmentation in the $Dll1^{-/-}$ embryos is also reflected in the *Fam181b* expression in the spinal nerve precursors, which migrate as a connected sheet of cells along the trunk rather than in distinct, separated streams. Whether or not *Fam181b* is a direct target of Notch signalling

remains to be elucidated.

3.2 *Fam181b* shows mouse strain-dependent expression differences

While investigating embryos derived from matings of heterozygous *Dkk1* knock-out animals (Mukhopadhyay *et al.*, 2001), the absence of detectable presomitic and lateral plate mesoderm expression of *Fam181b* was noted in all specimens, independently of their genotype (see Fig. 12A-A"). The embryos analysed were F1 offspring of 129s2 X C57BL/6J matings, while the earlier description of the *Fam181b* expression pattern was done on both CD1 and NMRI outbred embryos, and no differences were observed between these two latter strains. This suggests genetic background-dependent variation in transcriptional activity of *Fam181b*. To further investigate this, wild-type C57BL/6J and 129s2 embryos were analysed for their spatial *Fam181b* mRNA distribution patterns. While expression in the neural tissues and the limb anlagen was consistent in both inbred strains, *Fam181b* mRNA signals were undetectable in the presomitic and lateral plate mesoderm (see Fig. 12B-E'). This clearly demonstrated the genetic background-dependency of *Fam181b* expression with respect to these tissues. This finding is in line with a study performed by Kong *et al.* (2014), where the gene expression profiles of blood and brain cells, derived from either 129SvJae X C57BL/6J or pure C57BL/6J animals were compared. Among other genes, they identified *Fam181b* to be differentially expressed between these two wild-type lines.

The first domains of *Fam181b* expression which arose during the staining procedure of the WISH analysis were in neural tissues, namely the neural tube and the brain anlagen. Differences between the neural expression domains in C57BL/6J or 129s2 compared to the CD1 control embryos were not observed, neither regarding the time point when *Fam181b* mRNA signals became detectable, nor in the final staining intensity. This might argue for mesoderm-specific effects of the genetic background causing the observed differences. In line with this, neither presomitic nor lateral plate mesoderm expression became detectable after prolonged staining. The absence of a detectable signal in the WISH does not necessarily mean absent transcription. Another possibility would be that the *Fam181b* expression levels are generally reduced in the entire embryo. While domains with higher transcriptional activity in neural tissues and limb anlagen are still easily detectable by the WISH analysis, weaker expression domains might become undetectable due to the detection limit of the assay. The 129s2, C57Bl/6J, and the control CD1 embryos were all processed and stained simultaneously and no differences in the neural *Fam181b* expression domains were observed. This ar-

gues against a general reduction of *Fam181b* mRNA levels and shows the mesodermal specificity of the observed difference. Of course, it cannot be ruled out that there was a minor reduction of *Fam181b* levels which was undetectable using the WISH assay, while the parallel tissue-dependent impact of the genetic background was detected because it is stronger.

The *Dll1* mutants used in this thesis were originally generated on a mixed background between 129/Sv X 129/Sv-CP (R1 ES cells) and C57BL/6J (Nagy *et al.*, 1993; Hrabe de Angelis *et al.*, 1997). In our animal facility the line was kept on a CD1 outbred background. In the embryos *Fam181b* expression was easily detectable in the PSM of controls, and the lateral plate mesoderm (LPM) expression in both control and homozygous mutants (see Fig. 11). While not yet tested in a 129/Sv X 129/Sv-CP background, *Fam181b* expression was shown to be undetectable in the PSM of C57BL/6J. The finding of consistent *Fam181b* mRNA expression in the PSM and the LPM points to a large contribution of the CD1 background to the *Dll1* mouse line used. The loss of the PSM expression domain in the $Dll1^{-/-}$ embryos is thus thought to be caused by the impaired Notch signalling activity. It should be noted that, while pure CD1 and NMRI embryos showed signals for *Fam181b* mRNA in the PSM at a penetrance of 100% (n=13/13, see Fig. 12F-F'), the embryos wild-type or heterozygous for *Dll1* showed this in only 92.7% (n=51/55, see Fig. 11A/C). This discrepancy might be caused by the remaining contribution from the C57BL/6J and/or 129/Sv X 129/Sv-CP background.

If the findings described in this thesis hold true, *Fam181b* would be the first gene reported to show strain-dependent expression in the PSM. It remains to be investigated whether other genes identified by the two cycling screens are dependent on the genetic background withn respect to their cyclic and/or PSM expression. A cycling screen performed on other mouse strains would help to solve this question, and might reveal a new level of evolutionary plasticity and complexity in the mouse segmentation clock.

3.3 Expression data suggests function of *Fam181b* in neural tissues

This study has provided a first comprehensive analysis of *Fam181b* expression during murine embryonic development and in several adult tissues. The combined use of *in situ* hybridisation, quantitative and semi-quantitative PCR, and *in vitro* differentiation showed a direct positive correlation of *Fam181b* expression with neural tissues, starting during mid-gestational development at E7.5 and continuing into adulthood. The simultaneous presence of *Fam181b* mRNA detected in ganglia, nerves, and also

cartilaginous structures in the head of E14.5 embryos (see Fig. 10G-G""), reflects the common origin of these cells from the neural crest. This is in line with other findings made during this study, that link *Fam181b* to neural crest cells (NCCs). *Fam181b* expression was detected in several cranial nerves, namely in the ganglia of the trigeminal (V), the vestibulocochlear (VIII), the glossopharyngeal (IX), and the vagus (X) nerve (see Fig. 9C and Fig. 10G-G"), and in the dorsal root ganglia along the trunk (see Fig. 9D',E/E'). All of these neuronal structures are derivatives of the neural crest (Serbedzija *et al.*, 1990; Chai *et al.*, 2000). The hyoid bone is another structure originating from NCCs, and partially from those located near rhombomere 4 (Couly *et al.*, 1993; Frohman *et al.*, 1993). *Fam181b* was detectable in both the rhombomere 4 at E8.5-E9.5 (see Fig. 8C-D") and in the hyoid bone at E14.5 (see Fig. 10G""). Overall these findings support the notion that *Fam181b* expression is linked not only to neural structures of the central nervous system, but also to those of the peripheral nervous system mainly deriving from NCCs. A more detailed analysis is required to identify at which stage of NCC development and migration *Fam181b* transcription becomes activated.

The influence of NCCs is not limited to the developing embryo. So-called neural-crest derived stem cells (NCSCs) are present in different adult tissues, e.g. heart (Tomita *et al.*, 2005), the bone marrow of the femur and tibia, and the whisker pads (Nagoshi *et al.*, 2008). A characteristic feature of these NCSCs is their capability to differentiate into various cell types typically formed by NCCs (Nagoshi *et al.*, 2008). The study of Nagoshi *et al.* (2008) further revealed differences in the expression of NCC marker genes between different types of NCSCs, mainly depending on the tissue they were derived from. *Fam181b* mRNA was also detected in the whisker pads (see Fig. 8H and Fig. 10G"'), in progenitor structures of the limb skeleton (see Fig. 8G-H"' and ig. 10A-F), and the adult heart (see Fig. 13). However, the expression of *Fam181b* in NCSCs remains to be investigated.

The *in vitro* differentiation of murine ES cells into the neural lineage as described by Bibel *et al.* (2004, 2007) generates pyramidal glutamatergic neurons, positive for the tyrosine kinase receptors TrkB and TrkC from Pax6-positive radial glia cells. Using this differentiation protocol it was possible to show that *Fam181b* expression was correlated with neural differentiation (see Fig. 14). Although *Fam181b* was already detectable at day 2 of differentiation (day8+2 in Bibel *et al.*, 2007), its levels rapidly increased upon application of retinoic acid at day 4, making it comparable to the *Pax6* expression. The maximum *Fam181b* expression levels were observed in neural progenitor cells (day8 to day8+2hours after seeding). With the terminal differentiation into the glutamatergic neurons, its transcription decreased again. This might reflect a restriction of *Fam181b*

expression to neural progenitor cells, however, that does not exclude that transcription may continue in non-neuronal cells of the nervous system. In line with this is the finding that *Fam181b* transcripts are enriched in astrocytes (Lovatt *et al.*, 2012) and the observation that its expression was also found in the adult brain (see Fig. 13), when neuronal precursors become less frequent. It should be noted, that the differentiation program was stopped 1 day after the start of terminal differentiation. Thus, it cannot be ruled out that *Fam181b* levels are maintained in neuronal cells at lower levels. Maintaining neural differentiation for a longer period of time would be one possibility to investigate this issue, at least for glutamatergic TrkB- and TrkC-positive neurons.

Notch-signalling is very important for neural development and maintenance of proper brain function in adulthood, as reviewed in Louvi and Artavanis-Tsakonas (2006). It can activate the expression of the bHLH transcription factors of the *Hairy and enhancer of split Hes* gene family, thereby preventing the differentiation into neurons (Coffman *et al.*, 1993; Ishibashi *et al.*, 1994; Sakamoto *et al.*, 2003). While the downregulation of Notch activity leads to increased formation of neurons (Austin *et al.*, 1995), Notch activity can both maintain progenitor cells and promote the differentiation into glial lineage (Scheer *et al.*, 2001). The $Dll1^{-/-}$ embryos show, besides the segmentation defects mentioned above, also defects in neural development (Hrabe de Angelis *et al.*, 1997). *Fam181b* expression was visibly reduced in the telencephalic regions of these embryos (see Fig. 11B,D-D'). This might be due to premature neuronal differentiation due to impairment of Notch signalling activity in these embryos. This would be in line with the reduction of *Fam181b* seen during terminal differentiation into neurons (see Fig. 14) and supports the notion that *Fam181b* is expressed in neural progenitor and non-neuronal cells of the nervous system. Similar to the PSM, Notch signalling activity oscillates in neural progenitor cells, leading to cyclic expression of proneuronal *Dll1* and NPC-maintaining *Hes1* (Kageyama *et al.*, 2008; Shimojo *et al.*, 2008). In contrast to somitogenesis, this oscillatory gene expression does not appear spatially synchronized but rather presents as a salt-and-pepper pattern. A more detailed analysis of *Fam181b* expression in the different cell types of the developing and adult nervous system is required to identify to which of the neural lineages it is restricted. Given its oscillations during segmentation, *Fam181b* clearly fulfills the biochemical requirements for a cyclic gene. This makes it possible that *Fam181b* would oscillate in neural progenitor cells too.

A striking feature of the *Fam181b* expression pattern is the sharp juxtaposition of *Fam181b*-expressing cells in the midbrain to *Fam181b*-negative cells in the anterior hindbrain. The contact region between those domains correspond to the midbrain-hindbrain-boundary, also called isthmic organizer, an important organizing center for

proper brain development (reviewed in Wurst and Bally-Cuif, 2001). Initial positioning of this organizer depends on adjacent expression domains of the *Orthodenticle homolog 2* (*Otx2*) and *Gastrulation brain homeobox 2* (*Gbx2*) (Simeone *et al.*, 1992; Wassarman *et al.*, 1997), while Notch signalling seems to be required for specifying the boundary cell fate and cell sorting (Tossell *et al.*, 2011). In the *Dll1* mutants, the separation of the *Fam181b* positive and negative domains was maintained, though it appeared less distinct. This is likely due to partial compensation of *Dll1* function by another Notch-ligand, namely *Jagged 2* (*Jag2*, the mouse homologue of *Serrate 2*), both expressed in the anterior hindbrain region (Tossell *et al.*, 2011).

In summary, *Fam181b* shows a highly dynamic expression pattern during mouse embryonic development and remains present in various adult tissues. Strong expression was detected in neural tissues, potential neural progenitors. It seems thus likely that the main function of *Fam181b* resides in neural tissues.

3.4 FAM181 proteins are conserved in vertebrates with two paralogues per species

The *Fam181* gene family was identified based on sequence similarity from high throughput sequence annotations. The other family member of *Fam181b* is *Fam181a*. To investigate whether the lack of an obvious phenotype for the *Fam181b* loss-of-function could be caused by compensation through FAM181A, their protein sequences were compared and a phylogenetic analysis done including their vertebrate sequence homologues. Interestingly, the Esemble Genome Browser states that the murine *Fam181b* is a pseudogene (ENSMUSG00000051515) containing a frameshift mutation. Pseudogenes are considered to originate from functional genes by duplication events, followed by the acquisition of mutations leading to disruption of their processing, and thus absence of a protein product (rev in. Mighell *et al.*, 2000; Balakirev and Ayala, 2003). The results obtained during this study argue against the annotation of *Fam181b* as a pseudogene. First, by the knock-in of a C-terminal V5 tag into the endogenous *Fam181b* locus it was possible to detect a protein product of the expected size in transgenic embryos (see Fig. 17A). This protein was absent from unmodified wild-type embryos, ruling out unspecific detection by the antibody used. This clearly demonstrates the protein-coding capacity of the murine *Fam181b* gene. In line with this, other annotated pseudogenes have been shown to encode functional proteins (Betran *et al.*, 2002; Kandouz *et al.*, 2004; Zhang *et al.*, 2006) challenging their original annotations. Given the lack of any function, and thus the absence of a selective pressure, pseudogenes are further expected to show an increased mutation rate (Blake *et al.*, 1992). Though

the molecular function of Fam181b remains to be identified, the phylogenetic analysis performed in the course of this thesis proved the conservation of both FAM181A and B proteins throughout the vertebrate phylum (see Fig. 30B). Interestingly, in other species such as human, chimpanzee, and rat, *Fam181b* is annotated as protein-coding gene.

Within the FAM181 proteins investigated it was possible to identify 3 boxes highly conserved in respect to their amino acid sequence (see Fig. 30A, red boxed region). Further, a proline-rich stretch was found in all proteins, though the exact composition of this was variable (see Fig. 30A, highlighted in green). In line with the sequence conservation of the FAM181 paralogues, high similarity for the predicted secondary structures was identified for both murine proteins.

In most species investigated, two paralogues were identified. While one showed a higher similarity to the mFAM181A, the other seemed closer related to mFAM181B. From this it can be concluded that the presence of two FAM181 paralogues reflects the ancestral state in vertebrates. The only exception was the non-avian reptile *Alligator mississippiensis* (American alligator), where only a FAM181A orthologue was recovered. This is likely due to its still incomplete genome sequence (St John *et al.*, 2012), but might also reflect a secondary loss.

Taken together, the analysis reveals that the FAM181 protein family is highly conserved in vertebrates, usually with both paralogues present. Given their similarity, it is likely that both genes resulted from a duplication event. Additional investigations are required to identify homologues outside the vertebrate phylum and the evolutionary time-point, when this putative duplication occurred. The findings of this thesis provide evidence that the murine *Fam181b* gene is a functional, protein-coding gene rather than a pseudogene. The three boxes of highly conserved residues and the proline-rich stretch which were uncovered by bioinformatic approaches could possibly have a role in the function of the proteins.

Both murine FAM181 proteins were found to localize to the nucleus (see Fig. 15 and Fig. 35), though no known nuclear localization signal was uncovered. An *in silico* search for such signals using the NLStradamous tool (Nguyen Ba *et al.*, 2009) identified a possible motif in mFAM181B (amino acid residues 83-95), though a similar search for mFAM181A did not yield any results. Given their conservation it seems very likely that the mechanism for their localization to the nucleus is also conserved. Structural predictions revealed similarity of the conserved box 3 and a small region upstream of it with the YAP-TEAD4 interaction domain of the mouse YAP1 protein (Chen *et al.*, 2010). YAP requires TEAD proteins for its nuclear localization and to exert its function (Vassilev et al. 2001; Cao et al. 2008). However, deletion of box3 from the generated

FAM181B-V5 expression construct resulted in continued nuclear localization of the protein. Another, yet unidentified, domain within the FAM181 proteins is responsible for their subcellular localization. Further experiments are required to validate the localization of endogenous proteins under native conditions and to investigate their functions.

3.5 Gain- and loss-of-function of *Fam181b* do not interfere with normal embryonic development

To address the putative function of *Fam181b* during development and in adult mice, several approaches were used during this study. Two of these approaches relied on a modified version of the *Gt(ROAS26)Sor* locus. This locus is suitable for an ubiquitous expression in embryos (Zambrowicz *et al.*, 1997; Soriano, 1999) and upon further modification suitable for inducible expression of transgenes (Vidigal *et al.*, 2010; Riemer *et al.*, 2014). Therefore, this locus was used for both the expression of an additional copy of *Fam181b* to achieve a gain-of-function, and the expression of short hairpin RNAs to knock-down *Fam181b* transcripts. In both cases the functionality of the doxycycline-inducible transgene expression was verified on the level of ES cells and in embryos. Interestingly, for the gain-of-function approach the increase in *Fam181b* levels upon doxycycline treatment measured about 50-fold in ES cells (see Fig. 18C) and 8-fold change in whole embryos compared to controls (see Fig. 19C). While *Fam181b* mRNA was almost absent in ES cells, judged by real-time qPCR, there were several tissues showing endogenous *Fam181b* expression in the embryo (see Fig. 8). This could explain the discrepancy observed between the ES cells and the embryo samples. In tissues showing *Fam181* expression endogenously, the gain-of-function results in an upregulation of its mRNA levels, while in all other tissues ectopic expression is gained (compare Fig. 19D to D'). From the obtained results it seems likely that the missexpression of *Fam181b* in other tissues has no impact on the proper development of these. Its overexpression did not alter embryonic development either, though it can not be ruled out that the gain of expression levels was too low to achieve any disturbance in the *Fam181b* positive tissues. The usage of a stronger promoter or another transgenic system could help to address this point.

While the tdTomato fluorescence encoded by the gain-of-function transgene appeared homogeneously in E9.5 embryos, at E10.5 there were clear visible differences in the distribution of fluorescence intensity over the embryos. Such differences were not observed when an EmGFP was used as a fluorescence marker, as for the knock-down systems described here, or in other comparable approaches (Reinke, 2012 and personal

observations). It seems thus unlikely that these differences are due to expression differences from the *Gt(ROSA26)Sor* locus. In line with this, *Fam181b* expression in doxycyline-treated gain-of-function embryos was ubiquitously distributed, as revealed by WISH analysis. The non-homogeneous fluorescence distribution might, however, be an artefact resulting from the increased specimen thickness, tissue architecture and the microscopic setup used for image acquisition.

The more detailed analysis of E10.5 gain-of-function embryos showed a wild-type pattern of *Sox2* expression (see Fig. 20A-A'). This indicates that neither the ectopic expression of *Fam181b* in non-neural tissues, nor its overexpression in neural tissues had an impact on their proper development. The *Sox10* expression pattern and the skeleton preparation further showed normal NCC migration, segmental patterning, and limb development (see. Fig 20B-D'). Morphologically, all stages investigated were of a wild-type phenotype. Taken together, this suggests that the putative function of *Fam181b* in neural tissues resides downstream of neural induction. Further experiments are required to analyse whether *Fam181b* is able to disturb the ratio between neuronal versus non-neuronal cells. The generation of adult animals from embryos treated with doxycycline might help to identify such perturbations.

Knock-down of *Fam181b* showed wild-type expression patterns for *Sox2* and *Sox10*, suggesting no impact on neural induction, NCC development, or segmental patterning of the anteroposterior axis (see Fig. 24A-B). The latter was further demonstrated by the skeletal preparations, which showed no differences between induced and uninduced embryos (see Fig. 24F-F'). While up to E12.5 the morphology of doxycycline-treated embryos was unaltered compared to the controls, at E17.5 all induced embryos displayed bilaterally open eyelids (see Fig. 24C-E). During normal eyelid development in the mouse an epithelial sheet starts to protrude from the periphery over the cornea beginning at E15.5, and closed eyelids are observed by E17.5 (Harris and McLeod, 1982; Findlater *et al.*, 1993). The eyelid closure defect was observed in embryos derived from several foster mice with 100% penetrance.

Interestingly, this defect was not recapitulated in *Fam181b* knock-out embryos, suggesting that the open eyelids were not caused by the reduction of *Fam181b* levels. A possible explanation would be that the phenotype was caused by doxycycline administration, although a similar treatment was applied to the gain-of-function embryos, which did not display defects in eyelid closure. BLAST analysis of the targeting sequence used for the short hairpin RNAs confirmed their specificity for *Fam181b*, making it unlikely that another unintended gene was affected. In fact, double knock-down of both *Fam181a* and *b* genes lead to a less severe open eyelid phenotype at E17.5, though this observation was limited to a single embryo and thus requires further analy-

sis. Although a remote possibility, a compensatory feedback circuit between both genes may exist, which only becomes activated when one of their levels falls under a certain threshold. In the case of the *Fam181b*-null embryos this would allow for compensation by *Fam181a*, preventing the eyelid closure defect. The remaining *Fam181* activity in the case of both knock-downs, on the other hand, might be enough to prevent such a circuit from becoming activated.

In line with the results obtained from the *Fam181b* knock-down (except for the eyelid closure defects), the knock-out embryos generated during the course of the thesis were normally developed embryos at all stages investigated (see Fig. 26D and Fig. 27). The proper cranial nerve pattern observed in E10.5 embryos suggests that midbrain-hindbrain organization by the isthmic organizer was established correctly. Skeletons of the *Fam181b*-null embryos were indistinguishable from those of heterozygous and wild-type littermates. Further, $Fam181b^{-/-}$ offspring were viable and fertile.

An alteration in the ratios of neuronal versus non-neuronal cells is not necessary linked to embryonic or early postnatal lethality or morphological changes. They can also lead to neurological disorders that become overt as an abnormal behaviour. Two simple behavioural tests were done in adults to analyse the animals for such neurological phenotypes in general activity (Test for activity upon stimulation) and coordination (Tail-supsension test). While no difference were observed in the latter, the activity upon stimulation showed an non-significant increase in inactive animals. This observation is based on 1 litter, containing 5 homozygous and 2 heterozygous *Fam181b* knock-out animals. Several other tests are possible in order to assess neurological properties such as muscle strength or gait (rev in. Crawley, 2008). A comprehensive and standardized protocol for the identification and characterization of more subtle phenotypes is, for example, provided by SHIRPA (Rogers *et al.*, 1997). The tests described there, as well as a variety of other possible tests, all require special equipment, often authorization from the responsible federal governmental institution, along with a large number of age-matched litters to obtain conclusive results. Given that the capacity of our animal facility is limited and not specialized for the analysis of behaviour, a collaboration would be needed to continue the investigation of the behaviour of adult *Fam181b* knock-out animals.

The generated mutants were all produced in F1G4 ES cells, which are of a 129s6/SvEvTac X C57BL/6Ncr genetic background (George *et al.*, 2007). These strains have not been tested in detail for their *Fam181b* expression pattern so far. It could be possible, that expression in the presomitic and/or lateral plate mesoderm is reduced or absent from embryos of this background. This might exclude possible effects in these tissues *per se*. Further investigations are required to examine this possibility and to analyse the

functionality of *Fam181b* in the PSM and the LPM on backgrounds defined for their *Fam181b* expression.

In summary, the *Fam181b* mutants generated in this thesis appeared to develop normally up to E17.5. Loss-of-function of *Fam181b* lead to vital and fertile offspring. The failure in eyelid closure observed in the doxycyline induced knock-down embryos and the putative behavioural phenotype in adult loss-of-function animals requires a more detailed investigation before conclusive results can be drawn.

3.6 FAM181A might functionally compensate for loss of FAM181B

The comparison of the *Fam181* gene family on the protein level revealed the presence of two paralogues conserved in the vertebrate phylum. Further, these proteins share several highly similar regions. The *Fam181b* mutants generated in the course of this thesis showed no alterations in the developing embryo and/or adult mice, neither in gain-of-function nor in the loss-of-function approaches. This might due to a compensatory potential between the FAM181A and FAM181B proteins. The detailed, comprehensive analysis of the murine *Fam181a* expression described here, supports such a possibility.

Both *Fam181a* and *Fam181b* showed first signs of expression in the prospective midbrain region, where strong levels were maintained in all stages investigated, compared to surrounding tissues (compare Fig. 32 to 8). Both genes showed transcriptional activity in the neural tube. Notably, *Fam181a* was expressed along the entire dorsoventral length of the neural tube, while *Fam181b* seemed to be restricted to a medial portion and in later stages additionally to the roofplate. Partial overlap was also observed in the hindbrain, where *Fam181a* mRNA was detectable everywhere except for a temporally restricted gap at the position of rhombomere 5 (see Fig. 32C-D"). In contrast, *Fam181b* expression was mainly detected in the region around rhombomere 4, and formed a sharp boundary between the *Fam181b* positive midbrain and the *Fam181b* negative anterior hindbrain (see Fig. 8C-D"). An exclusive transcriptional domain for *Fam181a* was the eye anlagen (see Fig. 32D-H), while expression was undetectable in the PSM, the limb anlagen or the neural crest and its derivatives. Its strong association with the central nervous system might be indicative for a function of *Fam181a* in that tissue. In support of this idea, changes in its expression levels are observed in *in vitro* models for the neurodevelopmental disorders 18q21 deletion syndrome (Pitt-Hopkins syndrome) and 9q34 deletion syndrome (Chen *et al.*, 2014). In adults, both genes showed highest expression levels in the brain. *Fam181a* enrichment was higher

in the cerebrum than in the cerebellum, while the opposite was observed for *Fam181b*. In general, the amount of *Fam181a* transcripts detected in the brain exceeded those for *Fam181b*, though the efficiency of the used primer sets remains to be evaluated. Contrary to the strictly neural expression in the embryonic stages investigated, adults showed *Fam181a* expression in the ovary, similar to *Fam181b*, and in the lung. Lung expression is in line with studies reporting changes in CpG methylation of the *Fam181a* locus associated with asthma (Gunawardhana *et al.*, 2014; Wysocki *et al.*, 2014). Interestingly, one of the symptoms of the Pitt-Hopkins syndrome is breathing difficulties. This could be a hint for a possible link between *Fam181a* dysregulation and lung function. In the neural cells generated by *in vitro* differentiation of murine ES cells, *Fam181a* behaved comparably to its paralogue. It rapidly increased after the retinoic acid, treatment reaching its maximum expression between day 8 and the neural progenitor stage, before decreasing during terminal differentiation. This suggests that expression of *Fam181a* is either restricted to the progenitor cells or continues to be expressed in their non-neuronal descendants. The analysis of the FAM181A protein showed a localisation predominantly to the nucleus, overlapping with FAM181B.

In summary, *Fam181a* and *Fam181b* were partially coexpressed during development and in adults, especially in tissues of the central nervous system. Both showed comparable behaviour during the differentiation of ES cells into the neural lineage and their encoded proteins colocalised to the nucleus. With all of these findings it seems likely that *Fam181a* is indeed capable of at least partially compensating for the loss-of-function of its paralogue. It might be possible that *Fam181a* levels are increased in the *Fam181b*-null background by some kind of feedback mechanism. It remains to be investigated whether such a regulated compensatory mechanism might also account for tissues that displayed *Fam181b*, but not *Fam181a* expression in wild-type embryos and tissues. The double knock-down of both paralogues generated here was too weak to provide any conclusive results. Thus, the knock-out of *Fam181a* alone, and further the generation of a double knock-out, will help to further address these issues.

4 Abstract

In two independent screens for the identification of cyclically-expressed genes in the presomitic mesoderm (PSM) of the mouse embryo, *Fam181b* was predicted to display oscillating expression. This gene, as well as its closely related paralogue *Fam181a*, belong to the *Fam181* gene family which is thus far uncharacterized.

In this thesis, the expression patterns for *Fam181a* and *Fam181b* both during murine embryonic development, and in adult organs, are characterized. Both genes are mostly differentially expressed, starting at E7.5 and gaining complexity as development proceeds. *Fam181a* transcripts are mainly detectable in the neural tube, the brain vesicles, and the eye anlagen. *Fam181b* is also expressed in precursor structures of the central nervous system (CNS), and further in neural crest derived tissues, the PSM, the lateral plate mesoderm (LPM), and the limb anlagen. Since their expression patterns overlap in the CNS, this indicates a possible function for the *Fam181* gene family in the neural lineage.

The expression analysis further confirmed the predicted oscillation of *Fam181b* in the PSM. It was found to cycle in parallel to morphological somite formation (every 120 min in mice), and is in-phase with target genes of the Notch signalling pathway. Both PSM and LPM expression of *Fam181b* are detectable in wild-type CD1 and NMRI outbred strains, but not in the C57BL/6J and 129s2 mouse strains. This points to a dependency of *Fam181b* transcription on the genetic background. The proteins encoded by *Fam181a* and *Fam181b* localize to the nucleus and are both conserved within the vertebrate taxon. The presence of both paralogues per species is thus likely to be the ancestral state in vertebrates.

Despite its conservation in vertebrates, *Fam181b* gain- and loss-of-function embryos develop normally without any visible morphological phenotype. In addition, *Fam181b*-null animals are viable and fertile. The conservation of the FAM181 proteins, in combination with their partially overlapping expression, might be indicative of functional redundancy. Further investigations into the function of the *Fam181* gene family will thus require the generation of *Fam181a/b*-double mutants.

5 Zusammenfassung

In zwei unabhängigen Hochdurchsatzverfahren zur Identifizierung zyklisch exprimierter Gene im präsomitischen Mesoderm (PSM) des Mausembryos wurde eine oszillierende Expression von *Fam181b* vorhergesagt. Dieses Gen, ebenso wie dessen nahe verwandtes Paralog *Fam181a*, gehören zur *Fam181* Genfamilie und sind bisher noch uncharakterisiert.

In dieser Doktorarbeit werden die Expressionsmuster von *Fam181a* und *Fam181b* während der murinen Embryonalentwicklung und darüber hinaus in adulten Organen charakterisiert. Beide Gene sind in Embryonen von Tag 7.5 an differentiell exprimiert, wobei die Komplexität ihrer Expressionsmuster mit fortschreitender Entwicklung zunimmt. Die Transkripte von *Fam181a* sind überwiegend im Neuralrohr, den Gehirnventrikeln und den Augenanlagen detektierbar. *Fam181b* ist ebenfalls in den Vorläuferstrukturen des zentralen Nervensystems (CNS) exprimiert, darüber hinaus aber auch in von Neuralleistenzellen gebildeten Geweben, im PSM, im lateralen Plattenmesoderm und in den Anlagen der Extremitäten. Die Überlappung beider Expressionsmuster im CNS könnte auf eine Funktion der *Fam181*-Genfamilie in neuralen Geweben hindeuten.

Des weiteren konnte die vorhergesagte Oszillation von *Fam181b* im PSM durch die Expressionsanalyse bestätigt werden. Es oszilliert dabei parallel zur morphologischen Somitenbildung (alle 120 min in der Maus), in Phase mit Zielgenen des Notch-Signalweges. Sowohl die PSM-, als auch die im LPM-Expression sind in den Mausstämmen CD1 und NMRI, allerdings nicht in den Stämmen C57BL6J und 129s2 detektierbar. Das deutet auf eine Abhängigkeit der *Fam181b*-Transkription vom genetischen Hintergrund hin. Die von *Fam181a* und *Fam181b* kodierten Proteine sind im Zellkern lokalisiert und beide innerhalb der Wirbeltiere konserviert. Die Anwesenheit von zwei Paralogen scheint dabei der evolutionär ursprüngliche Zustand in Taxon der Vertebraten zu sein.

Trotz dieser Konservierung entwickeln sich Embryonen mit einem Funktionsverlust von *Fam181b* oder dessen Überexpression normal und ohne einen auffälligen morphologischen Phänotyp. Zudem sind adulte $Fam181b^{-/-}$-Tiere lebensfähig und fruchtbar. Die Konservierung der FAM181 Proteine, in Kombination mit deren partiell überlappender Expression, könnten Hinweise auf eine funktionelle Redundanz beider Gene sein. Für

eine weitere Untersuchung der Funktion der *Fam181*-Genfamilie wird es daher nötig sein, Doppelmutanten für *Fam181a* und *Fam181b* zu erzeugen.

6 Materials and Methods

6.1 General buffers and solutions

Standard buffers and solutions frequently used during the thesis are listed in Table 1. Their composition is indicated. All other buffers and solutions along with their composition are indicated when referred to.

Table 1. Standard buffers and solutions

Buffer/Solution	Composition
LB	1% Pepton/0.5% yeast extract/0.5% NaCl; adjusted to pH 7.8
PBS	137 mM NaCl/2.7 mM KCl/100 mM Na_2HPO_4/2mM KH_2PO_4; adjusted to pH 7.4
20x SSC	3 M NaCl/ 0.3 M Na-Citrat; adjusted to pH 7.0
TBS	50 mM Tris-HCl pH 7.5/150 mM NaCl
TE	10mM Tris-HCl pH 7.4/1mM EDTA pH 8.0

6.2 Sequences and sequence information

6.2.1 BACS

For the amplification of sequence elements from the *Fam181b* locus and its surrounding regions the*Fam181b* BAC (RP23-168D4 BAC; BACPAC Resources Center, Oakland, CA, USA) was used. Similarly, the *Fam181a* BAC (RP23-19B17; BAC-PAC Resources Center, Oakland, CA, USA) was used for the *Fam181a* locus and its surrounding regions.

6.2.2 Primer sequences

Table 2 lists all oligonucleotides used in the course of this study. Except for human (h) *Pmm2*-specific primers, all oligonucleotides were synthesized based on murine reference sequences. Stock solutions of 100 µM were prepared for each primer and stored at -20℃.

Table 2. Primer sequences

Primer Name	Sequence	Usage
Fam181b ISH fwd1	gtctgggtgacctggagaaa	Fam181b WISH probe (T7 antisense; T3 sense)
Fam181b ISH rev+T7 1	taatacgactcactataggggtagtcaggggaggacacca	Fam181b WISH probe (T7 antisense; T3 sense)
Fam181b ISH T3-fwd	aattaaccctcactaaaggggtctgggtgacctggagaaa	Fam181b WISH probe (T7 antisense; T3 sense)
Fam181a ISH fwd2	aattaaccctcactaaagggcaaggcccactctcagctac	Fam181a WISH probe (T7 antisense; T3 sense)
Fam181a ISH rev2	taatacgactcactatagggatgaacaagcgagatgcccc	Fam181a WISH probe (T7 antisense; T3 sense)
FamKO-Transcipt fwd2	aacaattgccaaagcctggctacgtaagc	Cloning Fam181b conditional KO
FamKO-Transcipt rev2	aagaattcgcaaagggggaaagaagggagg	Cloning Fam181b conditional KO
FKO 5'-loxP fwd	catgacaattgagccaatgtg	Cloning Fam181b conditional KO
FKO 5'-loxP rev	ggaagcttataacttcgtatagcatacattatacgaagtta tgatcttgtaagccagaggcg	Cloning Fam181b conditional KO
FamKO 3'arm fwd	aagcggccgcggaacagaggtatgtggtcattgag	Cloning Fam181b conditional KO
FamKO 3'arm rev	aagcggccgctgctatgccaccatccagta	Cloning Fam181b conditional KO
FKO-Seq1	ggttggaacacaggctttct	Sequencing Fam181b cKO targeting constructs
FKO-Seq2	gcttgatgttgctgg	Sequencing Fam181b cKO targeting constructs
FKO-Seq3	cgaagacgatgagagc	Sequencing Fam181b cKO targeting constructs
FKO-Seq4	cacccgaatcgttgcc	Sequencing Fam181b cKO targeting constructs
FKO-Seq5	gtgagtctgggtgac	Sequencing Fam181b cKO targeting constructs
FKO-Seq6	cccatcgttctctcc	Sequencing Fam181b cKO targeting constructs
FKO-Seq7	ggcatccagactgac	Sequencing Fam181b cKO targeting constructs
FKO-Seq8	gaagggactggctg	Sequencing Fam181b cKO targeting constructs

Primer Name	Sequence	Usage
FKO-Seq9	ccttcagcttccccac	Sequencing Fam181b cKO targeting constructs
FKO-Seq10	ctgcagcctgttgac	Sequencing Fam181b cKO targeting constructs
FKO-Seq11	gccgatatactatgccgatg	Sequencing Fam181b cKO targeting constructs
FKO-Seq12	caaacagctccctggtgtc	Sequencing Fam181b cKO targeting constructs
HindIII-FamA KOI 5' fwd	ggaagcttgacaagggctggatgtgtga	Cloning Fam181a KO
EcoRI-FamA KOI 5' rev	gggaattccaccacgagaactgtgcag	Cloning Fam181a KO
BamHI-FamA KOI 3' fwd	gaggatccctgaacaccctcagccctc	Cloning Fam181a KO
NotI-FamA KOI 3' rev	aagcggccgcccaatggaccagtgctgact	Cloning Fam181a KO
FKO5'-probe fwd1	acccctggagccatctcccttg	Fam181b 5' southern probe
FKO5'-probe rev1	ggcctcactgcttcatctgccc	Fam181b 5' southern probe
FAKO 5' probe1-fwd	ctgtgcaacggagggagaat	Fam181a 5' Southern probe
FAKO 5' probe1-rev	agtcccgagacctgtacctc	Fam181a 5' Southern probe
Neo probe fwd	ggcacaacagacaatcgg	Neo internal southern probe
Neo probe rev	taaagcacgaggaagcgg	Neo internal southern probe
Fam181a_nest1 fwd	ttgtcctccattcagcccac	cloning Fam181a transcript (incl. Intron; nested PCR)
Fam181a_nest1 rev	tgacgtcccatttgtcctgg	cloning Fam181a transcript (incl. Intron; nested PCR)
Fam181a transcript fwd	ctgcttctcagcctgca	cloning Fam181a transcript (incl. Intron; nested PCR)
Fam181a transcript rev	agaggtggaaactggaaaag	cloning Fam181a transcript (incl. Intron; nested PCR)
Fam181b-V5 transcript rev	cgtagaatcgagaccgaggagagggttagggataggcttac cgtctggatgccctccttcct	Fam181b transcript-V5 (fusion PCR)

Primer Name	Sequence	Usage
Fam181b-V5 transcript fwd	ggtaagcctatccctaaccctctcctcggtctcgattctac gtgactgcgaggaactcgttc	Fam181b transcript-V5 (fusion PCR)
Fam181b-delbox3 rev	gccgccgcagcccacagccactgagctcaccgcggtgccc	Fam181b-Box3 deletion (fusion PCR)
Fam181b-delbox3 fwd	gtgagctcagtggctgtgggctgcggcggcgccagcggcg	Fam181b-Box3 deletion (fusion PCR)
NdeI-Fam181a ORF-V5 fwd	aacatatggcagctgacagtgacgt	Fam181a-ORF-V5
SnaBI-Fam181a ORF-V5 rev	aagtacgtagaatcgagaccgaggagagggttagggatagg cttaccgaggtagccaaagacattga	Fam181a-ORF-V5
Fam181a-EmGFP Fam rev	ggtgaacagctcctcgcccttgctcaccatgaggtagccaa agacattga	Fam181a-ORF-EmGFP fusion (fusion PCR)
Fam181a-EmGFP GFP fwd	cccctatcttcaatgtctttggctacctcatggtgagcaa gggcgagga	Fam181a-ORF-EmGFP fusion (fusion PCR)
EmGFP rev	ggttacttgtacagctcgtcca	Fam181a-ORF-EmGFP fusion (fusion PCR)
Fam181b qPCR1 fwd	ggtgtcctcccctgactaca	qPCR/RT-PCR
Fam181b qPCR1 rev	gcagcgtccacctagcaaag	qPCR/RT-PCR
Fam181b (ORF) qPCR fwd1	cttcccagattgtgcgttgc	qPCR/RT-PCR
Fam181b (ORF) qPCR rev1	tctccagaggctggggtaaa	qPCR/RT-PCR
Fam181a real-time fwd1	cctatcccgactaagccagc	qPCR/RT-PCR
Fam181a real-time rev1	gccaaaagagagagggctga	qPCR/RT-PCR
Oct4 qPCR fwd	tgttcccgtcactgctctgg	qPCR/RT-PCR
Oct4 qPCR rev	ttgccttggctcacagcatc	qPCR/RT-PCR
Pax6 qPCr fwd	catggcaaacaacctgcctatg	qPCR/RT-PCR
Pax6 qPCR rev	gcacgagtatgaggaggtctgac	qPCR/RT-PCR

Primer Name	Sequence	Usage
TrkB qPCR fwd	agcagccctggtatcagcta	qPCR/RT-PCR
Trkb qPCR rev	cttgatgttcttccgggtgt	qPCR/RT-PCR
mPmm2 qPCR fwd	agggaaaggcctcacgttct	qPCR/RT-PCR
mPmm2 qPCR rev	aataccgcttatcccatccttca	qPCR/RT-PCR
Gapdh qPCR fwd	tcaagaaggtggtgaagcag	qPCR/RT-PCR
Gapdh qPCR rev	accaccctgttgctgtagcc	qPCR/RT-PCR
hPmm2 qPCR fwd	aagaagctgcagccaagaag	qPCR/RT-PCR
hPmm2 qPCR rev	gcctcctatggaaaacgtga	qPCR/RT-PCR
miR155 fwd	tgatctagagggcccgcggtt	qPCR/RT-PCR
miR155 rev	agcgcgggttccttccggtat	qPCR/RT-PCR
5' Dkk1 geno	gggagcctgagtataaaggc	Genotyping
3' Dkk1 geno	aagagtctggtacttgttcc	Genotyping
Dkk1_Mut 5'	gagagggcacagcgattaggt	Genotyping
Dkk1_Mut 3'	taccggtggatgtggaatgtg	Genotyping

6.2.3 Plasmids

The plasmids used during the thesis are listed in Table 3. Sequence elements were generally cloned into pBS (SK+) and sequenced before further usage. The pcDNA$^{(TM)}$ 6.2-GW/ +EmGFP-miR vector was used for shRNAmir cloning, chaining and their expression in eukaryotic cell lines. Except for pBS, the usage of all vectors listed below is mentioned in the results parts when concerned.

Table 3. Plasmids used

Plasmid	Usage	Resistance	Source/Reference
pBS (SK+)	standard cloning vector	Amp	Stratagene
pDONR	RMCE into mod. *Gt(ROSA26)Sor* locus	Amp	Vidigal *et al.* (2010)
pcDNA3	expression vector for eukaryotic cell lines	Amp	Clonetech
pcDNA$^{(TM)}$ 6.2-GW/ +EmGFP-miR	assembly and chaining of shRNAmirs	Spec	Life Technologies
PL451	assembly of homologous recombination constructs	Amp	Liu *et al.* (2003)
PGK-Cre	Cre-recombinase expression during RMCE	Amp	Dr. Heiner Schrewe

6.2.4 *In situ* hybridization probes

The *Fam181a*, *Fam181b*, and *Sox10 in situ* probes used in this thesis were synthesized as described in section 6.3.6. The DNA template for the *Sox10* probe was provided by Prof. Michael Wegner (Institute for Biochemistry, Emil-Fischer-Center, FAU Erlangen-Nürnberg). The *Dkk1* and *Lfng* probes were provided by Dr. Lars Wittler, the *T+Uncx* mixed probe by Dr. Joana DeCampos Vidigal, and the *Sox2* probe by Dr. Tracie Pennimpede, all ready-to-use. For WISH analysis, probes were added to hybridization buffer. This mixture was reused and stored at -20°C.

6.2.5 Reference sequences

For the phylogenetic analysis of the FAM181 proteins, the reference sequences listed in Table 4 were used.

Reference sequences for the *Fam181b* transcript (NM_021427.2), and for the *Fam181a* transcript (NM_001195726.1) were used. The *in situ* probes and oligonucleotides generated in this thesis were designed according to these sequences.

Table 4. Protein reference sequences

Species	Protein	Reference ID
Alligator mississippiensis	FAM181A	XP_006278984.1
Anolis carolinensis	FAM181A	XP_003214448.1
Anolis carolinensis	FAM181B	XP_008106372.1
Bos taurus	FAM181A	XP_594106.4
Bos taurus	FAM181B	NP_001094693.1
Danio rerio	FAM181A	XP_005169962.1
Danio rerio	FAM181B	XP_005157544.1
Gallus gallus	FAM181A	XP_003641418.1
Gallus gallus	FAM181B	XP_004939010.1
Homo sapiens	FAM181A	NP_612353.3
Homo sapiens	FAM181B	NP_787081.2
Macaca mulatta	FAM181A	gb|EHH28130.1
Macaca mulatta	FAM181B	NP_001180963.1
Monodelphis domestica	FAM181A	XP_001370835.2
Monodelphis domestica	FAM181B	XP_001377183.1
Mus musculus	FAM181A	NP_001182655.1
Mus musculus	FAM181B	NP_067402.2
Nematostella vectensis	predicted protein	XP_001627460.1
Pan troglodytes	FAM181A	XP_001143456.2
Pan troglodytes	FAM181B	XP_003313276.1
Xenopus tropicalis	FAM181A	gb|AAI35265.1
Xenopus tropicalis	FAM181B	XP_004912246.1

External Southern probes and homology arms for recombination were generated using the genomic regions surrounding the *Fam181a* and *b* loci. The according sequence information was extracted from the *Mus musculus* genome assembly GRCm38 (GCA_-000001635.4) using the Ensembl genome browser.

6.3 Nucleic acid methods

If not explicitly mentioned, molecular standard procedures on nucleic acids were carried out as described in the protocols provided by Sambrook and Russell (2001).

6.3.1 PCR, qPCR, and RT-PCR

The amplification of DNA fragments by polymerase chain reaction (PCR) was done using the PrimeSTAR® HS DNA polymerase kit (Takara Bio Inc., product no. R010A) according to the manufacturer's manual with slight modifications. The reaction volume was scaled down to 25 µl. If an increase in reaction stringency was required, 1 M Betaine (Sigma, product no. B0300-5VL) or 5% DMSO (v/v) were added to the reaction. The reactions were carried out in a thermal cycler (Mastercycler® Pro S, Eppendorf). If required, the amplified DNA was cleaned up directly from the PCR using the Wizard® SV Gel and PCR Clean-Up System (Promega, product no. A9281) according to the supplied protocol.

For real-time quantitative PCR (qPCR), the GoTaq® qPCR Master Mix (Promega, product no. A6001) was used with slight modifications to the protocol. The reaction volume was scaled down to 20 µl, containing the primers used in a concentration of 0.25 µM each. 0.5-1 µl cDNA was used per reaction and each analysis was carried out in triplicate. All reactions were set up in MicroAmp® Fast Optical 96-well Reaction Plates (Life Technologies, product no. 4346906). All qPCRs were carried out using a StepOnePlus Real-Time PCR System (Life Technologies). Visualization, evaluation, and relative quantification of the results was done using the StepOne Software v2.3 (Life Technologies). For the calculation of the mean normalized expression, the Q-Gene software was used (Muller *et al.*, 2002; Simon, 2003).

Semi-quantitative PCR (RT-PCR) was done using 2 µl of cDNA with the GoTaq® Flexi DNA polymerase Kit (Promega, product no. M7801) in a reaction as indicated in Table 5. As for standard PCR, the reaction was carried out in a thermal cycler (Mastercycler® Pro S, Eppendorf), with a PCR program according to the protocol.

Table 5. RT-PCR

Component	Volume	Final Concentration
5 x Green GoTaq® Flexi buffer	5 µl	1x
MgCl$_2$ (25 mM)	3 µl	3 mM
dNTP (10 mM each)	0.5 µl	0.2 mM each
Primer mix (5 µM each)	0.5 µl	0.1 µM each
GoTaq® DNA polymerase (5 U/µl)	0.13 µl	0.65 U
H$_2$O	13.87 µl	/

6.3.2 Preparation of plasmid and BAC DNA

To obtain plasmid DNA for analytical purposes the QIAprep Miniprep Kit (Qiagen) was used according to the supplied protocol. Large scale preparations were done using either the QIAprep Midi or Maxi Kit (Qiagen) according to the manufacturer's protocols.

To yield BAC DNA for use as a PCR template, this was extracted with a modified version of alkaline lysis purification (Bimboim and Doly, 1979) using the buffers supplied with the QIAprep Miniprep Kit (Qiagen). After centrifugation of the neutralized lysate, the DNA was precipitated by adding 0.6x vol. isopropanol and centrifugation for 10 min at 16.000 x g. This was followed by washing twice with 70% EtOH and centrifuged for 10 min at 16.000 x g. After drying, the DNA pellet was resuspended in 50µl 1xTE.

6.3.3 RNA extraction

For RNA extraction from embryos and tissues samples, these were transferred to Eppendorf tubes and lysed in TRIzol® Reagent (Life Technologies, product no. 15596-026) by vortexing vigorously. Cells in culture were lysed by adding the TRIzol® Reagent directly to the culture plate. After several minutes with slight shaking the suspension was transferred into an Eppendorf tube using wide-bored pipette tips. The samples were either stored in TRIzol® Reagent at -80°C or directly processed to RNA. Total RNA was extracted from the lysed samples using the RNeasy Plus Mini Kit (Qiagen, product no. 74134) according to the suppliers protocol with the following modification: the on-column RNaseI-digest was carried out for 30 min.

6.3.4 Quantification of nucleic acids

Quantification of DNA and RNA concentrations was done using the NanoPhotometer® (Implen). The reagent used for resuspension of the nucleic acid was also used for the blank reference.

6.3.5 cDNA synthesis

For synthesis of cDNA, 500-1000 ng of total RNA were reverse transcribed using the QuantiTect® Reverse Trancription Kit (Qiagen, product no. 205311) according to the supplied protocol. All incubations were carried out in a thermal cycler (Mastercycler® Pro S, Eppendorf). From one sample an additional reaction without reverse transcriptase was prepared as control for DNA contamination.

6.3.6 *In vitro* transcription

The generation of *in situ* hybridization probes, *in vitro* transcription was used to produce digoxygenin (DIG)-labelled RNA fragments. Either PCR products or linearised plasmids, both containing the probe region fused to DNA-dependent RNA polymerase promoter were used as templates.

For *in vitro* transcription the following reaction was set up under RNAse-free conditions on ice (see Table 6). For the generated *in situ* probes, the T7 (Promega, poduct no. P2075) and T3 (Promega, product no. P2083) RNA polymerases were used. To inhibit RNase A family members and thus protect the generated RNAs from degradation the Recombinant RNasin® Ribonuclease Inhibitor protein (Promega, product no. N2511) was added to the reaction.

Table 6. *In vitro* transcription reaction

Reagent	Volume	Stock concentration
Template DNA	up to 14.25 µl	/
RNAse-free H$_2$O	14.25-Volume of DNA template	/
Transcription buffer	6 µl	5x
ACG-Mix	3 µl	4 mM each
DIG-UTP	0.75 µl	4 mM
DTT	3µl	100 µM
RNasin	1.5 µl	40 U/µl
RNA polymerase	1.5 µl	17 U/µl

The transcription reaction was carried out at 37°C for 2.5 h. For removal of the template DNA, 2 µl RNase-free DNaseI (10 U/µl; Roche, product no. 10104159001) was added. The reaction was then incubated further for 15 min at 37°C. Then the reaction volume was diluted to 50 µl with RNase-free H$_2$O and unincorporated nucleotides removed using illustra ProbeQuant$^{(TM)}$ G50 Micro columns (GE Healthcare, product no. 28-9034-08) according to the supplied manual. Using this step, the volume of the purified probe was now 70 µl. It was the diluted to 100 µl with RNase-free H$_2$O. Efficiency of the of the *in vitro* transcription was tested by running 5µl of the labelled RNA probe an agarose gel. The remaining probe was stored at -80°C until further usage.

6.3.7 Radioactive labelling of DNA fragments

For the synthesis of DNA fragments radioactively-labelled with $[\alpha^{32}P]dCTP$ (Hartmann Analytik GmbH, produc no. SRP-405) the Amersham Rediprime$^{(TM)}$ II DNA labelling system (GE Healthcare, product no. RPN1633) was used. Briefly, 20 ng of template DNA in a total volume to 45 µl 1x TE were denatured for 5 min at 95°C, cooled down on ice and used to resuspend the pelleted reaction mix supplied with the kit. Next, 5 µl of $[\alpha^{32}P]dCTP$ were added and the reaction incubated for 30 min at 37°C. Unincorporated nucleotides were removed using the illustra ProbeQuant$^{(TM)}$ G50 Micro columns (GE Healthcare, product no. 28-9034-08) according to the manual. Prior to usage, the labelled probe was denatured for 5 min at 95°C and the kept on ice until hybridization.

6.3.8 DNA ligation

Ligation of blunt and sticky end DNA fragments were done using the Quick Ligase$^{(TM)}$ Kit (New England BioLabs, product no. M2200S) according to the supplied manufacturer's protocol with minor modifications. Ligation reactions were carried out at 25°C for at least 30 min.

6.3.9 DNA extraction from agarose gels

DNA fragments were extracted from agarose gels by cutting the desired fragment from the gel followed by purification using the Wizard® SV Gel and PCR Clean-Up System (Promega, product no. A9281) according to the manufacturer's protocol.

6.3.10 Chemical transformation of *E. coli* bacterial cells

In the course of the study DH5α were generally used. Large and recombination-prone constructs were cloned in JM109 cells instead. Table 7 lists the genotypes and the cultivation conditions for both strains.

For transformation of *E. coli* cells, approximately 100 µl of $CaCl_2$-competent cells were added to an entire ligation reaction and incubated at 4°C for 10 min. After 1 min heatshock at 42°C, 500 µl of LB without antibiotics was added directly to the suspension and the mixture incubated at the temperature indicated in 7. Depending on the encoded antibiotic resistance of the transformed DNA, this incubation time varied between ≤30 min for bacteriostatic and ≥ 60 min for bacteriotoxic antibiotics. After the incubation, the cells were pelleted, plated on LB/Agar dishes containing the appropriate antibiotic and cultured overnight.

<div align="center">**Table 7.** *E. coli* strains used</div>

Strain	Genotypen	Cultivation	Reference
DH5α	F$^-$ *endA1 glnV44 thi-1 recA1 relA1 gyrA96 deoR nupG Φ80dlacZΔM15 Δ(lacZYA-argF)U169, hsdR17(r_k^- m_k^+)*	37°C	Meselson and Yuan (1968)
JM109	*endA1 glnV44 thi-1 relA1 gyrA96 recA1 mcrB$^+$ Δ(lac-proAB) e14- [F' traD36 proAB$^+$ lacI^q lacZΔM15] hsdR17(r_k^- m_k^+)*	30°C	Yanisch-Perron *et al.* (1985)

6.3.11 Generation of the *Fam181a/b* shRNAmir constructs

The shRNAmirs targeting *Fam181a* or *b* respectively were designed using BLOCK-iT$^{(™)}$ RNAi Designer tool (Life Technologies) and supplied by Life Technologies in the form of two separate, partially overlapping oligonucleotides each. These were reconstituted to achieve a stock concentration of 100µM each. The corresponding primers were annealed together using 1 µl of each added to 16 µl ddH2O and 2 µl 1M KAc/300 mM HEPES (pH 7.5). This solution was then incubated for 30 sec at 90°C, before slowly cooling down to 4°C with a cooling rate of 0.1°C/sec. The annealed pairs were cloned into the linearized pcDNA$^{(™)}$ 6.2-GW/ +EmGFP-miR vector supplied with the BlockiT$^{(™)}$ Pol II miR RNAi Expression Vector Kit with EmGFP (Life Technologies, product no. K4936-00). Analytical digests and chaining of several shRNAmirs were done in accordance to the supplied protocol. Table 8 lists the generated shRNAmirs, their sequences and the element within the corresponding transcript they are targeting. The sequence parts highlighted in red letters correspond to the region which would be processed into the miRNA duplexes by the RNAi machinery. The control shRNAmir cloned into pcDNA$^{(™)}$ 6.2-GW/ +EmGFP-miR vector was provided with the kit.

<div align="center">**Table 8.** ShRNAmir sequences</div>

ShRNAmir name	Sequence	Target region
Fam181b miRNA#1	tgctgttcactttccgcttagacttggttttggccactgac tgaccaagtctacggaaagtgaacagg	ORF
Fam181b miRNA#2	tgctgactcaaagaactcaacggcctgttttggccactgac tgacaggccgttgttctttgagtcagg	ORF
Fam181b miRNA#3	tgctgtttacttgcgttctcccatcggttttggccactgac tgaccgatgggaacgcaagtaaacagg	3'UTR
Fam181a miRNA#1	tgctgtttccatgaagagcatgggctgttttggccactgac tgacagcccatgcttcatggaaacagg	5'UTR

ShRNAmir name	Sequence	Target region
Fam181a miRNA#2	tgctgtagaaaggcattcctccctaagttttggccactgac tgacttagggagatgcctttctacagg	ORF
Fam181a miRNA#3	tgctgagaactacgggtctgtacactgttttggccactgac tgacagtgtacacccgtagttctcagg	ORF

6.3.12 Southern blot analysis

For Southern blot analysis the restriction digest setup was scaled to 30 µl total volume containing 25 µl of resuspendend gDNA, and prepared in 1.5 ml Eppendorf tubes according to Table 9. The restriction enzymes used in the course of this study were *BamH*I (Promega, product no. R4024) and *Hind*III (Promega, product no. R4044). The restriction digest reaction was carried out at 37°C in a Thermomixer (Eppendorf) under slight agitation (500 rpm) overnight.

Table 9. Restriction digest for Southern blot analysis

Reagent	Volume	Supplier/Stock concentration
Restriction buffer	3 µl	Promega/10x
RNase A	0.3 µl	Thermo Scientific Fischer/10 mg ml^{-1}
BSA	0.3 µl	Promega/10 mg ml^{-1}
Spermidin	0.033 µl	0.9 mM
Restriction enzyme	x µl (60 U)	Promega/40-80 U ml^{-1}
H$_2$O	1,367 µl - used enzyme volume	/

The next day, the restriction digest was supplied with a sufficient amount of loading dye and separated on a 0.6% agarose gel at 60-80 V until the appropriate resolution was achieved. The gel was documented with the GelDoc$^{(TM)}$ (Bio-Rad), incubated in 0.25 N HCl twice for 10 min, washed in H$_2$O for 5 min, and then in 0.5 N NaOH for 40 min. Afterwards the gDNA was blotted by capillary force onto a pre-equilibrated nylon Zeta-Probe® membrane (Bio-Rad) overnight. After blotting, the gDNA was crosslinked by exposure to UV-light of 5000 µJ/cm$_2$, followed by washing twice in 2x SSC for 10 min. The membrane was either air-dried and stored at 4°C or directly used for hybridization. The membrane was incubated for at least 30 min with ExpressHyb$^{(TM)}$ Hybridization Solution (Clontech, product no. 636832) rotating at 65°C. After this pre-hybridization, the radioactively-labelled, denatured probe (see 6.3.7) was directly added

to the ExpressHyb, avoiding direct pipetting onto the membrane. Hybridization was carried out under rotation at 65°C overnight. On the following day, the membrane was washed twice with 2 x SSC/0.1% SDS to remove unbound probe. Then it was wrapped in clingfilm and used to expose a phosphor screen film (Fuji) overnight. The film was then scanned using the Phosphorimager Storm$^{(TM)}$ 820 (Amersham Biosciences).

6.3.13 Genotyping

Animals of the generated *Fam181b* targeted and knock-out mouse lines were genotyped from tail or ear biopsies prepared by the responsible animal caretaker in 1.5ml Eppendorf tubes. The samples were lysed in 300 µl Laird's buffer (100 mM Tris pH8.3/5 mM EDTA/0.20% SDS/200 mM NaCl) supplemented 1:100 with Protinase K (Sigma, product no. P4850) at 56°C in a Thermomixer under agitation of 800 rpm. To remove insoluble components, especially hair, the lysate was centrifuged for 5 min at 16.000 x g and the supernatant transferred into a new Eppendorf tube. The DNA was then precipitated with 1 ml 100% EtOH. After centrifugation for 15 min at 16.000 x g and 4°C, the DNA pellet was washed twice with 70% EtOH and then air-dried. Finally it was taken up in 50 µl or 25 µl 0.1x TE for tail or ear biopsies, respectively.

For genotyping of embryos, the yolk sac and/or the amnion were used. After washing quickly in 1x PBS, the gDNA was extracted as described for biopsy samples.

For genotyping of ES cells grown on 48-well plates or larger surfaces, the cells were wahsed twice with 1x PBS and the Laird's buffer directly applied to the cells in a sufficient volume. After 5 min at 37°C, gDNA of the lysed cells was transferred into 1.5 ml Eppendorf tubes using wide-bored pipette tips. DNA was then precipitated by adding 0.6x volume Isopropanol and centrifuged for 30 min at 16.000 x g and 4°C. Processing was continued as described above.

The extracted gDNA was subjected to Southern blot analysis as described in section 6.3.12. Southern probes were synthesised using primers listed in Table 2 and radioactively-labelled (see section 6.3.7).

For genotyping of *Dkk1* embryos, these were dissected in ice-cold PBS and the amnia removed. These tissues were used for extraction of gDNA and genotyping by PCR using the REDExtract-N-Amp$^{(TM)}$ Tissue PCR Kit (Sigma-Aldrich, product no. 254-457-8) according to the manual. The PCR was executed as indicated in Table 10. The embryos were stored individually and those of similar genotype pooled after evaluation of the genotyping PCR.

Table 10. PCR for *Dkk1* genotyping

Cycles	Temperature [°C]	Duration
1x	94	5'
5x	94	45"
	60	45"
	72	1'
35x	94	45"
	58	45"
	72	1'
1x	72	7'
1x	4	overnight

6.3.14 *In silico* sequence maintenance and analysis

Sequence management and *in silico* cloning was done using the Vector NTI Advance® software (Life Technologies). Design of restriction digests was done with NEBcutter V2.0 (Vincze *et al.*, 2003, New England BioLabs® Inc.) online tool. If not done by eye, oligonucleotides were designed with NCBI primer blast (Ye *et al.*, 2012).

6.4 Protein methods

6.4.1 Protein extraction

For whole embryo protein lysates, the embryos were dissected in ice-cold PBS, transferred into an 1.5 ml Eppendorf tube and the PBS removed as much as possible. Then the embryos were lysed using TOPEX buffer (300 mM NaCl/50 mM Tris-HCL (pH7.5)/0.5% Triton X-100/1 mM DTT/1x complete EDTA free protease inhibitor (Roche)) supplemented with 33.33 U/ml Benzonase® (Sigma, product no. E1014-25KU) at a ratio of 10:1 v/v of the embryonic sample. The protein lysate was incubated for 5 min at RT and the gDNA meanwhile sheared using an appropriate syringe. Then the lysate was incubated at 95°C, shock frozen on dry-ice and stored at -20°C until further usage.

For protein extraction from cell lines, cells were trypsinized, resuspended in PBS and transferred into 1.5 ml Eppendorf tubes. After centrifugation the cells were taken up in 300 µl TOPEX buffer with Benzonase® and the gDNA sheared by pipetting up and down at RT until viscosity disappeared. Then the sample was incubated for 5 min at

95°C, quickly cooled down on dry-ice and stored at -20°C.

6.4.2 Protein quantification

Protein quantification was done using the Qubit® 1.0 fluorometer (Life Technologies) with the Qubit® protein assay kit (Life Technologies, product no. Q33211) according to the suppliers manual.

6.4.3 SDS-PAGE and immunoblot analysis

For immunoblot analysis, 30 µg total of quantified protein lysate was supplemented with NuPAGE® LDS sample buffer (Life Technologies, product no. NP0007) and 50 mM DTT. This solution was denatured at 95°C for 5 min. The proteins were then separated by SDS-PAGE using NuPAGE® Novex® 10% Bis-Tris protein gels (Life Technologies, product no. NP0301BOX) in a XCell SureLock$^{(\text{TM})}$ mini-cell chamber (Life Technologies) and 1x NuPAGE® MOPS SDS running buffer (Life Technologies, product no. NP0001) until an appropriate resolution was achieved. The proteins were blotted using iBlot® transfer stack, PVDF, mini (Life Technologies, product no. IB4010) on an iBlot® gel transfer device (Life Technologies)with the default program 03. After the transfer, the membrane was blocked for at least 30 min at RT in TBS/1% Tween-20/5% skim milk powder (w/v).

Protein detection was done using the α-V5 monoclonal antibody (Life Technologies, product no. R960-25) at 1:2000 dilution for cell line- and at 1:500 dilution for embryo-derived protein samples. The α-mouse LamininB1 primary antibody (Abcam, product no. ab16048) was used in both as loading-control at 1:3500 dilution. Primary antibody incubation was carried out at 4°C overnight. The next day, membranes were washed three times in TBST for 5 min each, followed by 1 h incubation at RT with the secondary antibody. As secondary antibodies, either α-mouse or α-rabbit HRP-linked IgG (Cell Signaling, product no. 7076 and 70745, respectively) were used, both at 1:2000 dilution. After TBST washing, chemiluminescence detection was performed using the Amersham$^{(\text{TM})}$ ECL$^{(\text{TM})}$ Western Blotting Detection Reagents (GE Healthcare, product no. RPN2232) and images were acquired on a Fusion SL Vilber Lourmat device (Peqlab).

6.4.4 Immunofluorescence staining

For indirect immunofluorescence staining PBS-washed cells attached to gelatinized cover slides were fixed for 15 min in 4% PFA/PBS at RT, followed by washing twice with PBS. Membrane permeabilization was done by 5 min incubation with PBS/0.5%

Triton X-100 at RT followed by two PBS-washes. For blocking of non-specific antibody binding, the cells were then treated for 30 min at RT with DMEM/10% FBS. For primary antibody incubation the cells were incubated for 1 h at 37°C either with α-V5 monoclonal antibody (Life Technologies) generally at 1:1000 dilution for the detection of V5-tagged proteins, or an α-GFP antibody (Life Technologies, product no. A11122) at 1:500 dilution for detectaion of FAM181A-EmGFP. . For the detection of endogenous, V5-tagged proteins the α-V5 antibody concentration was increased to 1:500 dilution. After primary antibody incubation, cells were washed twice with PBS, followed by secondary antibody incubation for 1h at RT. Secondary antibodies used were α-rabbit IgG-Alexa488 conjugated (Life Technologies, product no. A11034), and α-mouse IgG-Alexa546 conjugated (Life Technologies, product no. A11030), both at 1:1000. Unbound antibody was removed by washing two times with PBS. Counterstaining was performed by incubation with FITC-phalloidin at 1:500 (Sigma; Cat. No. P5282), and slides were mounted using VECTASHIELD HardSet Mounting Medium with DAPI (Vector Laboratories).

6.5 Cell culture methods

The experimental procedures and techniques were done according to protocols previously described (Robertson, 1987; Colowick *et al.*, 1993; Behringer and Gertsenstein, 2014). All cell culture work was performed under sterile conditions in a laminar flow hood (HERAsafe®, Heraeus)

6.5.1 ES cell lines used and their maintenance

All constructs generated during this thesis were based on G4 embryonic stem (ES) cells (George *et al.*, 2007) and have a F1 129s6/SvEvTac X C57BL/6NCr background. The ROSA26A cells used to generate inducible knock-down and overexpression constructs were also of F1G4 background and described previously (Vidigal *et al.*, 2010).

Cultivation of ES cells was done in ES cell medium, composed as described below (see Table 11). The cells were cultured on gelatinized dishes (0.1% gelatine (v/v), Sigma) on top of monolayers of mitomycin C-treated feeder cells (primary embryonic fibroblasts). If not handled, the cells were cultivated at 37°C under 5% CO_2 atmosphere. The medium was changed every day, and cells split every 2-3 days. Briefly, they were washed twice with DPBS (Lonza) and incubated with trypsin-EDTA (0.5 g/l, Gibco) for 5-10 min. Under slight agitation the cells were detached from the plate, resuspended in ES cell medium and split onto new plates, previously prepared as described above.

Table 11. ES cell medium

Components	Concentration	Supplier
Knock-out DMEM (4.5 g/l D-glucose, sodium pyruvate)	/	Gibco
ES cell-qualified FCS	15% (v/v)	PAN Biotech GmbH
L-glutamine	2 mM	Lonza
Pen/Strep stock	50 U $^{-1}$ penicillin/50 µg $^{-1}$ streptomycin	Lonza
Non-essential amino acids	1x	Gibco
β-mercaptoethanol	0.1 µM	AppliChem
Nucleosides	1x	EmbryoMax®, Millipore
LIF	1000 U $^{-1}$	ESGRO®, Millipore

For storage of ES cells, these were trypsinized as described above an resuspendend in ES cell medium. Cells were then harvested by centrifugation for 5 min at 200 x g. The cell pellet was resuspended in ES cell medium supplemented with 20% (instead of 15% as described in Table 11). ES cell medium containing 20% DMSO was then added 1:1 to the cell suspension, mixed gently py pipetting once up and down and aliquoted into cryo vials. After cooling down slowly to -80°C in a freezing box overnight, the vials were stored in liquid N_2.

For thawing, the vials were shortly incubated at 37°C in a water bath and then the cell suspension taken up in ES cell medium. For removal of the DMSO cell were harvested by centrifugation for 5 min at 200 x g and the pellet resuspended again in ES cell medium. Afterwards the cell suspension was plated and maintained as described above.

6.5.2 Picking of ES cell colonies

For picking of ES cell colonies 20 µl trypsin-EDTA (0.5 g/l, Gibco) was added to as many wells of a 96-well U-bottom plate as colonies were picked. The single colonies were picked using sterile pipette tips and transferred into the trypsin. After the desired number of colonies was picked, the plate was incubated for 10 min at 37°C/5% CO_2. Then 120 µl of selection medium was added and colonies disaggregated by pipetting up and down. Cells were then transferred to either 96- or a 48-well plates prepared as described above using neomcyin resistant feeder cells (see section 6.5.1).

6.5.3 Recombinase-mediated cassette exchange

For RMCE into the modified *Gt(ROSA26)Sor* locus 3x10^5 ROSA26A ES cells/well were plated on a 6-well plate prepared as described above (see 6.5.1) and cultured overnight. Counting of cells was done using the Luna$^{(TM)}$ automated cell counter (Logos Biosystems) according to the supplied manual. On the next day, the medium was exchanged for ES cell medium without Pen/Strep. The cells were transfected with 5 µg of target construct DNA and 1 µg of Cre-Recombinase expression plasmid (PGK-Cre, see Table 3) using Lipofectamine$^®$ 2000 Transfection Reagent (Life Technologies, product no. 11668019) according to the manufacturer's protocol. Approximately 6 h after the transfection, the cells were split 1:1 onto to 6cm dishes prepared with neomycin resistant feeder cells as described above. On the next day the selection was started with ES cell medium containing 250 µg/ml Geneticin$^®$ Selective Antibiotic (Life Technologies, product no. 10131-027) and maintained for 6-8 days. The selection medium was replaced every day. When the growing colonies reached an appropriate size, they were picked as described under 6.5.2 onto 48-well plates prepared with neomycin resistant feeder cells. The selection was continued two days further to ensure that the colonies were indeed made up by resistant clones only. When the cells reached an appropriate density, they were split. Thereby,4/5 of the cell suspension were frozen and stored until further expansion and usage. The remaining 1/5 was plated back to the 48-well plate and cultured in ES cell medium without LIF for 2-3 days. The gDNA was extracted and, while the remaining 1/5 was plated back to the 48-well plate and used for genotyping (see 6.3.13).

6.5.4 Electroporation of ES cells

To insert transgenes by homologous recombination into the genome, ES cells were subjected to electroporation. Therefore, 5-10x10^6 cells were counted using the Luna$^{(TM)}$ automated cell counter, centrifuged for 5 min at 200 x g, and then resuspended in 800 µl DPBS. About 25 µg of linearised targeting construct DNA was added to the cell suspension and the mixture transferred into a 0.4 cm Gene Pulser$^®$ electroporation cuvette (Bio-Rad, product no. 165-2091). The cell suspension was electroporated at 240 V and 500µF using a Gene Pulser$^®$ (Bio-Rad). Afterwards, the cells were taken up in ES cell medium and split $^1/_6$:$^2/_6$:$^3/_6$ onto three 6-cm dishes prepared with neomycin-resistant feeders as described above (see section 6.5.1). Selection was started $\geq$24 h after electroporation with ES cell medium containing 250 µg/ml Geneticin$^®$ Selective Antibiotic (Life Technologies, product no. 10131-027) and was maintained for 6-8 days. The selection medium was replaced every day. At least 200 colonies were picked onto

96-well plates as described above (see section 6.5.2). When the majority of the picked clones reached an appropriate density (usually after about 2-3 days), the entire plate was washed twice with DPBS, trypsinized using 30 µl/well trypsin-EDTA (0.5 g/l, Gibco), and disaggregated in additional 120µl/well resuspension medium (see Table 12) by pipetting up and down.

Then 50 µl of the cell suspension were transferred into a U-bottom 96-well plate already containing 50µl/well of 2x Hepes freezing medium (see Table 12). This plate was then cooled down slowly overnight to -80°C and then stored at this temperature. The remaining 100µl/well cell suspension was equally distributed onto two gelatinized 96-well plates, supplemented with 100 µl ES cell medium without LIF per well, and further cultured until the majority of the colonies reached again an appropriate density. These plates were used for extraction of genomic DNA for Southern analysis (see section 6.5.5).

Table 12. ES cell media for split/freeze of 96-well plates

Medium	Composition (Supplier)
Resuspension medium	HCO_3^--free DMEM (Gibco)/10 mM HEPES pH7.2 (Sigma)/20% ES cell-qualified FCS (v/v) (PAN Biotech GmbH)
2 x HEPES freeze medium	Resuspension medium/20% DMSO (v/v) (Sigma)

6.5.5 gDNA extraction in 96-well format for Southern blot

To prepare gDNA from 96-well plates, cells were washed twice with PBS and then 50 µl/well Laird's buffer (see section 6.3.13) with Proteinase K (Sigma, product no. P4850) at 1:100 dilution was added. The plates were incubated in a humidified chamber at 37°C overnight. On the next day, gDNA was precipitated by adding 100 µl/well 100% EtOH/75mM NaCl and incubated at RT for 30 min. To ensure that the gDNA was pelleted, the plate was then centrifuged at 3220 x g and 4°C for 15 min. The solution was then discarded by carefully inverting the plate. The plate was washed three times with 200 µl/well 70% EtOH with 5 min centrifugation steps in between to ensure stability of the DNA pellet. After air-drying, 25 µl of 1x TE were added to each well and the plate incubated in a humidified chamber at 37°C overnight. The entire plate was then subjected to Southern blot analysis as described under section 6.3.12.

6.5.6 *In vitro* differentiation into neural cells

For the differentiation of F1G4 ES cells and the *Fam181b* V5 knock-in ES cell line, cells were thawed on 6 cm-dishes as described above (see 6.5.1). After 3 days of culture, cells were made feeder-free by trypsinizing and resuspension in 3 ml/plate ES cell medium. The cell suspension was plated back onto the 6 cm-dish and the cells were allowed to settle for 30 min. During that time, feeder cells already start to attach to the plate, while ES cells remain in the solution. This was repeated four times with fresh gelatinzed 6 cm-dishes. Thereby the mainly feeder-free ES cells remained on the last plate and were expanded under feeder-free conditions with ES cell medium.

After reaching an appropriate density on a 10 cm-dish, the cells were subjected to *in vitro* differentiation into neural cells according to the protocol established by Bibel *et al.* (2007). During the differentiation, samples were taken for RNA extraction using TRIzol® Reagent (Life Technologies, product no. 15596-026). The neural progenitor cells (day 8+8 according to Bibel *et al.*, 2007) were seeded onto µ-Slide 8 well slides (ibidi®, product no. 80826) and samples either used for RNA extraction or subjected to indirect immunofluorescence.

6.5.7 Maintenance of non-ES cell lines used

Eukaryotic non-ES cell lines used during the thesis were the HEK293 cell line or the murine NIH3T3 and C2C12 (data not shown) cell lines.

These were maintained on gelatinized cell culture plates in cell culture medium (DMEM/10% FCS/1% Gln/50 U ml^{-1} penicillin/ 50µg ml^{-1} streptomycin) as described for ES cells. Medium was changed every 2nd day and cells split at about 75% confluence. For splitting the cells were washed twice with DPBS, then trypsinized und taken up in cell culture medium and plated. For freezing cells were taken up in cell culture medium/10% DMSO, aliquoted into cryo vials and slowly cooled down overnight to -80°C. The vials were stored in liquid N$_2$. Thawing was done as for ES cells using cell culture medium instead.

6.5.8 Transient transfection

For the shRNAmir tests and the immunofluorescence experiments on non-ES cell lines performed in this thesis, transient transfection was used for temporal insertion of expression plasmids. For immunofluoresce, cell were grown on gelatinized 15 mm ⌀ glass cover slides and transferred to 12-well plates for further processing.

Transient transfection was done using Lipofectamine® 2000 Transfection Reagent (Life Technologies, product no. 11668019) according to the manufacturer's protocol.

The amount of DNA and the volume of Lipofectamine$^{®}$ 2000 were adjusted to the used culture plate format according to the supplied manual.

6.6 Mouse husbandry and embryo analysis

6.6.1 Animal husbandry

For gene expression analysis the mouse outbred strains CD1 (*Hsd:ICR(CD-1$^{®}$)*), and NMRI (*HsdHan:NMRI*), as well as the inbred strains C57Bl/6J (*C57BL/6JOlaHsd*) and 129s2 (*129S2/SvHsd*) were used. They were purchased from Harlan Laboratories (Harlan Winkelmann GmbH, Borchen, Germany). To generate *Fam181b* null animals the CMV-Cre line established by Schwenk *et al.* (1995) and kept on a C57Bl/6J background was used. The generated knock-out animals are currently being crossed back to C57Bl/6J to generate a congenic line.

All mice used in the course of this thesis were maintained in the animal facility of the Max Planck Institute for Molecular Genetics, Berlin, under conditions according to international standards and protocols. For transgene induction, 4mg ml^{-1} doxycyline and 1% sucrose (w/v) were present in the drinking water.

Animal maintenance and all procedures performed on mice described in this thesis were done in accordance to the German animal welfare act (Tierschutzgesetz,TSchG) and approved by the Berlin federal office for health and social affairs (LaGeSo).

6.6.2 Mouse embryo dissection

For harvesting embryos, mice were euthanized at the required day post coitum (dpc) by cervical dislocation. If not indicated differently, embryos were removed from the uteri in ice-cold PBS. The harvested embryos were then kept in PBS on ice until fixation with 4% paraformaldehyde (PFA)/PBS (w/v). In case of protein analysis, fixation was done for 2 to 4 h, for RNA analysis overnight, in both cases at 4℃ under rotation.

6.6.3 Caudal end half preparation and culture

The preparation of tail halves was done for two purposes, either the comparison of two different genes on the two segmentation phase-matched halves, or to visualize the changes in RNA expression occurring within one segmentation cycle.

For the first purpose, E9.0-9.5 embryos were dissected as described above (see section 6.6.2) and transferred to a 6 cm dish half filled with 1% agarose (w/v)/PBS, half with ice-cold PBS. The caudal end was roughly removed from the embryo using forceps and

pined down onto the bottom in a way that leaves the psm flat on the agarose with its dorsal side facing up. Using a tungsten needle, the caudal and was then separated along the midline starting at the caudal-most tip and moving anteriorly. After reaching the somite IV level, the generated halves were removed carefully from the remaining caudal end and immediately fixed. During WISH analyses (see section 6.6.4), both samples were separated before *in situ* hybridisation and merged for processing after removal of unbound probe.

In *Xenopus* and *Danio* embryos it was shown the segmentation clock period is temperature-sensitive (Elsdale *et al.*, 1976; Schröter *et al.*, 2008), although it remains to be investigated how far this applies to *ex utero* mouse embryos. To prevent possible disturbances of the clock period, for the second purpose embryos were dissected in PBS prewarmed to RT, and after dissection quickly transferred to M2 medium prewarmed to 37°C. Separation of the tail halves was done in a 6 cm dish half-filled with 1% agarose (w/v)/PBS, half with M2 medium prewarmed to 37°C as described above. Both halves were transferred to DMEM/F-12/10% FCS (v/v) and incubated for 30 min at 37°C/7.5%CO_2. Then one half was fixed, while the other one further incubated for 60 min, 90 min, or 120 min respectively before fixation. Both halves were further processed together.

6.6.4 Whole-mount *in situ* hybridization (WISH)

If not indicated otherwise, all steps were carried out at 4°C under shaking incubation and with RNase-free solutions.

After overnight fixation, samples were washed twice in PBST (see Table 14) and then stepwise dehydrated in 25%, 50% and 75% (v/v) MeOH/PBST and 100% MeOH. Each incubation step was carried out for 5 to 15 min. The specimens were either directly further processed or stored in 100% MeOH at -20°C. After rehdyation in reversed stepwise MeOH/PBST-series (75%, 50%, 25%) for 5 to 15 min, the samples were washed twice with PBST before bleaching for 45 min with 6% H_2O_2/PBST (v/v) followed by three PBST-washes 5 min each. For increase of probe and antibody permeability, the specimens were treated with proteinase K (10 µg/ml in PBST). The incubation time was adapted to the stage of the embryos used or the size of the tissue, respectively (see Table 13) and carried out at RT.

Inactivation of proteinase K was done by incubation with glycine (2 mg/ml in PBST) for 5 min at RT. After this the specimens were washed twice with PBST, then postfixed in 0.2% glutaraldehyde (v/v) /4% PFA/PBS for 20 min and again washed twice in PBST. For E12.5 embryos an additional 30 min incubation with RIPA buffer (see Table 14), followed by two 5 min PBST-washes were done prior to the postfixation.

Table 13. Proteinase K treatment time

embryos	incubation time
mouse E6.5	3 min
mouse E7.5	4 min
mouse E8.5	5 min
mouse E9.5	8 min
mouse E10.5	10 min
mouse E11.5	15 min
mouse E12.5	20-25 min
tissue samples	**incubation time**
tail halves (E9.5)	2 min
limb anlagen (E14.5)	8 min

After this the samples were either transferred to storage mix (see Table 14) and stored at -20°C. Alternatively, they were directly preincubated in prewarmed hybridisation solution (see Table 14) for $\geq$ 1h at 68°C. After preincubation, the RNA probe was added and and allowed to hybridise overnight at 68°C under shaking incubation.

The next day the RNA probe/hybridisation solution mixture was collected and stored at -20°C for reuse. Unbound probe was removed by washing at 68°C twice for 30 min in solution 1, and once for 30 min in solution 3T (see Table 14). Next the specimens were incubated 30 min at RT in 50% MABT (see Table 14)/50% solution 3T (v/v), prewarmed to 68°C. After washing three times in MABT at RT, the samples were blocked in 2% blocking reagent (w/v, Roche, product no. 11096176001)/20% fetal calf serum (FCS, v/v)/MABT for $\geq$ 1 h at RT. Then the alkaline phosphatase-conjugated α-digoxygenin antibody (Roche, product no. 11093274910) was added at a 1:2000 dilution and the samples incubated overnight at 4°C.

On the following day the specimens were washed in MABT at RT three times for 5 min, once for 15 min and twice for 30 min, before the MABT was changed every hour for the rest of the day. Washing was continued every hour the next day and could be extended for further 2 days if necessary. Overnight the samples were always kept at 4°C.

In preparation of the staining reaction, the specimens were incubated at RT twice for 10 min and once for 40 min in NTMT (see Table 14), before the BM Purple staining solution (Roche, product no. 11442074001) was applied. The progress of the staining was checked at regular intervals. If necessary the samples were transferred into NTT

(see Table 14), kept overnight at 4°C and the staining continued the next day. To stop the staining reaction, the samples were washed twice in PBST for 10 min, then post-fixed in 4% PFA/PBS and stored at 4°C.

Table 14. WISH buffers and their composition

buffer	composition
PBST	PBS+1% Tween-20
RIPA buffer	50 mM Tris-HCl/150 mM NaCl/1% NP-40 (v/v)/0.25% NaDOC (w/v)/0.1% SDS (w/v)/1 mM EDTA
storage mix	50% formamide/2.5xSSC (pH 4.5) (v/v)
hybridisation solution	50% formamide (v/v)/1% SDS (w/v)/50 ng/ml yeast RNA (Sigma-Aldrich)/50 ng/ml heparin (Sigma-Aldrich)/5xSSC (pH 5.0)
solution 1	50% formamide (v/v)/1% SDS (w/v)/5xSSC (pH 4.5)
solution 3T	50% formamide (v/v)/0.1% Tween-20 (v/v)/2xSSC pH 4.5
MABT	100 mM maleic acid/150 mM NaCl/0.8% NaOH (w/v)/ 0.1% Tween-20; adjusted to pH 7.5
NTMT	100 mM Tris-HCl (pH 9.5)/50 mM $MgCl_2$/100 mM NaCl/0.1% Tween-20
NTT	as NTMT but without $MgCl_2$

6.6.5 Vibratome sections

For a more detailed analysis of the RNA expression pattern, vibratome sections were used on WISH-stained specimens. The postfixed samples were incubated in 5% sucrose/PBS (w/v), 15% sucrose/PBS (w/v) and 30% sucrose/PBS (w/v) for 1 h each at 4°C, before incubating overnight in 30% BSA (w/v)/20% sucrose (w/v)/0.5% gelatine/PBS.

The next day the samples were embedded by adding 2.5% glutaraldehyde (v/v), which led to polymerisation of the gelatine. Embedding was done on ice to slow down the polymerisation, giving time to proper position the specimens according to the planed sectioning. From the embedded specimens sections of 35 µm thickness were produced using Microm HM650 V (Thermo Fisher Scientific[TM]), transferred to microscope slides and mounted with HYDRO-MATRIX® (Micro-Tech-Lab).

6.6.6 Paraffin sections

For paraffin sections of E14.5 mouse embryos, fixed specimens were washed three times with PBS for 5 min and the directly transferred to 70% EtOH for at least one hour. The following processing was done using a Microm STP120 (Thermo Fisher Scientific$^{(TM)}$) using the following program:

Table 15. Processing for paraffin sections

step	reagent	time [h]	agitation [0/1/2]
1	70% EtOH	2:00	2
2	70% EtOH	1:50	2
3	80% EtOH	1:40	2
4	90% EtOH	2:00	2
5	96% EtOH	2:00	2
6	100% EtOH	1:00	2
7	100% EtOH	1:00	1
8	100% EtOH	1:00	1
9	Xylol	1:30	2
10	Xylol	1:30	2
11	Paraffin (56°C-58°C)	2:00	2
11	Paraffin (56°C-58°C)	2:00	1

After the incubation program the specimens were embedded in fresh paraffin, allowed to solidify and stored at 4°C until sectioning. The generated blocks were cut into sections of 5 µm using a HM 355 S microtome (Microm). Section were transferred onto Menzel Gläser SUPERFROST ULTRA PLUS® microscopy slides (Thermo Scientific Fisher$^{(TM)}$), dried at 37°C for several hours and stored at 4°C.

6.6.7 *In situ* hybridization on paraffin sections

All steps were carried out under RNase-free conditions with solutions freshly prepared before. If not explicitly mentioned, all steps were done at RT. If not already described above, the solutions used and their compositions are listed in Table 16.

First, the slides were incubated at 63°C for 30 min. This should help to remove paraffin and increase the attachment of the specimens to the glass surface. Remaining paraffin was removed by washing twice for 5 min each in Xylol. After two incubation steps of 5 min each in 100% EtOH, the samples were processed through 95%, 85%, 70%, 50%, and 30% EtOH with 2 min per step. This was followed by washing in 1x

PBS two times for 5 min. Postfixation was done by 15 min incubation in 4% PFA/PBS, followed by two 5 min 1xPBS washes.After incubating for 2 min in 100mM Tris-HCl (pH 7.5), acetylation was carried out by incubation for 10 min in 100 mM Tris-HCl (pH 7.5)/0.25% acetic anhydride, followed by two 2x SSC (pH 5.0) washes of 2 min each. Then the samples were dehydrated stepwise in 30%, 50%, 70%, 85%, 95%, and 100% EtOH with 2 min per step and allowed to air-dry for 0.5-4 h after. For hybridization, 120 µl of the probe mix (0.8-1 µg RNA probe/ml in hybridization solution, see Table 14) were added per slide and overlaid by a HybriSlip$^{(TM)}$ (Sigma, product no. GBL716022). The slides were incubated in a chamber humidified with 0.2x SSC/50% fomamide (v/v) at 63°C overnight.

The following day unbound probe was removed by washing once in 5x SSC/50% fomamide (v/v) for 10 min, twice for 10 min in 2x SSC/50% formamide, twice in 1x SSC for 15 min each, and finally once for 30 min in 0.2x SSC. All washing steps were carried out at 60°C with prewarmed solutions. Then the slides were incubated two times in TBST for 5 min each, before 700 µl of Blocking solution was applied, the specimens blocked for 1 h and the blocking solution removed afterwards. For the antibody incubation, the alkaline phosphatase-conjugated α-digoxygenin antibody (Roche, product no. 11093274910) was prepared in a 1:2000 dilution in Blocking solution and 120 µl of it added per slide. Antibody binding was allowed overnight at 4°C in a humidified chamber.

On the next day, the slides were washed 6 times for 30 min each in TBST, before being incubated in NTMT/2 mM Levamisole twice for 10 min. Staining was done by using BM Purple staining solution (Roche, product no. 11442074001) with about 120 µl per slide. The specimens were stained in the dark for 2 h up to several days. After adequate staining intensity was achieved, the slides were dehydrated again and mounted with with Entellan$^{®}$ (Merck Millipore, product no. 107960) and cover slides.

Table 16. ISH buffers for paraffin sectiones

buffer	composition
TBST	TBS+1% Tween-20
Blocking solution	80% MABT (v/v)/20% Fetal lamb serum (FLS, v/v)/2% Roche Blocking Reagent(w/v)/2 mM Levamisole

6.6.8 Skeletal preparation

Skeletal preparations of E17.5-18.5 mouse embryos were done by removal of the uterus, transferring it into a Falcon tube with PBS followed by incubation at -20°C for 30-60 min to sacrifice the embryos. These were then dissected and stored in ice-cold PBS until further preparation. Single embryos were incubated for 30-60 sec in tap water heated to 60°C for easier removal of the skin, and then carefully flayed and eviscerated using forceps. The prepared carcasses were collected and incubated overnight in 95% EtOH at RT with slight agitation.

On the next day cartilage staining was done by incubation Alcian Blue stain (76% EtOH (v/v) /5% glacial acetic acid (v/v) /0.015% Alcian Blue 8GX (w/v, Sigma)) for 24-48 h at RT with soft agitation. After another agitated overnight incubation in 95% EtOH the bulk of the remaining soft tissues were removed by treatment with 1% KOH (w/v) solution. This was done without agitation and until the bones became visible. For staining of the bones the solution was next changed to Alizarin Red stain (1% KOH (w/v)/ 0.015% Alizarin Sodium Sulfate (w/v, Sigma)) and the specimens incubated overnight. Afterwards the skeletons were de-coloured in 20% glycerol (v/v)/ 1% KOH (v/v) over the course of 1-2 weeks. During this time the solutions was changed several times to guarantee removal of excess Alizarin Red stain. The skeletons were stored and imaged in 50% glycerol/ 35% EtOH.

6.6.9 Neurofilament immunostaining on embryos

To visualize cranial and spinal nerves a neurofilament whole mount immunostaining was applied. Therefore, embryos were dissected at E10.5 and, after 2 h of 4% PFA/PBS fixation, transferred to 100% MeOH and incubated overnight at -20°C. At this point the specimens can be stored, though long term storage can lead to a reduction in staining quality. For bleaching of the embryos, these were then incubated in 5:1 MeOH/30% H_2O_2 at RT for 3-5 h, followed by transfer back into 100% MeOH and storage at -20°C overnight. The next day, embryos were rehydrated in 50% MeOH/PBS, 15% MeOH/PBS, and PBS for 30 min at 4°C each. For blocking, the specimens were incubated for 1 h at RT in PBSMT (see Table 17) and then incubated with the primary antibody at 4°C overnight. For this step the 2H3 monoclonal antibody (Developmental Studies Hybridoma Bank) was used at 1:50 dilution in PBSMT. For removal of unbound antibody, on the next day, the embryos were washed twice at 4°C and three times at RT in PBSMT for 30 min each. Secondary antibody incubation was done overnight at 4°C using an HRP-linked α-mouse antibody (Cell Signaling, product no. 7076) at 1:500 dilution. Removal of the secondary antibody was done as described for the primary

antibody plus an additional PBT (see 17) wash step at RT for 20 min. Then specimens were incubated in PBT/0.5% NiCl$_2$ (w/v)/0.03% DAB (w/v, Sigma, product no. D-5905) for $\geq$30 min at RT. After adding H$_2$O$_2$ to 0.0003% the samples were incubated until an appropriate staining intensity was achieved. When this was the case, they were rinsed in PBT, shortly incubated in 50% MeOH/PBS and then stored in 100% MeOH at 4°C. For imaging, the embryos were transferred into 1:1 (v/v) PBT/fomamide and kept in this solution during image acquisition.

Table 17. Buffers for neurofilament immunostaining

buffer	composition
PBSMT	PBS/2% skim milk powder (w/v)/0.1% Triton X-100(v/v)
PBT	PBS/0.2% BSA (w/v)/0.1% Triton X-100(v/v)

6.7 Imaging

For imaging of WISH-stained embryos, the MZ16A dissection microscope (Leica) fitted with an AxioCam MRc5 (Carl Zeiss MicroImaging) was used in combination with the AxioVision Special Edition 64-bit Release 4.9.1SP1 software (Carl Zeiss MicroImaging).

Caudal end half specimens were imaged using a Zeiss SteREO Discovery .V12 with an AxioCam (Carl Zeiss MicroImaging) in combination with the AxioVision Release 4.8.2 software (Carl Zeiss MicroImaging). Both corresponding halves were imaged in a single picture.

Vibratome and paraffin sections were imaged using a Zeiss Observer.Z1 microscope with an AxioCam MRc (Carl Zeiss MicroImaging) in combination with the AxioVision Release 4.6.3SP1 software (Carl Zeiss MicroImaging) and either the EC Plan-Neofluar 10x/0.30 Ph 1 or the Plan-Apochromat 20x/0.8 M27 objective (both Carl Zeiss MicroImaging). For tile scans the image were acquired with $\geq$ 15% overlap and stitched by the software. If necessary, stitching was improved by hand. Live imaging of fluorescent ES cells and transiently transfected HEK293 cells was also done with this microscope using the AxioCamMR3_2 (Carl Zeiss MicroImaging) in combination with the EC Plan-Neofluar 10x/0.30 Ph 1 objective.

Fluorescence microscopy on embryos and immunostained cells was performed on an LSM710NLO laser-scanning microscope using the ZEN 2012 software (Carl Zeiss MicroImaging) and a Plan-Apochromat 10x/0.3 M27 objective for embryos or a Plan-

Apochromat 63x/1.40 Oil DIC M27 obejctive for cells. For embryos, tile scans with overlaps of $\geq 20\%$ and z-Stacks of about 15µm distance were produced. The number of tiles and range of the z-stacks were adopted for each embryo to fit its dimensions. EmGFP, Alexa 488, and FITC-conjugated phalloidin were excited using a laser of 488 nm, tdTomato and Alexa 546 of 543 nm wavelength. DAPI was excited using the Coherent Chameleon$^{(TM)}$ laser 710 nm wavelength. The T-PMT detector was used to generate bright field images. Stitching of tiles and Maximum Intensity Projection of z-planes was done with the Zen software package.

Colour and brightness adjustments were done in Adobe® Photoshop® CS6 or Microsoft® PowerPoint and applied to the entire images only.

6.8 Phylogenetic analysis

Sequence alignment of human and murine FAM181 proteins was generated using CLC DNA workbench. Multiple sequence alignment of the selected vertebrate species was produced using Clustal Omega (Sievers *et al.*, 2011) with default settings. This alignment was used as input for ClustalW version 2 (Larkin *et al.*, 2007) to generate the phylogenetic tree. The distance correction was enabled by the software, while other settings remained default. Conversion of the Newick tree into an SVG tree, was done using TreeVector (http://supfam.cs.bris.ac.uk/TreeVector/index.html). Sequence identities were calculated using William Pearson's lalign program (http://www.ch.embnet.org/software/LALIGN_form.html). *In silico* search for putative nuclear localization signals was performed using NLStradamous (Nguyen Ba *et al.*, 2009).

Danksagung

Als erstes möchte ich mich bei Prof. Dr. Bernhard G. Herrmann für die Möglichkeit bedanken, meine Doktorarbeit in seiner Abteilung anzufertigen. Auch danke ich ihm für seine Betreuung und Unterstützung während der gesamten Zeit, sowie die Freiheit, eigene Wege und Ideen zu verfolgen. Ich danke Prof. Dr. Stephan Sigrist, dass er sich als Zweitgutachter meiner Arbeit bereiterklärt hat.

Großer Dank gilt Lisette Lange. Du hast mir so oft in späten Stunden und an den Wochenenden tatkräftig hilfreich zur Seite gestanden und mich, wenn nötig, immer wieder aufs Neue motiviert. Ohne dich wäre diese Arbeit nie möglich gewesen.

Mein besonderer Dank gebührt auch Dr. Tracie Pennimpede für die schöne gemeinsame Zeit, die wir in Labor 5 hatten, für all die Diskussionen, all die Dinge, die ich von dir lernen konnte, und nicht zuletzt für deine große Hilfe, vor allem auch während des Schreibens der Arbeit und das trotz deines Umzugs nach Kanada.

Ganz besonderer Dank gilt auch Dr. Lars Wittler und Dr. Phillip Grote, die mich zu Beginn meines Masterstudiums als Praktikant aufnahmen und mich überhaupt erst in Kontakt mit der Entwicklungsbiologie führten. Mein heutiges Verständnis von Wissenschaft beruht zum größten Teil auf dem, was ich von euch gelernt habe. Vielen Dank für all die wissenschaftlichen Diskussionen, aber auch die nicht-wissenschaftlichen Gespräche über Video Games, Fantasy und anderen Kram.

Vielen Dank auch an Andrea, Gaby, Manuela und Sandra für all die Hilfe und Unterstützung in allen Zellkultur-Belangen, bei Wochenendarbeiten, und vor allem auch während der Zeit des Schreibens der Arbeit. Auch danke ich allen anderen Mitgliedern der Abteilung Entwicklungsgenetik (einschließlich jener, welche die Abteilung bereits verlassen haben) für ihre Hilfsbereitschaft, die freundliche Atmosphäre und die vielen schönen Momente, die wir zusammen erlebt haben.

Bei Dijana und Christin möchte ich mich ganz herzlich für ihre gute Arbeit bei der Betreuung meiner Mäuse, das Ansetzen der Verpaarungen, und bei Dijana auch für ihren Einsatz bei den Verhaltensexperimenten bedanken.

Letztlich danke ich auch meiner Familie und besonders meinen Eltern. Ohne ihre bedingungslose Unterstützung und vor allem auch ihr Verständnis für meinen Weg wäre es nie zu dieser Arbeit gekommen.

Bibliography

Aulehla, A. and Johnson, R. L. Dynamic expression of lunatic fringe suggests a link between notch signaling and an autonomous cellular oscillator driving somite segmentation. *Developmental biology*, 207(1):49–61, March 1999.

Aulehla, A. and Herrmann, B. G. Segmentation in vertebrates: clock and gradient finally joined. *Genes & development*, 18(17):2060–7, September 2004.

Aulehla, A., Wehrle, C., Brand-Saberi, B., Kemler, R., Gossler, A., Kanzler, B., and Herrmann, B. G. Wnt3a Plays a Major Role in the Segmentation Clock Controlling Somitogenesis. *Developmental Cell*, 4(3):395–406, March 2003.

Austin, C., Feldman, D., Ida, J., and Cepko, C. Vertebrate retinal ganglion cells are selected from competent progenitors by the action of Notch. *Development*, 121(11): 3637–3650, November 1995.

Avilion, A. A., Nicolis, S. K., Pevny, L. H., Perez, L., Vivian, N., and Lovell-Badge, R. Multipotent cell lineages in early mouse development depend on SOX2 function. *Genes & development*, 17(1):126–40, January 2003.

Ay, A., Knierer, S., Sperlea, A., Holland, J., and Özbudak, E. M. Short-lived Her proteins drive robust synchronized oscillations in the zebrafish segmentation clock. *Development (Cambridge, England)*, 140(15):3244–53, August 2013.

Balakirev, E. S. and Ayala, F. J. Pseudogenes: are they "junk" or functional DNA? *Annual review of genetics*, 37:123–51, January 2003.

Behringer, R. R. and Gertsenstein, M. Manipulating the mouse embryo: A laboratory manual. 2014.

Betran, E., Wang, W., Jin, L., and Long, M. Evolution of the Phosphoglycerate mutase Processed Gene in Human and Chimpanzee Revealing the Origin of a New Primate Gene. *Molecular Biology and Evolution*, 19(5):654–663, May 2002.

Bettenhausen, B. and Gossler, A. Efficient isolation of novel mouse genes differentially expressed in early postimplantation embryos. *Genomics*, 28(3):436–41, August 1995.

Bettenhausen, B., Hrabe de Angelis, M., Simon, D., Guénet, J. L., and Gossler, A. Transient and restricted expression during mouse embryogenesis of Dll1, a murine gene closely related to Drosophila Delta. *Development (Cambridge, England)*, 121 (8):2407–18, August 1995.

Bibel, M., Richter, J., Lacroix, E., and Barde, Y. Generation of a defined and uniform population of CNS progenitors and neurons from mouse embryonic stem cells. *Nature protocols*, 2(5):1034–43, January 2007.

Bibel, M., Richter, J., Schrenk, K., Tucker, K. L., Staiger, V., Korte, M., Goetz, M., and Barde, Y.-A. Differentiation of mouse embryonic stem cells into a defined neuronal lineage. *Nature neuroscience*, 7(9):1003–9, September 2004.

Bimboim, H. and Doly, J. A rapid alkaline extraction procedure for screening recombinant plasmid DNA. *Nucleic Acids Research*, 7(6):1513–1523, November 1979.

Blake, R. D., Hess, S. T., and Nicholson-Tuell, J. The influence of nearest neighbors on the rate and pattern of spontaneous point mutations. *Journal of Molecular Evolution*, 34(3):189–200, March 1992.

Capecchi, M. R. Gene targeting in mice: functional analysis of the mammalian genome for the twenty-first century. *Nature reviews. Genetics*, 6(6):507–12, June 2005.

Chai, Y., Jiang, X., Ito, Y., Bringas, P., Han, J., Rowitch, D., Soriano, P., McMahon, A., and Sucov, H. Fate of the mammalian cranial neural crest during tooth and mandibular morphogenesis. *Development*, 127(8):1671–1679, April 2000.

Chen, E., Gigek, C., Rosenfeld, J., Diallo, A., Maussion, G., Chen, G., Vaillancourt, K., Lopez, J., Crapper, L., Poujol, R., Shaffer, L., Bourque, G., and Ernst, C. Molecular Convergence of Neurodevelopmental Disorders. *The American Journal of Human Genetics*, October 2014.

Chen, L., Chan, S. W., Zhang, X., Walsh, M., Lim, C. J., Hong, W., and Song, H. Structural basis of YAP recognition by TEAD4 in the hippo pathway. *Genes & development*, 24(3):290–300, February 2010.

Christ, B. and Ordahl, C. P. Early stages of chick somite development. *Anatomy and Embryology*, 191(5):381–396, May 1995.

Coffman, C. R., Skoglund, P., Harris, W. A., and Kintner, C. R. Expression of an extracellular deletion of Xotch diverts cell fate in Xenopus embryos. *Cell*, 73(4): 659–671, May 1993.

Colowick, S. P., Kaplan, N. O., Wassarman, P. M., and DePamphilis, M. L. *Methods in Enzymology: Guide to techniques in mouse development / edited by Paul M. Wassarman, Melvin L. DePamphilis, Volume 225*. Academic Press, 1993.

Cooke, J. and Zeeman, E. A clock and wavefront model for control of the number of repeated structures during animal morphogenesis. *Journal of Theoretical Biology*, 58 (2):455–476, January 1976.

Cordes, S. P. Molecular genetics of cranial nerve development in mouse. *Nature reviews. Neuroscience*, 2(9):611–23, September 2001.

Couly, G., Coltey, P., and Le Douarin, N. The triple origin of skull in higher vertebrates: a study in quail-chick chimeras. *Development*, 117(2):409–429, February 1993.

Crawley, J. N. Behavioral phenotyping strategies for mutant mice. *Neuron*, 57(6): 809–18, March 2008.

Dale, J. K., Maroto, M., Dequeant, M.-L., Malapert, P., McGrew, M., and Pourquie, O. Periodic notch inhibition by lunatic fringe underlies the chick segmentation clock. *Nature*, 421(6920):275–8, January 2003.

del Corral, R. D., Olivera-Martinez, I., Goriely, A., Gale, E., Maden, M., and Storey, K. Opposing FGF and Retinoid Pathways Control Ventral Neural Pattern, Neuronal Differentiation, and Segmentation during Body Axis Extension. *Neuron*, 40(1):65–79, September 2003.

Dequéant, M.-L. and Pourquié, O. Segmental patterning of the vertebrate embryonic axis. *Nature reviews. Genetics*, 9(5):370–82, May 2008.

Dequéant, M.-L., Glynn, E., Gaudenz, K., Wahl, M., Chen, J., Mushegian, A., and Pourquié, O. A complex oscillating network of signaling genes underlies the mouse segmentation clock. *Science (New York, N.Y.)*, 314(5805):1595–8, December 2006.

Detrick, R., Dickey, D., and Kintner, C. R. The effects of N-cadherin misexpression on morphogenesis in xenopus embryos. *Neuron*, 4(4):493–506, April 1990.

Downs, K. and Davies, T. Staging of gastrulating mouse embryos by morphological landmarks in the dissecting microscope. *Development*, 118(4):1255–1266, August 1993.

Dubrulle, J. and Pourquié, O. fgf8 mRNA decay establishes a gradient that couples axial elongation to patterning in the vertebrate embryo. *Nature*, 2004a.

Dubrulle, J. and Pourquié, O. Coupling segmentation to axis formation. *Development (Cambridge, England)*, 131(23):5783–93, December 2004b.

Dubrulle, J., McGrew, M. J., and Pourquié, O. FGF Signaling Controls Somite Boundary Position and Regulates Segmentation Clock Control of Spatiotemporal Hox Gene Activation. *Cell*, 106(2):219–232, July 2001.

Eakin, G. S. and Hadjantonakis, A.-K. Production of chimeras by aggregation of embryonic stem cells with diploid or tetraploid mouse embryos. *Nature protocols*, 1 (3):1145–53, January 2006.

Elsdale, T., Pearson, M., and Whitehead, M. Abnormalities in somite segmentation following heat shock to Xenopus embryos. *J Embryol Exp Morphol*, 35(3):625–635, June 1976.

Evans, D. J. R. and Noden, D. M. Spatial relations between avian craniofacial neural crest and paraxial mesoderm cells. *Developmental dynamics : an official publication of the American Association of Anatomists*, 235(5):1310–25, May 2006.

Findlater, G. S., McDougall, R. D., and Kaufman, M. H. Eyelid development, fusion and subsequent reopening in the mouse. *Journal of anatomy*, 183 (Pt 1:121–9, August 1993.

Fiúza, U.-M. and Arias, A. M. Cell and molecular biology of Notch. *The Journal of endocrinology*, 194(3):459–74, September 2007.

Folger, K. R., Wong, E. A., Wahl, G., and Capecchi, M. R. Patterns of integration of DNA microinjected into cultured mammalian cells: evidence for homologous recombination between injected plasmid DNA molecules. *Molecular and cellular biology*, 2(11):1372–87, November 1982.

Forsberg, H., Crozet, F., and Brown, N. A. Waves of mouse Lunatic fringe expression, in four-hour cycles at two-hour intervals, precede somite boundary formation. *Current Biology*, 8(18):1027–1030, September 1998.

Fortini, M. E. Notch signaling: the core pathway and its posttranslational regulation. *Developmental cell*, 16(5):633–47, May 2009.

Frohman, M., Martin, G., Cordes, S., Halamek, L., and Barsh, G. Altered rhombomere-specific gene expression and hyoid bone differentiation in the mouse segmentation mutant, kreisler (kr). *Development*, 117(3):925–936, March 1993.

Geffers, L., Herrmann, B., and Eichele, G. Web-based digital gene expression atlases for the mouse. *Mammalian genome : official journal of the International Mammalian Genome Society*, 23(9-10):525–38, October 2012.

George, S. H. L., Gertsenstein, M., Vintersten, K., Korets-Smith, E., Murphy, J., Stevens, M. E., Haigh, J. J., and Nagy, A. Developmental and adult phenotyping directly from mutant embryonic stem cells. *Proceedings of the National Academy of Sciences of the United States of America*, 104(11):4455–60, March 2007.

Gilbert, S. F. *Developmental Biology*. Sinauer, 10th editi edition, 2014.

Gomez, C., Ozbudak, E. M., Wunderlich, J., Baumann, D., Lewis, J., and Pourquié, O. Control of segment number in vertebrate embryos. *Nature*, 454(7202):335–9, July 2008.

Götz, M., Stoykova, A., and Gruss, P. Pax6 Controls Radial Glia Differentiation in the Cerebral Cortex. *Neuron*, 21(5):1031–1044, November 1998.

Gracy, J., Le-Nguyen, D., Gelly, J.-C., Kaas, Q., Heitz, A., and Chiche, L. KNOTTIN: the knottin or inhibitor cystine knot scaffold in 2007. *Nucleic acids research*, 36 (Database issue):D314–9, January 2008.

Gräper, L. Die Rhombomeren und ihre Nervenbeziehungen. *Archiv für Mikroskopische Anatomie*, 83(1):A371–A426, September 1913.

Gunawardhana, L. P., Baines, K. J., Mattes, J., Murphy, V. E., Simpson, J. L., and Gibson, P. G. Differential DNA methylation profiles of infants exposed to maternal asthma during pregnancy. *Pediatric pulmonology*, 49(9):852–62, September 2014.

Harima, Y. and Kageyama, R. Oscillatory links of Fgf signaling and Hes7 in the segmentation clock. *Current opinion in genetics & development*, 23(4):484–90, August 2013.

Harris, M. J. and McLeod, M. J. Eyelid growth and fusion in fetal mice. *Anatomy and Embryology*, 164(2):207–220, July 1982.

Harrison, S. M., Houzelstein, D., Dunwoodie, S. L., and Beddington, R. S. Sp5, a new member of the Sp1 family, is dynamically expressed during development and genetically interacts with Brachyury. *Developmental biology*, 227(2):358–72, November 2000.

Heins, N., Malatesta, P., Cecconi, F., Nakafuku, M., Tucker, K. L., Hack, M. A., Chapouton, P., Barde, Y.-A., and Götz, M. Glial cells generate neurons: the role of the transcription factor Pax6. *Nature neuroscience*, 5(4):308–15, April 2002.

Hernández, A. R., Klein, A. M., and Kirschner, M. W. Kinetic responses of β-catenin specify the sites of Wnt control. *Science (New York, N.Y.)*, 338(6112):1337–40, December 2012.

Holley, S. A., Geisler, R., and Nusslein-Volhard, C. Control of her1 expression during zebrafish somitogenesis by a Delta-dependent oscillator and an independent wavefront activity. *Genes & Dev.*, 14(13):1678–1690, July 2000.

Hrabe de Angelis, M., McIntyre, J., and Gossler, A. Maintenance of somite borders in mice requires the Delta homologue DII1. *Nature*, 386(6626):717–21, April 1997.

Hubaud, A. and Pourquié, O. Signalling dynamics in vertebrate segmentation. *Nature Reviews Molecular Cell Biology*, 15(11):709–721, October 2014.

Ishibashi, M., Moriyoshi, K., Sasai, Y., Shiota, K., Nakanishi, S., and Kageyama, R. Persistent expression of helix-loop-helix factor HES-1 prevents mammalian neural differentiation in the central nervous system. *The EMBO journal*, 13(8):1799–805, May 1994.

Jimenez-Guri, E. and Pujades, C. An ancient mechanism of hindbrain patterning has been conserved in vertebrate evolution. *Evolution & Development*, 13(1):38–46, 2011.

Kageyama, R., Ohtsuka, T., Shimojo, H., and Imayoshi, I. Dynamic Notch signaling in neural progenitor cells and a revised view of lateral inhibition. *Nature neuroscience*, 11(11):1247–51, November 2008.

Kandouz, M., Bier, A., Carystinos, G. D., Alaoui-Jamali, M. A., and Batist, G. Connexin43 pseudogene is expressed in tumor cells and inhibits growth. *Oncogene*, 23 (27):4763–70, June 2004.

Kelley, L. A. and Sternberg, M. J. E. Protein structure prediction on the Web: a case study using the Phyre server. *Nature protocols*, 4(3):363–71, January 2009.

Kim, S.-E., Huang, H., Zhao, M., Zhang, X., Zhang, A., Semonov, M. V., MacDonald, B. T., Zhang, X., Garcia Abreu, J., Peng, L., and He, X. Wnt stabilization of β-catenin reveals principles for morphogen receptor-scaffold assemblies. *Science (New York, N.Y.)*, 340(6134):867–70, May 2013.

Kimura-Yoshida, C., Nakano, H., Okamura, D., Nakao, K., Yonemura, S., Belo, J. A., Aizawa, S., Matsui, Y., and Matsuo, I. Canonical Wnt signaling and its antagonist regulate anterior-posterior axis polarization by guiding cell migration in mouse visceral endoderm. *Developmental cell*, 9(5):639–50, November 2005.

Klein, R., Martin-Zanca, D., Barbacid, M., and Parada, L. F. Expression of the tyrosine kinase receptor gene trkB is confined to the murine embryonic and adult nervous system. *Development (Cambridge, England)*, 109(4):845–50, August 1990.

Knoetgen, H., Teichmann, U., Wittler, L., Viebahn, C., and Kessel, M. Anterior neural induction by nodes from rabbits and mice. *Developmental biology*, 225(2):370–80, September 2000.

Kong, S. W., Sahin, M., Collins, C. D., Wertz, M. H., Campbell, M. G., Leech, J. D., Krueger, D., Bear, M. F., Kunkel, L. M., and Kohane, I. S. Divergent dysregulation of gene expression in murine models of fragile X syndrome and tuberous sclerosis. *Molecular autism*, 5(1):16, January 2014.

Kuan, C.-Y. K., Tannahill, D., Cook, G. M. W., and Keynes, R. J. Somite polarity and segmental patterning of the peripheral nervous system. *Mechanisms of development*, 121(9):1055–68, September 2004.

Kuhlbrodt, K., Herbarth, B., Sock, E., Hermans-Borgmeyer, I., and Wegner, M. Sox10, a Novel Transcriptional Modulator in Glial Cells. *J. Neurosci.*, 18(1):237–250, January 1998.

Larkin, M. A., Blackshields, G., Brown, N. P., Chenna, R., McGettigan, P. A., McWilliam, H., Valentin, F., Wallace, I. M., Wilm, A., Lopez, R., Thompson, J. D., Gibson, T. J., and Higgins, D. G. Clustal W and Clustal X version 2.0. *Bioinformatics (Oxford, England)*, 23(21):2947–8, November 2007.

Li, V. S. W., Ng, S. S., Boersema, P. J., Low, T. Y., Karthaus, W. R., Gerlach, J. P., Mohammed, S., Heck, A. J. R., Maurice, M. M., Mahmoudi, T., and Clevers, H. Wnt signaling through inhibition of β-catenin degradation in an intact Axin1 complex. *Cell*, 149(6):1245–56, June 2012.

Liu, C., Kato, Y., Zhang, Z., Do, V. M., Yankner, B. A., and He, X. Beta-Trcp couples beta-catenin phosphorylation-degradation and regulates Xenopus axis formation. *Proceedings of the National Academy of Sciences*, 96(11):6273–6278, May 1999.

Liu, P., Jenkins, N. A., and Copeland, N. G. A highly efficient recombineering-based method for generating conditional knockout mutations. *Genome research*, 13(3): 476–84, March 2003.

Logan, C. Y. and Nusse, R. THE WNT SIGNALING PATHWAY IN DEVELOPMENT AND DISEASE. October 2004.

Louvi, A. and Artavanis-Tsakonas, S. Notch signalling in vertebrate neural development. *Nature reviews. Neuroscience*, 7(2):93–102, February 2006.

Lovatt, D., Nedergaard, M., Kettenmann, H., and Ransom, B. The astrocyte transcriptome. *Neuroglia*, 2012.

MacDonald, B. T., Tamai, K., and He, X. Wnt/beta-catenin signaling: components, mechanisms, and diseases. *Developmental cell*, 17(1):9–26, July 2009.

Marks, M. Characterization of genes involved in somitogenesis. *Master Thesis*, 2010.

McGrew, M. J., Dale, J., Fraboulet, S., and Pourquié, O. The lunatic Fringe gene is a target of the molecular clock linked to somite segmentation in avian embryos. *Current Biology*, 8(17):979–982, August 1998.

Meno, C., Saijoh, Y., Fujii, H., Ikeda, M., Yokoyama, T., Yokoyama, M., Toyoda, Y., and Hamada, H. Left-right asymmetric expression of the TGF beta-family member lefty in mouse embryos. *Nature*, 381(6578):151–5, May 1996.

Meselson, M. and Yuan, R. DNA restriction enzyme from E. coli. *Nature*, 1968.

Mighell, A., Smith, N., Robinson, P., and Markham, A. Vertebrate pseudogenes. *FEBS Letters*, 468(2-3):109–114, February 2000.

Morales, A. V., Yasuda, Y., and Ish-Horowicz, D. Periodic Lunatic fringe Expression Is Controlled during Segmentation by a Cyclic Transcriptional Enhancer Responsive to Notch Signaling. *Developmental Cell*, 3(1):63–74, July 2002.

Moreno, T. A. and Kintner, C. Regulation of Segmental Patterning by Retinoic Acid Signaling during Xenopus Somitogenesis. *Developmental Cell*, 6(2):205–218, February 2004.

Mukhopadhyay, M., Shtrom, S., Rodriguezesteban, C., Chen, L., Tsukui, T., Gomer, L., Dorward, D., Glinka, A., Grinberg, A., and Huang, S. Dickkopf1 Is Required for Embryonic Head Induction and Limb Morphogenesis in the Mouse. *Developmental Cell*, 1(3):423–434, September 2001.

Muller, P., Janovjak, H., Miserez, A., and Dobbie, Z. Short technical report processing of gene expression data generated by quantitative Real-Time RT-PCR. *Biotechniques*, 2002.

Nagoshi, N., Shibata, S., Kubota, Y., Nakamura, M., Nagai, Y., Satoh, E., Morikawa, S., Okada, Y., Mabuchi, Y., Katoh, H., Okada, S., Fukuda, K., Suda, T., Matsuzaki, Y., Toyama, Y., and Okano, H. Ontogeny and multipotency of neural crest-derived stem cells in mouse bone marrow, dorsal root ganglia, and whisker pad. *Cell stem cell*, 2(4):392–403, May 2008.

Nagy, A., Rossant, J., Nagy, R., Abramow-Newerly, W., and Roder, J. C. Derivation of completely cell culture-derived mice from early-passage embryonic stem cells. *Proceedings of the National Academy of Sciences*, 90(18):8424–8428, September 1993.

Nguyen Ba, A. N., Pogoutse, A., Provart, N., and Moses, A. M. NLStradamus: a simple Hidden Markov Model for nuclear localization signal prediction. *BMC bioinformatics*, 10(1):202, January 2009.

Nichols, J., Zevnik, B., Anastassiadis, K., Niwa, H., Klewe-Nebenius, D., Chambers, I., Schöler, H., and Smith, A. Formation of Pluripotent Stem Cells in the Mammalian Embryo Depends on the POU Transcription Factor Oct4. *Cell*, 95(3):379–391, October 1998.

Niida, A., Hiroko, T., Kasai, M., Furukawa, Y., Nakamura, Y., Suzuki, Y., Sugano, S., and Akiyama, T. DKK1, a negative regulator of Wnt signaling, is a target of the beta-catenin/TCF pathway. *Oncogene*, 23(52):8520–6, November 2004.

Niwa, Y., Masamizu, Y., Liu, T., Nakayama, R., Deng, C.-X., and Kageyama, R. The initiation and propagation of Hes7 oscillation are cooperatively regulated by Fgf and notch signaling in the somite segmentation clock. *Developmental cell*, 13(2):298–304, August 2007.

Nye, J. S. and Kopan, R. Developmental Signalling: Vertebrate ligands for Notch. *Current Biology*, 5(9):966–969, September 1995.

Ordway, J. M., Tallaksen-Greene, S., Gutekunst, C.-A., Bernstein, E. M., Cearley, J. A., Wiener, H. W., Dure, L. S., Lindsey, R., Hersch, S. M., Jope, R. S., Albin, R., and Detloff, P. J. Ectopically Expressed CAG Repeats Cause Intranuclear Inclusions and a Progressive Late Onset Neurological Phenotype in the Mouse. *Cell*, 91(6):753–763, December 1997.

Osumi-Yamashita, N., Ninomiya, Y., Doi, H., and Eto, K. Rhombomere formation and hind-brain crest cell migration from prorhombomeric origins in mouse embryos. *Development, Growth and Differentiation*, 38(1):107–118, February 1996.

Palmeirim, I., Henrique, D., Ish-Horowicz, D., and Pourquié, O. Avian hairy Gene Expression Identifies a Molecular Clock Linked to Vertebrate Segmentation and Somitogenesis. *Cell*, 91(5):639–648, November 1997.

Pan, D. The hippo signaling pathway in development and cancer. *Developmental cell*, 19(4):491–505, October 2010.

Patthey, C., Gunhaga, L., and Edlund, T. Early development of the central and peripheral nervous systems is coordinated by Wnt and BMP signals. *PloS one*, 3(2): e1625, January 2008.

Perea-Gomez, A., Vella, F. D., Shawlot, W., Oulad-Abdelghani, M., Chazaud, C., Meno, C., Pfister, V., Chen, L., Robertson, E., and Hamada, H. Nodal Antagonists in the Anterior Visceral Endoderm Prevent the Formation of Multiple Primitive Streaks. *Developmental Cell*, 3(5):745–756, November 2002.

Pusch, C., Hustert, E., Pfeifer, D., Südbeck, P., Kist, R., Roe, B., Wang, Z., Balling, R., Blin, N., and Scherer, G. The SOX10 / Sox10 gene from human and mouse: sequence, expression, and transactivation by the encoded HMG domain transcription factor. *Human Genetics*, 103(2):115–123, September 1998.

Reinke, S. Improvement of an inducible transgene system in mice. *Master Thesis*, 2012.

Riemer, P., Sreekumar, A., Reinke, S., Rad, R., Schäfer, R., Sers, C., Bläker, H., Herrmann, B. G., and Morkel, M. Transgenic expression of oncogenic BRAF induces loss of stem cells in the mouse intestine, which is antagonized by β-catenin activity. *Oncogene*, August 2014.

Robertson, E. J. *Teratocarcinomas and embryonic stem cells: a practical approach.* IRL Press, 1987.

Rogers, D. C., Fisher, E., Brown, S., Peters, J., Hunter, A., and Martin, J. Behavioral and functional analysis of mouse phenotype: SHIRPA, a proposed protocol for comprehensive phenotype assessment. *Mammalian Genome*, 8(10):711–713, October 1997.

Sakamoto, M., Hirata, H., Ohtsuka, T., Bessho, Y., and Kageyama, R. The basic helix-loop-helix genes Hesr1/Hey1 and Hesr2/Hey2 regulate maintenance of neural precursor cells in the brain. *The Journal of biological chemistry*, 278(45):44808–15, December 2003.

Sambrook, J. and Russell, D. Molecular cloning: a laboratory manual (3-volume set). 2001.

Scheer, N., Groth, A., Hans, S., and Campos-Ortega, J. An instructive function for Notch in promoting gliogenesis in the zebrafish retina. *Development*, 128(7):1099–1107, April 2001.

Schoenwolf, G. C. Histological and ultrastructural studies of secondary neurulation in mouse embryos. *The American journal of anatomy*, 169(4):361–76, April 1984.

Schoenwolf, G. C. *Laboratory Studies of Vertebrate and Invertebrate Embryos: Guide and Atlas of Descriptive and Experimental Development.* 2009.

Schröter, C., Herrgen, L., Cardona, A., Brouhard, G. J., Feldman, B., and Oates, A. C. Dynamics of zebrafish somitogenesis. *Developmental dynamics : an official publication of the American Association of Anatomists*, 237(3):545–53, March 2008.

Schwenk, F., Baron, U., and Rajewsky, K. A cre-transgenic mouse strain for the ubiquitous deletion of loxP-flanked gene segments including deletion in germ cells. *Nucleic acids research*, 23(24):5080–1, December 1995.

Serbedzija, G., Fraser, S., and Bronner-Fraser, M. Pathways of trunk neural crest cell migration in the mouse embryo as revealed by vital dye labelling. *Development*, 108 (4):605–612, April 1990.

Shimizu, H., Uchibe, K., and Asahara, H. Large-scale whole mount in situ hybridization of mouse embryos. *Methods in molecular biology (Clifton, N.J.)*, 577:167–79, January 2009.

Shimojo, H., Ohtsuka, T., and Kageyama, R. Oscillations in notch signaling regulate maintenance of neural progenitors. *Neuron*, 58(1):52–64, April 2008.

Sievers, F., Wilm, A., Dineen, D., Gibson, T. J., Karplus, K., Li, W., Lopez, R., McWilliam, H., Remmert, M., Söding, J., Thompson, J. D., and Higgins, D. G. Fast, scalable generation of high-quality protein multiple sequence alignments using Clustal Omega. *Molecular systems biology*, 7:539, January 2011.

Simeone, A., Acampora, D., Gulisano, M., Stornaiuolo, A., and Boncinelli, E. Nested expression domains of four homeobox genes in developing rostral brain. *Nature*, 358 (6388):687–90, August 1992.

Simon, P. Q-Gene: processing quantitative real-time RT-PCR data. *Bioinformatics*, 19(11):1439–1440, July 2003.

Soriano, P. Generalized lacZ expression with the ROSA26 Cre reporter strain. *Nature genetics*, 21(1):70–1, January 1999.

Soza-Ried, C., Öztürk, E., Ish-Horowicz, D., and Lewis, J. Pulses of Notch activation synchronise oscillating somite cells and entrain the zebrafish segmentation clock. *Development (Cambridge, England)*, 141(8):1780–8, April 2014.

St John, J. A., Braun, E. L., Isberg, S. R., Miles, L. G., Chong, A. Y., Gongora, J., Dalzell, P., Moran, C., Bed'hom, B., Abzhanov, A., Burgess, S. C., Cooksey, A. M., Castoe, T. A., Crawford, N. G., Densmore, L. D., Drew, J. C., Edwards, S. V., Faircloth, B. C., Fujita, M. K., Greenwold, M. J., Hoffmann, F. G., Howard, J. M., Iguchi, T., Janes, D. E., Khan, S. Y., Kohno, S., de Koning, A. J., Lance, S. L., McCarthy, F. M., McCormack, J. E., Merchant, M. E., Peterson, D. G., Pollock, D. D., Pourmand, N., Raney, B. J., Roessler, K. A., Sanford, J. R., Sawyer, R. H., Schmidt, C. J., Triplett, E. W., Tuberville, T. D., Venegas-Anaya, M., Howard, J. T., Jarvis, E. D., Guillette, L. J., Glenn, T. C., Green, R. E., and Ray, D. A. Sequencing three crocodilian genomes to illuminate the evolution of archosaurs and amniotes. *Genome biology*, 13(1):415, January 2012.

Strumpf, D., Mao, C.-A., Yamanaka, Y., Ralston, A., Chawengsaksophak, K., Beck, F., and Rossant, J. Cdx2 is required for correct cell fate specification and differentiation of trophectoderm in the mouse blastocyst. *Development (Cambridge, England)*, 132 (9):2093–102, May 2005.

Swindell, E. C., Thaller, C., Sockanathan, S., Petkovich, M., Jessell, T. M., and Eichele, G. Complementary domains of retinoic acid production and degradation in the early chick embryo. *Developmental biology*, 216(1):282–96, December 1999.

Taelman, V. F., Dobrowolski, R., Plouhinec, J.-L., Fuentealba, L. C., Vorwald, P. P., Gumper, I., Sabatini, D. D., and De Robertis, E. M. Wnt signaling requires sequestration of glycogen synthase kinase 3 inside multivesicular endosomes. *Cell*, 143(7): 1136–48, December 2010.

Takahashi, Y., Yasuhiko, Y., Kitajima, S., Kanno, J., and Saga, Y. Appropriate suppression of Notch signaling by Mesp factors is essential for stripe pattern formation leading to segment boundary formation. *Developmental biology*, 304(2):593–603, April 2007.

Tam, P. P. L. The control of somitogenesis in mouse embryos. *J Embryol Exp Morphol*, 65(Supplement):103–128, October 1981.

Tax, F. E., Yeargers, J. J., and Thomas, J. H. Sequence of C. elegans lag-2 reveals a cell-signalling domain shared with Delta and Serrate of Drosophila. *Nature*, 368 (6467):150–4, March 1994.

Theiler, K. *The house mouse: atlas of embryonic development*. Springer-Verlag, New York, 1989.

Thomas, K. R. and Capecchi, M. R. Site-directed mutagenesis by gene targeting in mouse embryo-derived stem cells. *Cell*, 51(3):503–512, November 1987.

Thomas, K. R., Folger, K. R., and Capecchi, M. R. High frequency targeting of genes to specific sites in the mammalian genome. *Cell*, 44(3):419–428, February 1986.

Tomita, Y., Matsumura, K., Wakamatsu, Y., Matsuzaki, Y., Shibuya, I., Kawaguchi, H., Ieda, M., Kanakubo, S., Shimazaki, T., Ogawa, S., Osumi, N., Okano, H., and Fukuda, K. Cardiac neural crest cells contribute to the dormant multipotent stem cell in the mammalian heart. *The Journal of cell biology*, 170(7):1135–46, October 2005.

Tossell, K., Kiecker, C., Wizenmann, A., Lang, E., and Irving, C. Notch signalling stabilises boundary formation at the midbrain-hindbrain organiser. *Development (Cambridge, England)*, 138(17):3745–57, September 2011.

Valenta, T., Hausmann, G., and Basler, K. The many faces and functions of β-catenin. *The EMBO journal*, 31(12):2714–36, June 2012.

van der Weyden, L., White, J. K., Adams, D. J., and Logan, D. W. The mouse genetics toolkit: revealing function and mechanism. *Genome biology*, 12(6):224, January 2011.

Vidigal, J. A., Morkel, M., Wittler, L., Brouwer-Lehmitz, A., Grote, P., Macura, K., and Herrmann, B. G. An inducible RNA interference system for the functional dissection of mouse embryogenesis. *Nucleic acids research*, 38(11):e122, June 2010.

Vincze, T., Posfai, J., and Roberts, R. J. NEBcutter: A program to cleave DNA with restriction enzymes. *Nucleic acids research*, 31(13):3688–91, July 2003.

Wassarman, K., Lewandoski, M., Campbell, K., Joyner, A., Rubenstein, J., Martinez, S., and Martin, G. Specification of the anterior hindbrain and establishment of a normal mid/hindbrain organizer is dependent on Gbx2 gene function. *Development*, 124(15):2923–2934, August 1997.

Weidinger, G., Thorpe, C. J., Wuennenberg-Stapleton, K., Ngai, J., and Moon, R. T. The Sp1-related transcription factors sp5 and sp5-like act downstream of Wnt/beta-catenin signaling in mesoderm and neuroectoderm patterning. *Current biology : CB*, 15(6):489–500, March 2005.

Wilkinson, D. G. In situ hybridization: a practical approach. 1998.

Winston, J. T., Strack, P., Beer-Romero, P., Chu, C. Y., Elledge, S. J., and Harper, J. W. The SCFbeta-TRCP-ubiquitin ligase complex associates specifically with phosphorylated destruction motifs in Ikappa Balpha and beta-catenin and stimulates Ikappa Balpha ubiquitination in vitro. *Genes & Development*, 13(3):270–283, February 1999.

Wolpert, L., Jessell, T., Lawrence, P., Meyerowitz, E., Robertson, E. J., and Smith, J. *Principles of Development*. Oxford University Press, 3rd editio edition, 2007.

Wu, G. and He, X. Threonine 41 in beta-catenin serves as a key phosphorylation relay residue in beta-catenin degradation. *Biochemistry*, 45(16):5319–23, April 2006.

Wurst, W. and Bally-Cuif, L. Neural plate patterning: upstream and downstream of the isthmic organizer. *Nature reviews. Neuroscience*, 2(2):99–108, March 2001.

Wysocki, K., Conley, Y., and Wenzel, S. Epigenome Variation in Severe Asthma. *Biological research for nursing*, pages 1099800414553463–, October 2014.

Yanisch-Perron, C., Vieira, J., and Messing, J. Improved M13 phage cloning vectors and host strains: nucleotide sequences of the M13mpl8 and pUC19 vectors. *Gene*, 33(1):103–119, January 1985.

Ye, J., Coulouris, G., Zaretskaya, I., Cutcutache, I., Rozen, S., and Madden, T. L. Primer-BLAST: a tool to design target-specific primers for polymerase chain reaction. *BMC bioinformatics*, 13:134, January 2012.

Zambrowicz, B. P., Imamoto, A., Fiering, S., Herzenberg, L. A., Kerr, W. G., and Soriano, P. Disruption of overlapping transcripts in the ROSA betageo 26 gene trap strain leads to widespread expression of -galactosidase in mouse embryos and hematopoietic cells. *Proceedings of the National Academy of Sciences*, 94(8):3789–3794, April 1997.

Zhang, J., Wang, X., Li, M., Han, J., Chen, B., Wang, B., and Dai, J. NANOGP8 is a retrogene expressed in cancers. *The FEBS journal*, 273(8):1723–30, April 2006.

List of Figures

List of Tables